# Design and Implementation of a Compact Receiver Module for an Ice Penetrating Radar Depth Sounder

By

Austin Ryan Arnett

B.S. Electrical Engineering
University of Kansas, 2010

Submitted to the graduate degree program in Electrical Engineering and the Graduate Faculty of the University of Kansas in partial fulfillment of the requirements for the degree of Master of Science

_____

Dr. Carl Leuschen
Chairperson

_____

Dr. Fernando Rodriguez-Morales

_____

Dr. Swapan Chakrabarti

Date Defended: June 19, 2012

The Thesis Committee for Austin Ryan Arnett
certifies that this is the approved version of the following thesis:

Design and Implementation of a Compact Receiver Module
for an Ice Penetrating Radar Depth Sounder

_____

Dr. Carl Leuschen
Chairperson

Date Approved: June 19, 2012

## Abstract

The study of global climate change is an important issue in the scientific community and radar depth sounding and imaging data is very useful in modeling and predicting the changes to the ice sheets in Greenland and Antarctica. A compact radar receiver module for CReSIS's MCoRDS/I system was developed to standardize the system across various platforms and accommodate future upgrades to the system that will increase its performance and produce more complete and accurate data products of the most challenging target areas. Design parameters for the receiver module were determined by considering all possible current and future operation conditions of the MCoRDS/I system. The receiver module was designed, simulated, implemented, and tested in the field and shown to achieve its design goals.

## Acknowledgements

I would first like to thank my parents for their love, support, guidance, and encouragement throughout my education as well as my life. They have taught me that determination and hard work can take you anywhere you want to go and have inspired me to always strive to be the best I can be and take pride in everything I do.

I would also like to thank my committee. Each one has offered a tremendous amount of help and guidance along the way which made this all possible.

The facility, staff, and students at CReSIS have been a big help in assisting my research and made my time here much easier and more enjoyable.

Lastly, I would like to thank Kevin Player for his hard work in making this project become a reality. Without his efforts this project would have never been accomplished on time.

## Table of Contents

## List of Figures

## List of Tables

# Chapter 1

## *Introduction*

### *1.1 Background*

Among the scientific community, global climate change is an important and widely discussed topic. The impact of global climate change could be very significant and have an extreme impact on the Earth as we know it today. It is thus very important to study and fully understand its ramifications. One important consequence of global climate change is its impact on the polar land ice sheets in Greenland and Antarctica. The ice sheets in Greenland and Antarctica contain almost 2% of the world's total water. If the Greenland ice sheet were to melt into the ocean, the sea level could rise as much as 7 meters [1]. With approximately 100 million people living within 1 vertical meter of the current sea level and 2.5 billion people living in coastal regions within 100 km of the current coast, a rise in sea level would have a significant impact on humanity [2, 3]. The ability to understand and predict the changes in the ice sheets is vital to predicting sea level rise. To better understand and accurately model the changes in the polar ice sheets a large amount of information and data is needed such as bedrock topography, land ice mass flux, and sea ice thickness.

## *1.2 Motivation*

In 2005, the National Science Foundation (NSF) established the Center for Remote Sensing of Ice Sheets (CReSIS) to generate data that will advance the scientific understanding of polar ice sheets and assist in modeling their complex and dynamic behavior. CReSIS has developed a suite of radar systems to generate this data that assists scientists in measuring and understanding ice thickness, internal layering, basal conditions below the ice surface, liquid water layers and channels, and various other parameters. To map and image the ice-bedrock interface in the most challenging and fast moving areas of the polar ice sheets CReSIS has developed the Multi-Channel Coherent Radar Depth Sounder/Imager (MCoRDS/I) system. The MCoRDS/I system is deployed on airborne science laboratories such as NASA's P-3 and DC-8 for Operation Ice Bridge as well as a Twin Otter aircraft. In the past, each different airborne platform required a different configuration of the MCoRDS/I system. Recently, the MCoRDS/I system has been upgraded to utilize a National Instruments (NI) PCI extension for instrumentation (PXI) chassis to control the system and digitize the received signal. The development was done for the following reasons: to provide a user interface that was much easier to use, allow the radar operator to detect problems quickly and easily, and make the system much smaller in physical size and weight which is important for airborne platforms. The size and weight reduction also served to standardize the system across

all the different airborne platforms so that the same system could be used on any of the platforms without modification. The next step in fully utilizing the capabilities of the NI PXI chassis and making the MCoRDS/I system even smaller and lighter is to design a receiver module integrated inside the chassis. The receiver module is contained within and controlled by the NI PXI chassis creating an RF receiver module integrated with the digital back-end of the MCoRDS/I system. Figure 1.1 shows a photo of the MCoRDS system before and after the utilization of the NI PXI chassis. The green circle on the left shows the old digital control system with the arrow pointing to its replacement, the NI PXI chassis. The red circle on the right outlines the current receiver box and the red arrow shows where the receiver modules will replace the box and be integrated into the NI PXI chassis.

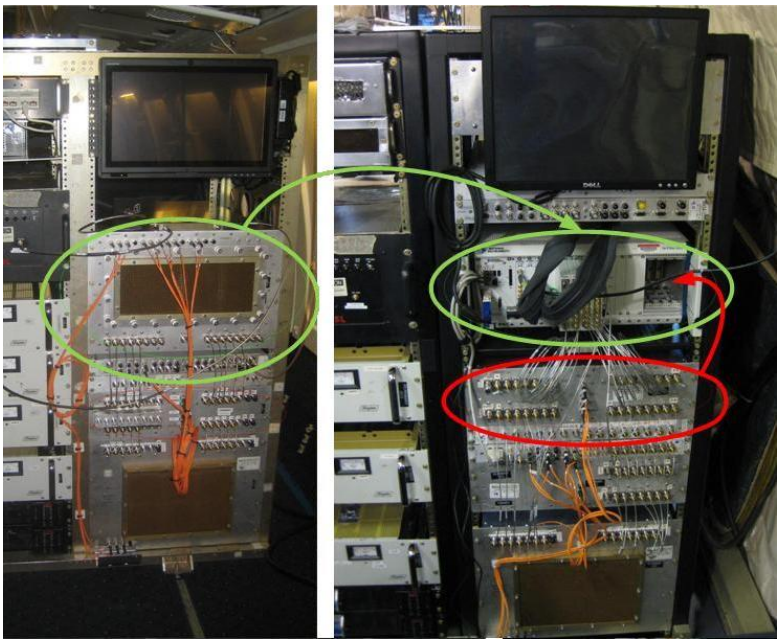

*Figure 1.1 - Comparison of Previous MCoRDS Hardware to MCoRDS/I Hardware and Placement of Receiver Modules*

## *1.3 Chapter Summaries*

The basic operation of the MCoRDS/I system and its platforms will be introduced in Chapter 2. This chapter will include a description of the subsystems of the MCoRDS/I system that affect the design parameters of the receiver module. A set of design requirements will also be derived and presented. Chapter 3 addresses the design of the receiver modules including the analysis of different topologies that were considered. This chapter includes an analysis of each component in the receiver chain as well as a simulation and analysis of the receiver chain S parameters. The physical design and testing of the receiver RF test board is presented in Chapter 4. The final design and test results are also discussed and compared with the simulation results. Chapter 4 concludes by presenting results gathered from field testing of the receiver modules. Chapter 5 offers conclusions and possible future work.

# Chapter 2

## *System Background and Theory*

### *2.1 MCoRDS/I System*

The MCoRDS/I system is CReSIS's primary airborne radar sensor for nadir depth sounding and SAR imaging of the bedrock interface. It is a high power multi-channel VHF system with a 195 MHZ center frequency, 30 MHZ of bandwidth, and approximately 150 W of transmitting power per transmitting element. Figure 2.1 is a simple block diagram of the current MCoRDS/I system.

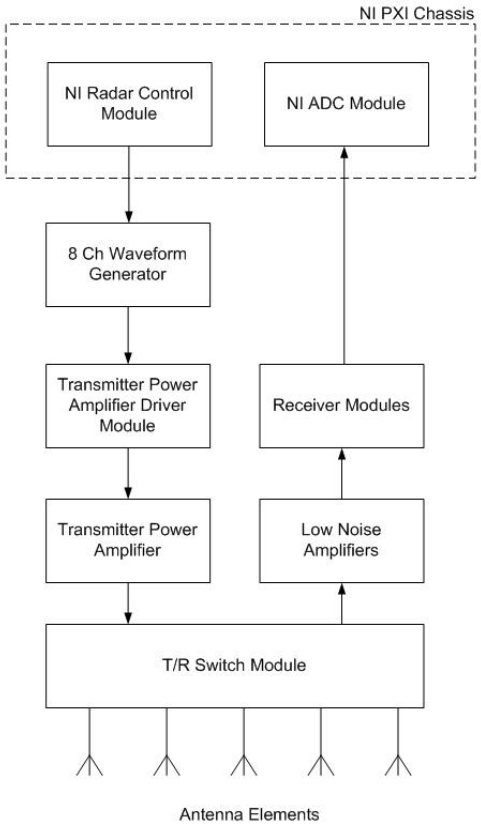


*Figure 2.1 - MCoRDS/I Simple Block Diagram*

### *2.1.1 MCoRDS/I Platforms*

There are three primary platforms that the MCoRDS/I system is deployed on, the NASA P-3 and DC-8 airborne laboratories for Operation IceBridge (OIB) as well as a DCH-6 Twin Otter aircraft. Each of these platforms have a different antenna configuration on the underside of the aircraft with a different number of transmitting and receiving antenna elements. Figures 2.2, 2.3, and 2.4 illustrate the antenna configurations on each of the different platforms. On the P-3 platform, there are a total of 15 antenna elements, four on each wing and seven under the fuselage. The seven antenna elements under the fuselage are used for both transmit and receive while the eight wing elements are used for receive only. The DC-8 aircraft has a five antenna element array under the fuselage with all five being used for both transmit and receive. The Twin Otter platform has a twelve element array, six under each wing. The six elements under the starboard (right) side are used for transmit and receive while the six antennas under the port (left) side are used for receive only.

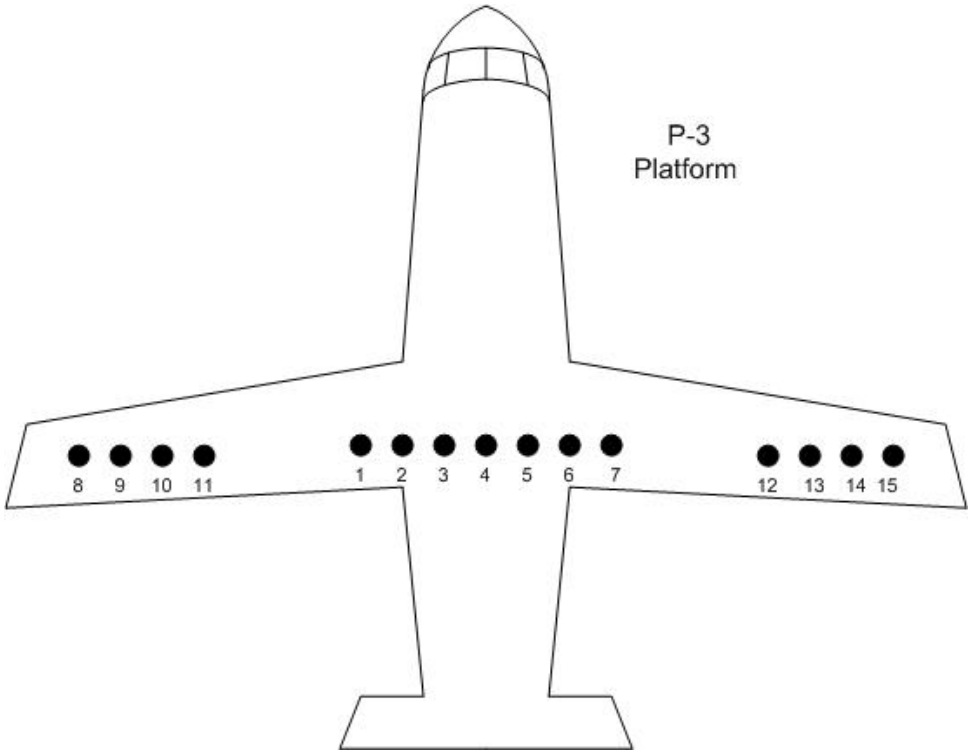


*Figure 2.2 - MCoRDS/I Antenna Placement for the P-3 Platform*

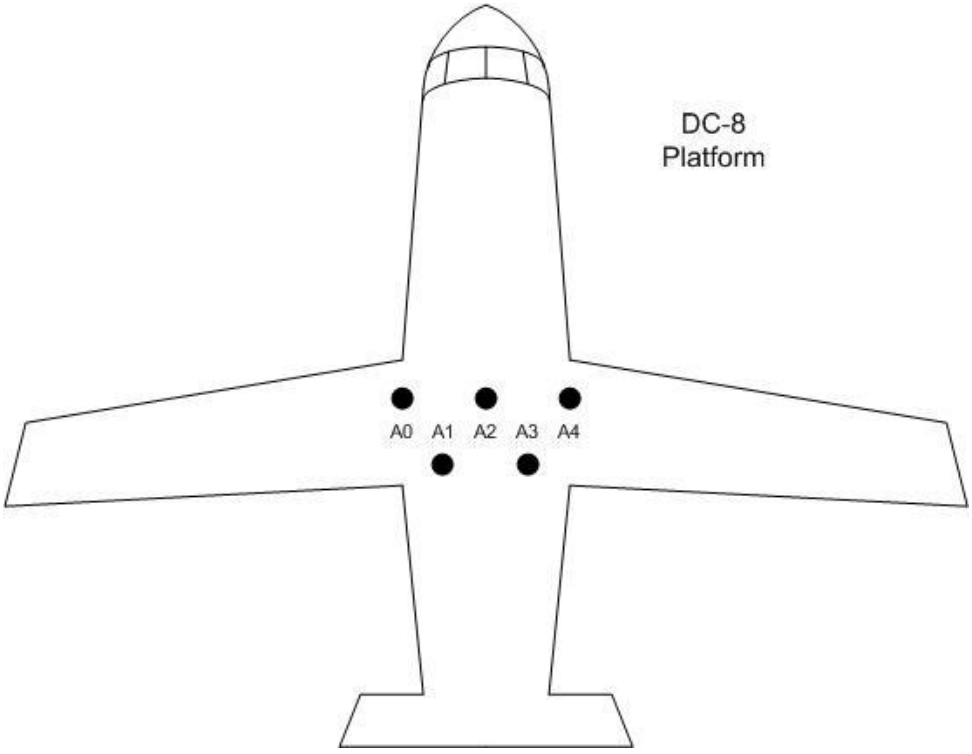


*Figure 2.3 - MCoRDS/I Antenna Placement for the DC-8 Platform*

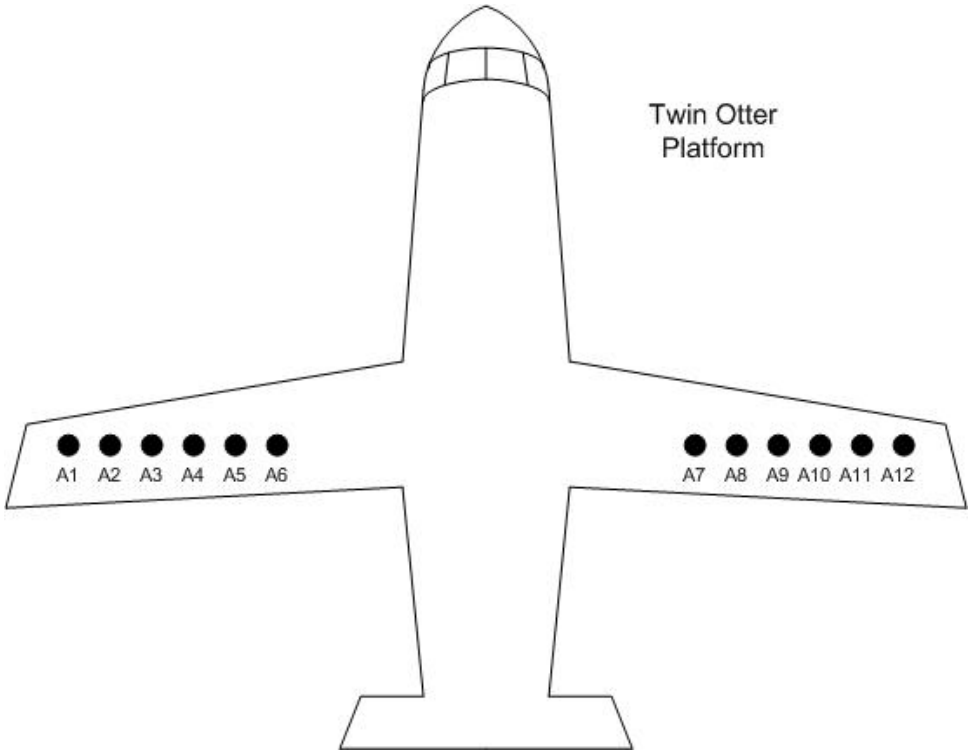


*Figure 2.4 - MCoRDS/I Antenna Placement for the Twin Otter Platform*

### *2.1.2 MCoRDS/I System Improvements*

The MCoRDS/I system is constantly upgraded to enhance its performance. There are many improvements currently under development. The largest and most impactful upgrade to the system that is being developed is a new power amplifier architecture that will increase the maximum transmit power of the system. In the near future, the system will see an increase in transmit power from the current 150 W per transmitting channel to at least 300 W. There is also a long term project in development to increase the transmit power to 1000 W per channel. This will allow the system to increase the illuminating power to

sound the most challenging areas in the polar ice sheets. In addition, the pursuit of increased miniaturization of the system is being developed to support a larger number of antenna elements.

## *2.2 MCoRDS/I Subsystems*

When approaching a new receiver design for the MCoRDS/I system many factors need to be accounted for to ensure that the receiver will operate properly. The MCoRDS/I system is very adaptable to its different platforms and ice targets. It uses multiple pulse lengths, transmit power levels, transmitting antenna arrays, transmit array phase and amplitude, and presums among other variable parameters depending on geographic location. All of these possible parameter variations must be taken into account so the receiver will operate optimally for any possible set of operating conditions the MCoRDS/I system might use. This section will introduce the figures of merit and design requirements of the receiver design.

### *2.2.1 MCoRDS/I Link Budget*

To set the required minimum saturation input power for the MCoRDS/I receiver the largest possible return signal must be calculated. To calculate the link budget for the MCoRDS/I system we first need to address the simple radar equation. Equation 2.1 shows the power that

will be received $P_R$ given the total transmit power $P_T$, transmit antenna gain at nadir $G_T$, receive antenna gain at nadir $G_R$, wavelength of the signal $\lambda$, one way range to the target R and reflection coefficient of the target $\Gamma$. This equation assumes the system is flying above a smooth specular surface which would provide the largest received power.

$$P_R = \frac{P_T G_T G_R \lambda^2 |\Gamma^2|}{(4\pi)^2 (2R)^2} \tag{2.1}$$

All the MCoRDS/I platforms utilize an antenna array for transmit. This can cause the gain pattern of the transmit array to be much different than the gain pattern of a single antenna. The transmit arrays on the P-3 and Twin Otter aircraft are linear half wavelength dipole arrays spaced by approximately half wavelength with a ground plane (wing or fuselage) located a quarter wavelength above the array structure. The DC-8 antenna array is arranged in a quarter wavelength inverted W configuration with a ground plane spaced approximately four inches above the antenna. To calculate the largest possible returned signal power, the largest possible array gain is needed. To simplify the calculations and provide the largest theoretical array gain, each platform will be assumed to have a dipole transmit array spaced a half wavelength apart with an infinite ground plane spaced a quarter wavelength above the array structure. This approximation is appropriate for the antenna configurations of the P-3 and Twin Otter platforms but will over estimate the array gain of the DC-8 antenna configuration. Equation 2.2 shows the

nadir gain of the transmit antenna array $G_T$ for the previously described case with N antenna elements with gain G. To approximate the dipoles used on the MCoRDS/I platforms 1 dBi will be used for the nadir element gain G.

$$G_T = 4GN \tag{2.2}$$

The platforms typically fly at a nominal altitude of 500 m above the ice surface but the altitude varies during flight and a lower altitude will provide a larger signal return thus 300 m will be used as the worst case. A smooth specular ice sheet surface provides a reflection coefficient of $\Gamma$=0.14 (-17 dB) [4].

| **Platform** | **units** | **P3** | **DC-8** | **Twin Otter** | | **300W P-3** | | **1000W P-3** |
|---|---|---|---|---|---|---|---|---|
| **Transmit Power / ch** | dBm | 51.76 | 51.76 | 51.76 | | 54.76 | | 60 |
| **Number of Elements** | | 7 | 5 | 6 | | 7 | | 7 |
| **Total Transmit power** | dBm | 60.21 | 58.75 | 59.54 | | 63.21 | | 68.45 |
| **Antenna Gain** | dBi | 7 | 7 | 7 | | 7 | | 7 |
| **Transmit Array Gain** | dBi | 15.45 | 13.99 | 14.78 | | 15.45 | | 15.45 |
| **Receive Gain** | dBi | 7 | 7 | 7 | | 7 | | 7 |
| **One Way Range** | m | 300 | 300 | 300 | | 300 | | 300 |
| **Two Way Range** | dB | 27.78 | 27.78 | 27.78 | | 27.78 | | 27.78 |
| **Wavelength** | m | 1.54 | 1.54 | 1.54 | | 1.54 | | 1.54 |
| **Wavelength^2** | dB | 3.74 | 3.74 | 3.74 | | 3.74 | | 3.74 |
| **4pi^2** | dB | 21.98 | 21.98 | 21.98 | | 21.98 | | 21.98 |
| **Reflection Coefficient** | dB | -17 | -17 | -17 | | -17 | | -17 |
| | | | | | | | | |
| **Max Received Power** | dBm | -8.14 | -11.07 | -9.48 | | -5.14 | | .10 |

*Table 2.1 - MCoRDS/I Link Budget*

Table 2.1 provides the link budget for the MCoRDS/I system for the different platforms as well as the worst case for both the 300 W and 1000 W transmitters in development to insure compatibility of this design with future upgrades. When examining Table 2.1, under the current 150 W per channel transmit power the P-3 platform provides the largest received signal at -8.14 dBm. Since the P-3 platform provides the largest received signal of the three platforms it was used as the worst case for the 300 W and 1000 W per channel transmit power upgrades that are currently under development. The largest received signal power for the 300 W case is -5.14 dBm and 0.10 dBm for the 1000 W case. To ensure that the receiver does not saturate, the compression point of the receiver needs to be set above the largest received signal power. A common rule of thumb states that the compression point of the receiver should be at minimum 3 dB above the largest received signal power thus the compression point of the receiver is required to be 3.1 dBm or greater. It should also be noted that if receiver compression becomes an issue over certain targets the MCoRDS/I system has the ability to decrease the transmit power to avoid compression of the receiver.

### *2.2.2 MCoRDS/I NI ADC*

The MCoRDS/I NI digital system uses the National Instruments 5761 Digitizer module to covert the received RF signal into a stream of binary words so the signal can be stored and processed in the digital domain. The NI 5761 is a four channel simultaneously sampled analog to digital converter. It has a maximum sample rate of 250 MS/s, 14 bits of resolution, and a 3 dB bandwidth that spans from 100 kHz to 500 MHz allowing for under sampling of a signal up to the fourth Nyquist zone. The MCoRDS/I system utilizes a bandpass sampling technique which samples at 111.11 MHz, placing the 180 MHz to 210 MHz signal in the forth Nyquist zone. The dynamic range of the NI 5761 extends from 10 dBm to -62 dBm and is very important when setting the gain requirements of the receiver module.

### *2.2.3 MCoRDS/I T/R Switch Module*

The MCoRDS/I system contains a high power T/R switch module for several purposes. It both allows the same antenna element to be used as both a transmitting and receiving element and protects the non-transmitting elements from the large signal power that will be present during transmit. The switch that is used to protect the receivers changes state just after the transmit pulse and introduces a transient signal known as video feed through. This video feed through is a high frequency

transient signal that will be present at the input of the receiver. To ensure that this transient does not saturate the receiver a low pass filter should be used to attenuate the video feed through signal. This will prevent the receiver from allowing the transient signal to propagate inside the receiver and saturate its components during operation.

### *2.2.4 MCoRDS/I Multiple Transmit Pulses, Signal Processing and Its Effect on Dynamic Range*

Depending on a variety of factors including thickness, attenuation, and surface roughness, outlet glaciers and ice sheet margins can be very difficult target for depth sounding radar systems to fully and accurately measure. A large amount of the transmitted signal is reflected off the surface of the ice and the rest of signal that is not reflected experiences a very large amount of attenuation when traveling all the way through the ice sheet. Once the signal reaches the bedrock only a small amount of the signal is reflected back off the bedrock and then it again gets largely attenuated when traveling back through the ice sheet. Outlet glaciers with a large amount of surface roughness and high altitude sounding of interior ice sheets further decrease the power of the bedrock reflection. This huge dynamic range in signal power between the surface and bedrock reflection make it very difficult for the MCoRDS/I system to accurately capture both the surface return and the bed rock return of a

single pulse. To solve this problem, the MCoRDS/I system currently utilizes two different transmit pulses of different pulse lengths: one to capture the surface return and one to capture the return from the bedrock. The large dynamic range in the returned signal power also places a difficult requirement on the receiver. The receiver must be able to handle the relatively large returned signal power from the surface return without saturating and amplify the signal with the proper gain to fit within the dynamic range of the ADC. It also must be extremely sensitive to very small returned signal power from the bedrock return and have the proper gain so the signal can be detected, often after extensive signal processing. These two very different and contrasting requirements on the receiver make it necessary for the receiver to have adjustable gain that can properly condition the wide dynamic range of return signals to all fit within the dynamic range of the ADC.

Because some the of antenna elements that are used to transmit the pulse are also used to receive the return signal and the elements that are not used to transmit the pulse experience a large direct path coupling of the transmitted signal, thus the returned signal cannot be measured until the transmit pulse has stopped. The pulse that is measuring the surface return must be shorter in time than the time it takes the transmitted pulse to be reflected off the ice surface and return to the antenna elements. With the MCoRDS/I platform flying at approximately 500 m, the transmitted pulse must be shorter than 3.3 μs to capture the surface

return. The MCoRDS/I system typically uses a 1 μs pulse to capture the surface return as well as shallow internal layers. This 1 μs transmit pulse is also capable of capturing the return from the bedrock, however, there are two factors that make this very difficult. First, due to the very large returned signal power from the ice surface a low and the very small signal power returned from the bedrock the dynamic range of these two returned signals is far greater than the dynamic range of the ADC. This would require the receiver to use a low gain setting to detect the surface return then switch to a higher gain setting during the listen period to detect the bedrock return. While it is possible for the receiver to switch gain settings during the listen period, this technique poses several challenges on both the hardware design of the receivers and the signal processing of the received signal. Second, even if the receiver was able to switch gain settings during the listen period the large amount of attenuation experienced by the transmit pulse when traveling all the way through the ice sheet, reflecting off the bedrock, and back through the ice sheet causes the SNR for the bedrock return to be too low for the ADC to detect even after extensive signal processing. To solve this problem, the MCoRDS/I system transmits more energy on the target and increases the time-bandwidth product of the transmit pulse by using a longer transmitted pulse length.

The MCoRDS/I system employs pulse compression to the received signal which increases the SNR of the processed signal. The SNR increase

is directly proportional to the time bandwidth product of the transmitted pulse. The time-bandwidth product is the duration of the transmitted pulse multiplied by its spectral width. This longer pulse will be blind to the surface return due to the direct coupling of the antennas but will provide a better SNR after signal processing. The MCoRDS/I system typically uses a 10 μs pulse with the same bandwidth as the 1 μs to detect the bedrock returns. Because of the pulse compression the 10 μs pulse effectively has a 10 dB better SNR after pulse compression when compared to the 1 μs pulse which is vital when detecting a very weak reflection from the bedrock.

Along with pulse compression, the MCoRDS/I system also uses presums to further increase the SNR of the processed signal and reduce the data rate that needs to be recorded. Presumming is simply adding together the received signal of several successive pulses and is done before pulse compression. It assumes that the successive pulses are all being reflected by the same target and similar to increasing the pulse duration, there is more energy directed onto the target by multiple pulses than one pulse and thus by adding them together the zero mean thermal noise integrate down as more and more pulses are added together while the returned signal from the target will remain constant and the signal returns will add together coherently. Presumming increases the SNR of the processed signal linearly, thus presumming two signals will increase the SNR of the processed signal by 3 dB, presumming 4 signals will

increase the SNR by 6 dB and so on. An important factor regarding presumming for the MCoRDS/I system is that it assumes the successive pulses are all being reflected by the same target but the MCoRDS/I platform is moving thus each successive pulse is looking at approximately the same target but not exactly. The velocity of the platform dictates how many presums that can be done before the approximation of each pulse being reflected from the same target becomes invalid. Each MCoRDS/I platform has a different nominal cruise speed but the MCoRDS/I system typically can perform 36 total presums. Since the MCoRDS/I system is designed to measure the surface and bedrock of the same target location, these 36 must be split up between the two transmitted pulse lengths, 6 presums for the 1 μs pulse and 30 presums for the 10 μs pulse. The 10 μs pulse gets the majority of the presums because the SNR of the surface return is much larger than the SNR of the bedrock return thus much more sensitivity is required to detect the bedrock return and increasing the presums is an easy way of increasing the processed signal SNR. Figure 2.5 shows the processed signal's dynamic range versus time for both the 1 μs and 10 μs pulses. This time axis accounts for the time that the receiver is blinded during transmit.

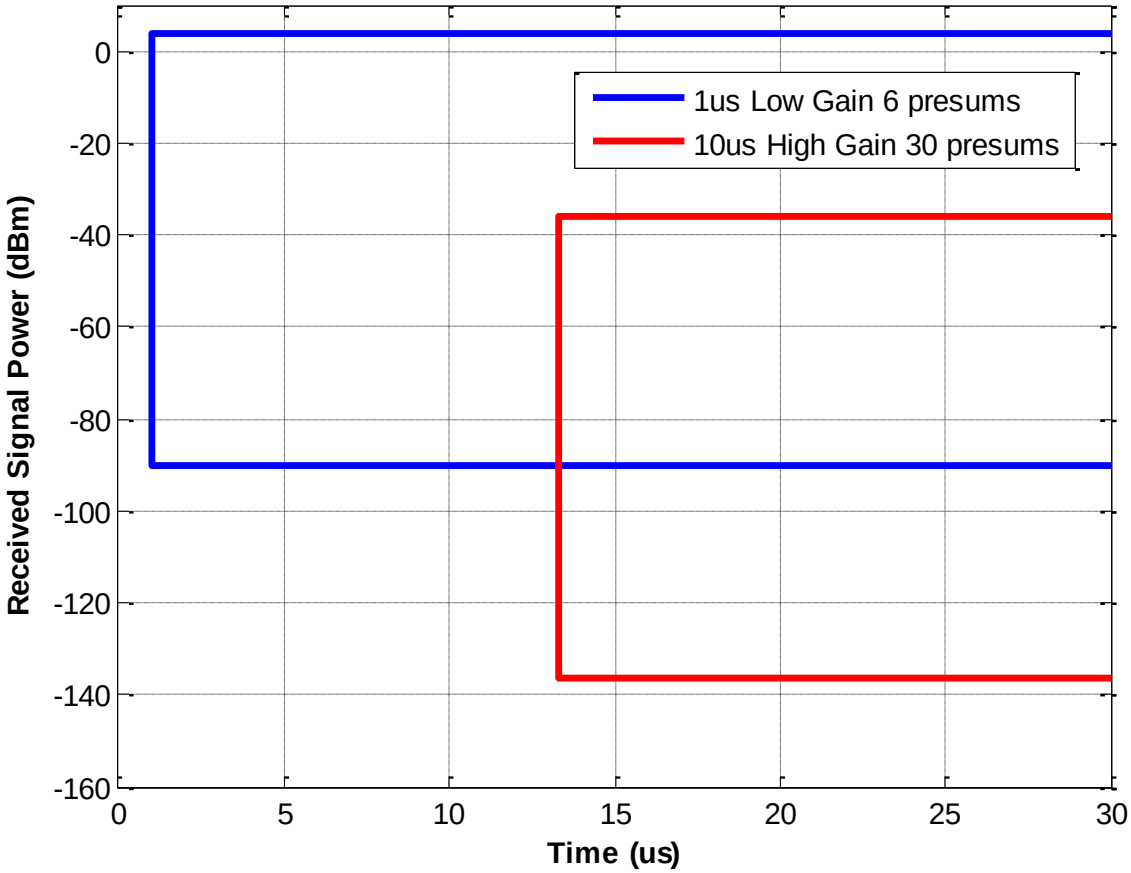


*Figure 2.5 - Processed Signal Dynamic Range for 1 μs and 10 μs pulses*

The typical power profile at the receiver input for an ice sheet target is shown in Figure 2.6. This figure was generated using MCoRDS/I data using a 1 μs pulse with the receivers set to the low gain setting from the Twin Otter platform in Antarctica in 2011. This plot shows the surface return at approximately 4 μs of approximately -14 dBm at the receiver input which is consistent with the link budget calculation in Table 2.1. The received power decreases quickly after the surface return and near the end of the record we can see what appears to be a return from the bedrock.

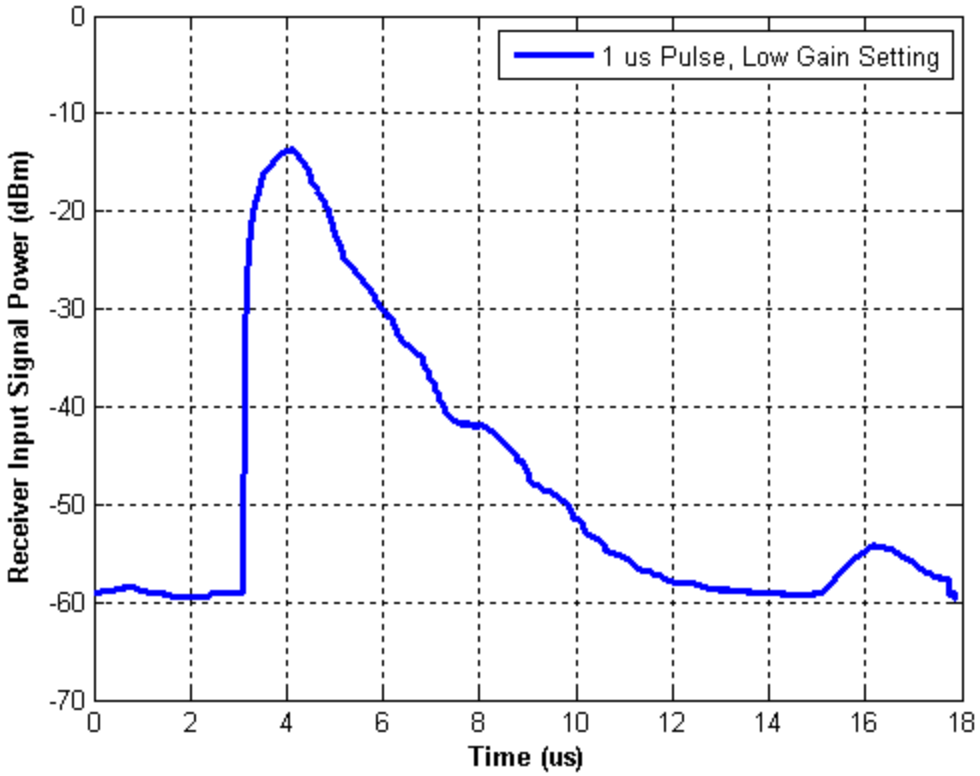


*Figure 2.6 - Typical Receiver Input Power Profile from the Twin Otter Platform using a 1 μs Pulse in the Low Gain Setting*

## *2.3 MCoRDS/I Receiver Requirements*

The receiver module must meet a specific set of design requirements for the MCoRDS/I system to operate properly. This section details these parameters that the receiver module must satisfy.

### *2.3.1 Receiver Bandwidth Requirement*

The bandwidth of the receiver is defined by the bandwidth of the transmit pulse and requires the bandwidth of each component of the receiver to operate optimally across that bandwidth. The current bandwidth of the MCoRDS/I transmit pulse extends from 180 MHz to 210 MHz. Due to the under sampling technique utilized by the MCoRDS/I ADC, the bandwidth of the receiver should be as tightly constrained to this bandwidth as possible. This is typically done by using an anti-aliasing bandpass filter at the end of the receiver channel that constricts the receiver response to the desired bandwidth and an attenuation of 50 dB or greater to signals in adjacent Nyquist zones to prevent a signal from aliasing into the MCoRDS/I frequency space. The sampling rate of the MCoRDS/I system is currently 111.11 MHz which places the transmitted signal in the fourth Nyquist zone which extends from 166.67 MHz to 222.22 MHz. The MCoRDS/I signal is approximately 13 MHz above the low boundary of the Nyquist zone and 12 MHz below the high boundary thus for a signal to alias into the MCoRDS/I frequency space it must be at least 13 MHz below the lower Nyquist zone boundary or 12 MHz above the higher boundary. This shows us that the anti-aliasing filter must attenuate signals at 153.3 MHz or lower and 234.4 MHz or higher by at least 50 dB. There is also a possibility that in future MCoRDS/I development the bandwidth of the transmit pulse could be extended to gain better resolution thus it is desirable for all components

except the anti-aliasing filter be as wideband as possible allowing for adjustments in the bandwidth of the transmit pulse be simply replacing the anti-aliasing filter with one that provides the receiver with the proper frequency response.

### *2.3.2 Receiver Gain Requirements*

It was shown earlier in section 2.2.4 that it is necessary for the gain of the receiver to be adjustable based on the desired target of the transmit pulse. To set the requirement for the minimum gain of the receiver, the receiver must amplify the maximum received signal up to the maximum input power of the ADC which in section 2.2.2 is shown to be 10 dBm. In table 1 it is shown that for the 1000 W per channel P-3 platform the maximum received signal power is 0.1 dBm thus the minimum gain of the receiver must be less than 10 dB. Due to unexpected variations in the target or platform altitude it is desirable for the receiver to be adjustable to a lower gain than the theoretical case shows, so the minimum gain requirement is set at 4 dB.

The maximum gain of the receiver is used to amplify the very small signal returns, like those from the bed rock of an ice sheet, up the dynamic range of the ADC so they can be accurately sampled. As the signal power gets amplified by the receiver, the thermal noise power increases by a larger amount than the signal gain alone typically due to

the noise generated by the amplifying components. This increase in signal to noise ratio (SNR) from input of the receiver to output of the receiver is unavoidable and the ratio of SNR at the output of the receiver to SNR at the input of the receiver is called noise figure. When setting the maximum gain of the receiver, it is important to understand that the thermal noise present at the output of the receiver will add to the quantization noise presented by the ADC to arrive at the total noise power of the received signal and thus the SNR of the received signal. Due to this addition of noise sources, the maximum gain of the receiver also sets the dynamic range of the received signal. There is a tradeoff that must be made between the SNR and dynamic range of the received signal. If the receiver gain is set such that the thermal noise at the output of the receiver is exactly equal to the quantization noise of the ADC the received signal will have a maximum dynamic range which is equal to the dynamic range of the ADC but the SNR at the output will be decreased by 3 dB due to the addition of the quantization noise and thermal noise of equal power. This case gives the maximum possible dynamic range but poor SNR for the received signal. As the receiver gain is increased so the thermal noise at the output of the receiver is much larger than the quantization noise the SNR of the received signal will effectively only be impacted by the noise figure of the receiver but the dynamic range will decrease by the difference of thermal noise power to quantization noise power (both expressed on a dB scale). In this application, the signals

that are being detected in the maximum gain mode are very small and have a very low SNR thus when examining this tradeoff the impact to the SNR is much more important than having the largest possible dynamic range. A common rule of thumb states that receiver should have enough gain so that the thermal noise at the output of the receiver was at least 10 dB larger than the quantization noise of the ADC which provides a 10 dB decrease in dynamic range but only degrades the SNR by 0.4 dB.

It was discussed earlier in section 2.2.2 that the quantization noise power of the ADC is -62 dBm thus the receiver must have enough gain so that the thermal noise at the output of the receiver is at least -52 dBm (6.31 μW). To calculate the gain required to fulfill this requirement it is first necessary to calculate the thermal noise at the input to the receiver as well as estimate the receiver's noise figure. Equation 2.3 gives the expression of the thermal noise power in terms of the noise temperature T, bandwidth of the noise B, and the Boltzmann constant k. To calculate the thermal noise power at the input of the receiver we will assume that the components of the receiver will be approximately at a room temperature of 290K (62°F) and the bandwidth BW of the noise power is the same as the bandwidth of the receiver, 30 MHz. Using these approximations the thermal noise at the input of the receiver is calculated to be .12 pW (-99.2 dBm).

$$P_n^{in} = kTB \tag{2.3}$$

Once the noise at the input of the receiver is known, Equation 2.4 gives the expression for the noise at the output of the receiver $P_n^{out}$ in terms of the thermal noise power at the input $P_n^{in}$, the gain of the receiver G, and the noise figure of the receiver F. For this approximation it can be assumed that the receiver will have a noise figure of approximately 2 dB. Since the all the terms of Equation 2.4 are known, we can rearrange it in Equation 2.5 to solve for the required gain of the receiver that causes the output noise power to be 10 dB larger than the quantization noise power of the ADC. By solving Equation 2.5 it is shown that the receiver must have at least 45.2 dB for the output noise power to be at least 10 dB larger than the quantization noise power of the ADC.

$$P_n^{out} = GFP_n^{in} \tag{2.4}$$

$$G = \frac{P_n^{out}}{FP_n^{in}} \tag{2.5}$$

$$G = \frac{6.31\mu W}{1.585 * 0.12pW}$$

$$G = 33{,}175 \; or \; 45.2 \; dB$$

### *2.3.3 Receiver Compression Point Requirement*

Typically amplifiers and receivers are defined by the output power at which 1 dB of compression occurs, however, in this case it is the input power at the compression point that is the important parameter. From Table 2.1 it is known that the maximum received signal power at the input to the receiver under normal operation is 0.1 dBm thus the receiver should linearly amplify signals up to that input power level. It should also be noted that at the 1 dB compression point the signal is already being amplified in a non-linear fashion thus to ensure that the MCoRDS/I receiver module remains linear for the largest expected signal power at the input it will be required that the input power at the 1 dB compression point of the receiver be at least 3 dB greater than the largest expected signal power at the input. This gives the requirement that the receiver cannot reach its 1 dB compression point at an input power of less than 3.1 dBm as discussed in Section 2.3.2.

### *2.3.4 Receiver Noise Figure Requirement*

The noise figure of a receiver is an important parameter that defines its relative noise performance. Noise figure defines the degradation of SNR from the input of the receiver to the output of the receiver assuming that the noise power present at the input to the receiver is equivalent to a thermal noise source at 290K. The sensitivity

of the receiver is very important due to the very small received signal power and thus very low SNR expected from typical bed rock returns of the ice sheet target. It is very desirable for the noise figure to be as low as possible but there are many engineering tradeoffs that occur when designing a receiver and thus a specific maximum noise figure requirement is needed. To obtain a noise figure comparable with previous versions of the MCoRDS/I receivers, the receiver noise figure must be 2 dB or less.

### *2.3.5 Receiver Channel Isolation Requirement*

To make the receiver module as compact as possible, it would be advantageous for a single printed circuit board (PCB) to contain more than one receiver channel. While this does make the receiver more compact, as always there are tradeoffs. Multiple channel receiver boards are susceptible to crosstalk between channels on the board. This crosstalk is a signal from one channel that couples onto an adjacent channel. The unwanted signal on the channel degrades performance of the receiver and can be thought of as noise. Channel to channel isolation is a measurement of that crosstalk between channels and can be calculated in many different ways. For this application each receiver will have a similar input power at a given point in time due to the size of the antenna array and the altitude of the platform. This simplifies the

channel to channel isolation requirement since there will not be a large received signal power and a small received signal power present in the receiver at the same time. The channel to channel isolation is measured as the ratio of the power of the unwanted channel's signal in the desired channel to the power of the desired channel's signal.

The channel to channel isolation of the receivers must be greater than the lowest channel to channel isolation in the MCoRDS/I system to ensure that the receivers are not lowering the total channel to channel isolation for the system. The antenna elements had the lowest channel to channel isolation of any component in the system at approximately 30 dB and thus the receivers must have greater than 30 dB of channel to channel isolation.

### *2.3.6 Receiver Robustness*

While there are expected operating parameters for the MCoRDS/I system, the targets are extremely unpredictable and the altitude of the airborne platforms can vary greatly during flight. Each day the system typically surveys the polar ice sheets for eight consecutive hours a day for several months and every second of the data that is collected is both scientifically significant and costly to obtain. It is very important that the MCoRDS/I system operates optimally for the entire field mission. Due to the very unpredictable target and platform altitude present while

MCoRDS/I is operating and the importance of the data is obtains it is crucial that the receiver module design is very robust and will not fail under the possible stresses that could be present during a field mission. The major concern for receiver failure during a field mission is a component failure due to a large RF input power. While under normal operating conditions, Table 1 shows that the largest expected input power is around 0 dBm, there can be large variations to that input power based in altitude of the platform and the surface of the target. To ensure that there will be no damage to the receiver components, it will be a requirement that the receiver can withstand 1 W of input power without damaging any of the components. Temperature is also a concern with the extreme temperature environments that the system will be operating in thus the receiver will be required to operate from -40 °C to 85 °C.

### *2.3.7 Receiver Interface Requirements*

The receiver is being designed, in part, to make the MCoRDS/I system more compact. To accomplish this goal, four receiver channels will be placed on a single PCB which should fully interface with the NI PXI chassis. The NI PXI chassis has “slots” where removable PCB cards can plug into the backplane of the chassis and be powered and controlled. A single receiver module will consist of four separate channels with SMA input and output connectors for each receiver channel, backplane

connectors to receive power and digital control signals from the backplane, a faceplate to secure the module into the chassis and provide an electromagnetic barrier, and a digital system to decode the control signals coming from the PXI controller over the backplane and properly set the gain of each receiver channel. A PXI module should be approximately 6.3" in length, 3.96" in height, and less than 0.7" in height.

### *2.3.8 Receiver Requirements Summary*

Table 2.2 below gives a summary of the MCoRDS/I receiver RF requirements described in the previous sections.

| Requirement | Min | Max |
|---|---|---|
| 1 dB Bandwidth | 180 MHz | 210 MHz |
| Out of Band Attenuation | 50 dB | |
| Gain | 4 dB | 46 dB |
| Input 1 dB Compression Point | 3.1 dBm | |
| Noise figure | | 2 dB |
| Channel to Channel Isolation | 30 dB | |
| No Damage Input level | 30 dBm | |

*Table 2.2 – Summary of MCoRDS/I Receiver RF Requirements*

# Chapter 3

## *Receiver Design*

### *3.1 Analysis of Receiver Topologies*

The first step in the design of the receiver is deciding on a topology. To build a receiver topology for the MCoRDS/I receiver there are several components that are required in any configuration to ensure proper operation. To achieve the required sensitivity, a low noise amplifier (LNA) is typically one of the first components in any receiver topology. The LNA is an extremely important component and in this case, if the receiver is designed properly it will set the noise figure as well as compression point of the receiver. The MCoRDS/I system uses a bandpass sampling technique thus there is no frequency conversion necessary in the receiver. The bandpass sampling technique does require an anti-aliasing bandpass filter to be utilized near the end of the receiver channel to attenuate any signals that exist outside the desired Nyquist zone that is being sampled. As discussed in Section 2.2.3, the video feed through of the T/R switching module requires a low pass filter to attenuate the large transient that is produced by the switch and keep it from saturating the receiver channel. Beyond the LNA, low pass video feed through filter and anti-aliasing filter, the rest of the receiver topology will be responsible for achieving the adjustable receiver gain requirement of the MCoRDS/I system. Figure 3.1 shows a simplified

version of the receiver topology required by the MCoRDS/I system. There are two distinct approaches to accomplish the adjustable gain requirement, a switched multiple RF path topology and a single RF path topology. These topologies will be discussed in the remainder of this section. Throughout the rest of the document, the terminology of "low gain setting" will refer to 4 dB of total receiver gain and "high gain setting" will refer to 46 dB of total receiver gain.

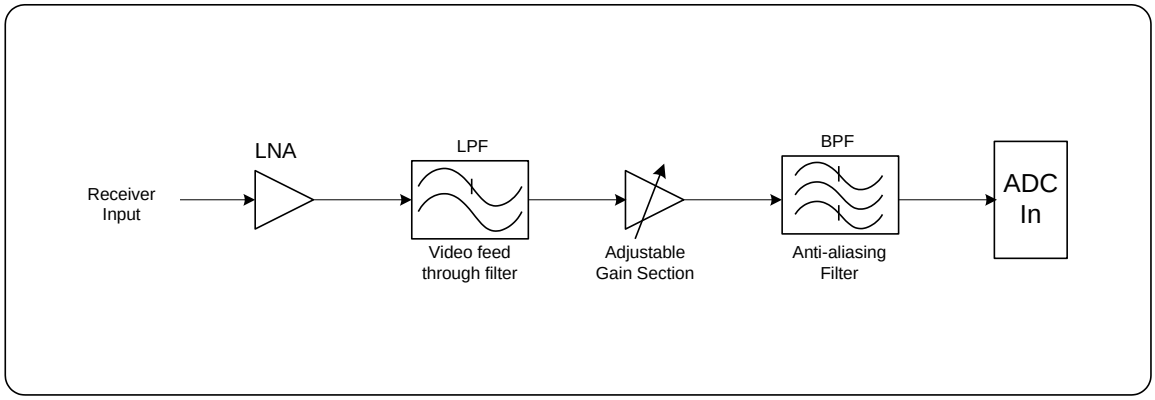


*Figure 3.1 - Simple MCoRDS/I Receiver Topology*

### *3.1.1 Switched Dual RF Path Topology*

The first topology that was considered for the receiver design was a switched dual RF path topology. This topology has two separate RF paths for the signal based on the desired amount of receiver gain. Figure 3.2 is a simple block diagram for the dual switched RF path topology.

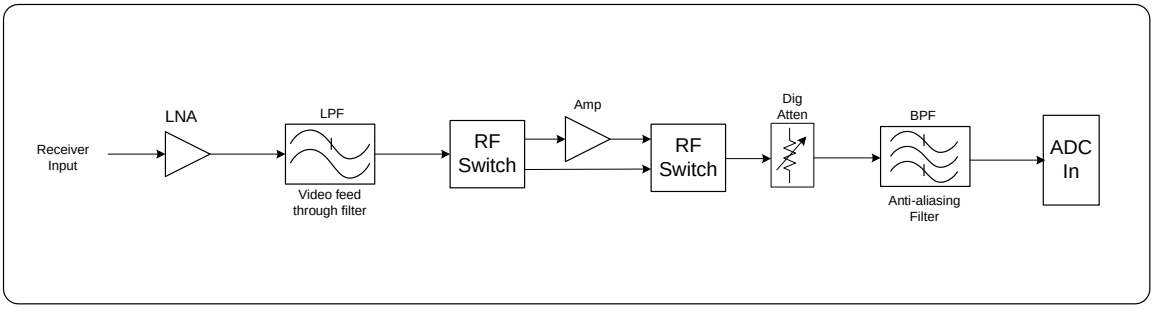


*Figure 3.2 - Simple Block Diagram for the Dual Switched RF Path Topology*

There are two main objectives achieved with this topology. The first is to allow the receiver to switch gain settings very quickly during the listen period so the surface return could be captured by the low gain setting and once the surface return is completed the receiver can switch to the high gain setting to have more sensitivity to capture small returns of the same pulse from internal layers and the bedrock return. The second motivation to use this topology is to provide good noise figure performance for the low gain setting. Figure 3.3 below shows the processed signal dynamic range for the switched dual RF path receiver topology assuming a noise figure of 2 dB for both the low and high gain settings and that the receiver switches gain settings from low to high right after the surface reflection is received.

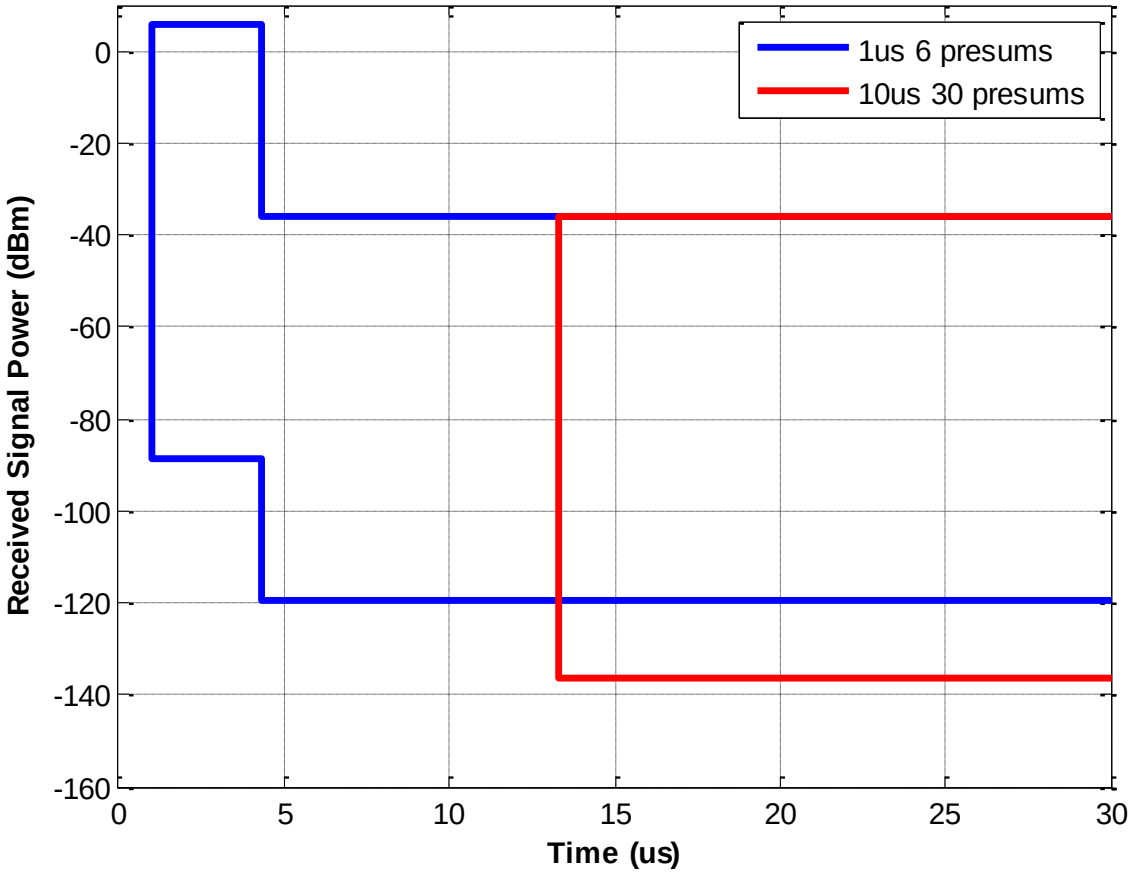


*Figure 3.3 - Processed Dynamic Range for Switched Gain Topology*

As mentioned above, the switched RF path topology has an advantage over a single RF path topology in two areas. It has a better noise figure in the low gain setting which makes it more sensitive to smaller returned signals in the low gain setting. It also is capable of switching gain settings while the signal returns are being received which makes it more sensitive to returns from the 1 µs pulse after the surface return. Figure 3.4 compares the processed signal dynamic range for the switched gain topology with the previous MCoRDS/I receiver processed signal dynamic range for the 1 µs pulse.

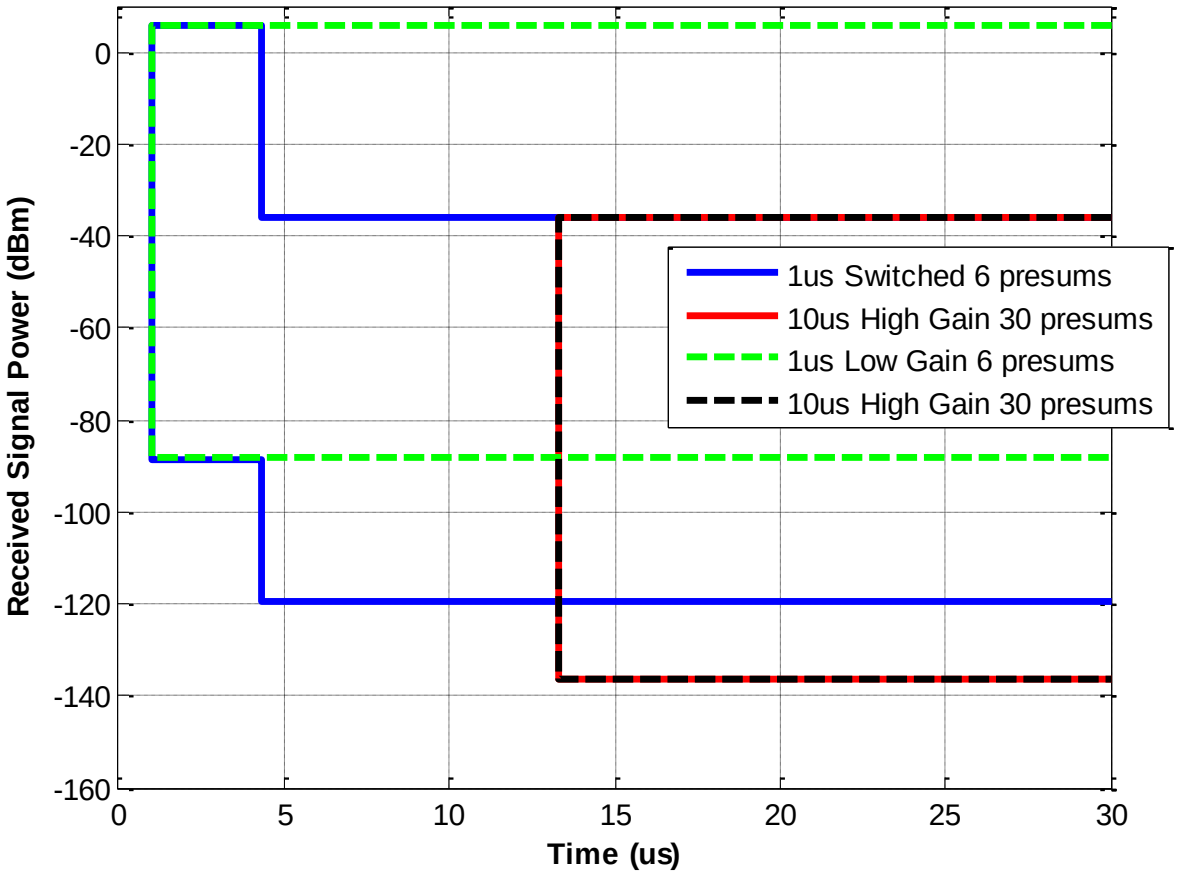


*Figure 3.4 - Processed Dynamic Range Comparison of Switched Gain Topology and Previous MCoRDS/I receiver*

When examining Figure 3.4 several important conclusions can be drawn. First, we can see that both the switched gain topology and the previous MCoRDS/I receiver use the high gain setting and have the same noise performance for the 10 µs pulse thus they have the same processed signal dynamic range. The differences of the switched RF path topology come when receiving the 1 µs pulse. When examining the low gain setting of both, you can see that the lower noise figure of the switched RF path receiver gives only a very slight improvement in sensitivity of about 0.2 dB. This occurs because the total received noise power is composed

of the sum of the thermal noise at the output of the receiver and the quantization noise of the ADC. As can be seen from Equation 2.4, the output thermal noise power is directly proportional to gain and in the low gain setting the thermal noise at the output of the receiver is much smaller than the quantization noise power of the ADC thus the total received noise power is dominated by the quantization noise power of the ADC. Even a large decrease in noise figure of the low gain setting, which was one of the goals of the switched path RF topology, has very little effect on the total received noise power and thus very little increased sensitivity. The main advantage of the switched gain topology occurs just after the switching event. As can be observed from Figure 3.4, the current MCoRDS/I receiver remains in the low gain setting while the switched RF path receiver switches to the high gain setting after the large surface return has been received. This allows the receiver to be more sensitive to the small signal returns from the shallow internal layers of the ice sheet that the 10 μs pulse cannot detect due to its inability to receive during transmit.

There are also several difficulties using the switched RF path topology. The biggest challenge arises from controlling the switching event. Ideally the switching event would occur just after the large surface return when the returned power falls below the saturation point of the high gain setting. Due to the dynamic nature of the MCoRDS/I airborne platforms the altitude of the platform is not constant and can

vary by several hundred meters. This variation in altitude causes the surface return to be received at different times in the listening period and thus the switching event could not be statically set to a certain time but must be dynamically changed based on the altitude and the received power profile. Along with the switching event tracking the surface, the switching event should also be moved slightly in time from pulse to pulse. During the switching event there will be a discontinuity during which the data will be corrupted and if it occurs at exactly the same time after the surface return there will be a certain depth inside the ice sheet that may not be recorded properly. Changing the time that elapses after the surface return for each pulse would allow the entire return to be recorded with a slight degradation in the SNR in the region in which the switching events occurred. This can all be achieved with the NI controller but adds significant complexity to the radar system control programming. Another difficulty of the switched RF path topology is the complexity it adds to the calibration and signal processing of the system. When completing the signal processing steps it is important to know the exact channel response of the receiver so the signal processing techniques can compensate for it. With two different RF paths and thus two different channel responses, the signal processing would need to use two different responses when processing a return where both the low gain setting and high gain setting were used in the same record which makes it more complex and time consuming.

### *3.1.2 Single RF Path Topology*

Due to the complexities that the switched RF path topology introduced for marginal performance improvements a single RF path topology was also considered. Figure 3.5 is a simple block diagram for the single RF path topology.

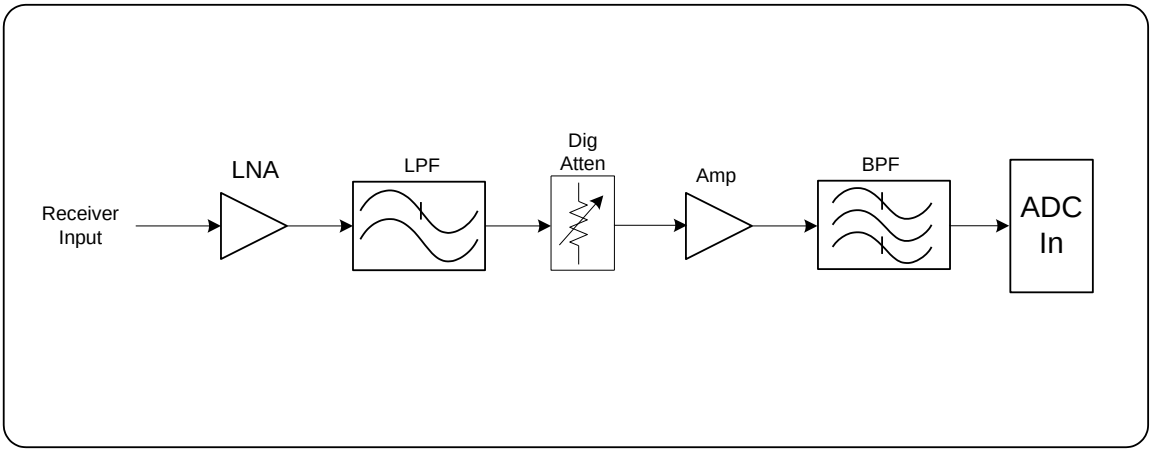


*Figure 3.5 - Simple Block Diagram for the Single RF Path Topology*

The two main differences between the switched RF path topology and the single RF path topology is a higher noise figure in the low gain setting and the inability to change gain settings during the listen period. It was described in the previous section that the total noise power in the low gain setting is dominated by the quantization noise and thus the noise figure in the low gain setting is inconsequential. The main performance difference lies in the inability to switch gain setting during the listen period. It was previously described that the switching of the gain setting from low to high during the listen period of the 1 μs pulse

allowed the receiver to be more sensitive to the small signal returns from the shallow internal layers of the ice sheet that the 10 μs pulse cannot detect due to its inability to receive during transmit. To solve this problem with the single RF path topology a third transmit pulse can be utilized which is intended to be sensitive to these small signal returns from the shallow internal layers. If a medium length pulse (between 2 μs and 6 μs) is used with the receiver in the high gain setting it is possible to capture the reflections from the internal layers with the required sensitivity. The tradeoff that adding another transmit pulse length introduces comes with the limited number of presums that can be performed as described in Section 2.2.4. The total number of presums must remain constant thus the additional pulse must be used in place of some of the 1 μs or 10 μs pulses. Because of the very small SNR of the bedrock returns and the very large SNR of the surface return it would most beneficial to keep the number of presums the same for the 10 μs pulse and use a few the presums for the medium length pulse. This will slightly decrease the sensitivity of the 1 μs pulse but the additional pulse will increase the sensitivity to the shallow internal layer reflections. Figure 3.6 shows the comparison of the processed signal dynamic range for the switched RF path topology versus the single RF path topology with a 1 μs pulse with 4 presums, a 3 μs pulse with 2 presums and a 10 μs pulse with 30 presums.

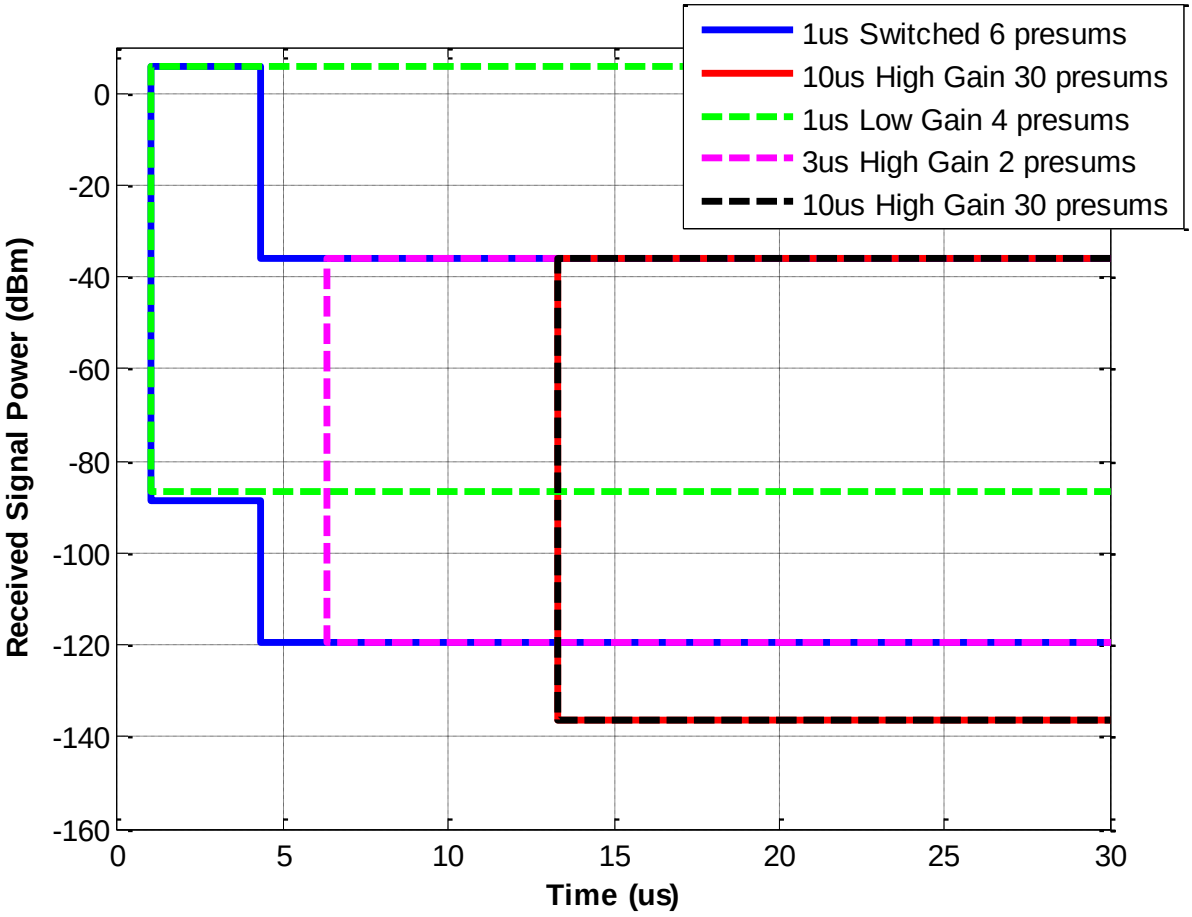


*Figure 3.6 - Processed Signal Dynamic Range Comparison of Switched RF Path Topology and Single RF Path Topology with 1 µs 3 µs and 10 µs pulses*

As can be seen from Figure 3.6 the processed signal dynamic range for the single RF path with the addition of a medium length pulse is very similar to the switched RF path topology. The sensitivity to the 10 µs pulse remains the same and the 3 µs pulse has the same sensitivity as the 1 µs pulse of the switched RF path topology. In the low gain setting, the switched RF path has approximately 2 dB better sensitivity due to lowering the number of presums from 6 to 4. Because the surface reflection has a very high SNR the sensitivity in the low gain setting is

typically not critical thus the 2 dB decrease is very likely to be insignificant. The only other difference in the dynamic range comes just after the surface return has been received and the switching event occurs in the switched RF path topology but if this region is deemed to be important and more sensitivity is required the medium length pulse can be shortened from 3 μs to capture this region.

The single RF path topology has a very similar performance to the switched RF path topology while being much simpler to implement. It has fewer components, is simpler for the radar system controller to control, and simpler to process the recorded data thus the single RF path topology was chosen for the MCoRDS/I receiver design.

## *3.2 Analysis of Receiver Components*

After the topology of the receiver has been decided, a large component search must be done to locate the components with the parameters that allow all the receiver design requirements to be met. This is an intricate process as there are many requirements to simultaneously consider and changing one component can have an effect on other components in the receiver chain and multiple receiver requirements. All S parameter measurements taken in this section were done with an Agilent N5230C network analyzer. The passive components were measured with an output power of 0 dBm while the amplifiers were measured with on output power of -20 dBm. Figure 3.7 shows the component level block diagram for the RF section of the MCoRDS/I receiver channel. Due to the compact nature of the receiver module it is desirable for all the components to be small in physical size, and operate at a low current from the same DC power supply voltage to minimize the size and number of DC power components required on the module.

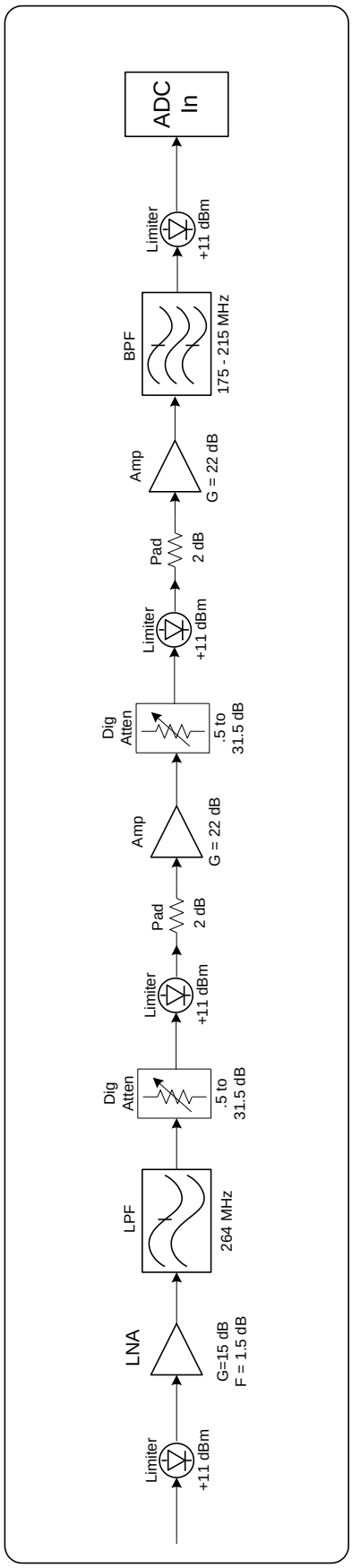


*Figure 3.7 - Block Diagram MCoRDS/I Receiver RF Channel*

### *3.2.1 RFHIC WL2208-L Low Noise Amplifier*

One of the most important components in the RF chain is the LNA. If the receiver is designed properly, the LNA effectively sets the noise figure and compression point of the receiver. The RFHIC WL2208-L LNA was chosen for its low noise figure and high compression point. It is Gallium Arsenide (GaAs) amplifier in a small surface mount package that operates using a 5 V DC power supply. Figures 3.8 and 3.9 provide the measured S parameters of the WL2208-L. When examining these S parameter plots it is shown the WL2208-L has a gain (|S21|) of 15.6 dB, input return loss (|-S11|) of 21.5 dB, output return loss (|-S22|) of 7.5 dB and reverse isolation (|-S12|) of 24.5 dB. It is desirable for the input and output return loss of a component to be greater than 10 dB within the bandwidth of the system. To increase the output return loss of the LNA, an output matching network was designed, simulated, and tested using Agilent's Advanced Design System (ADS). The matching network consists of the Minicircuits ADT1.5-1+ transformer, a 56 pF series capacitor, and a 6.8 pF shunt capacitor.

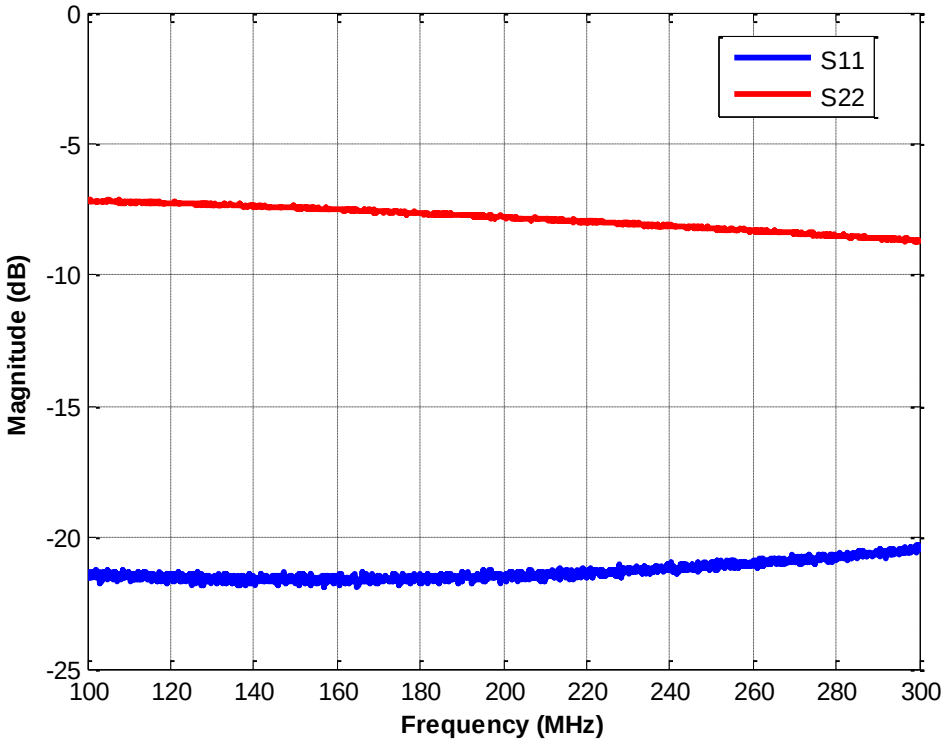


*Figure 3.8 - Measured S11 and S22 of RFHIC WL2208-L Low Noise Amplifier*

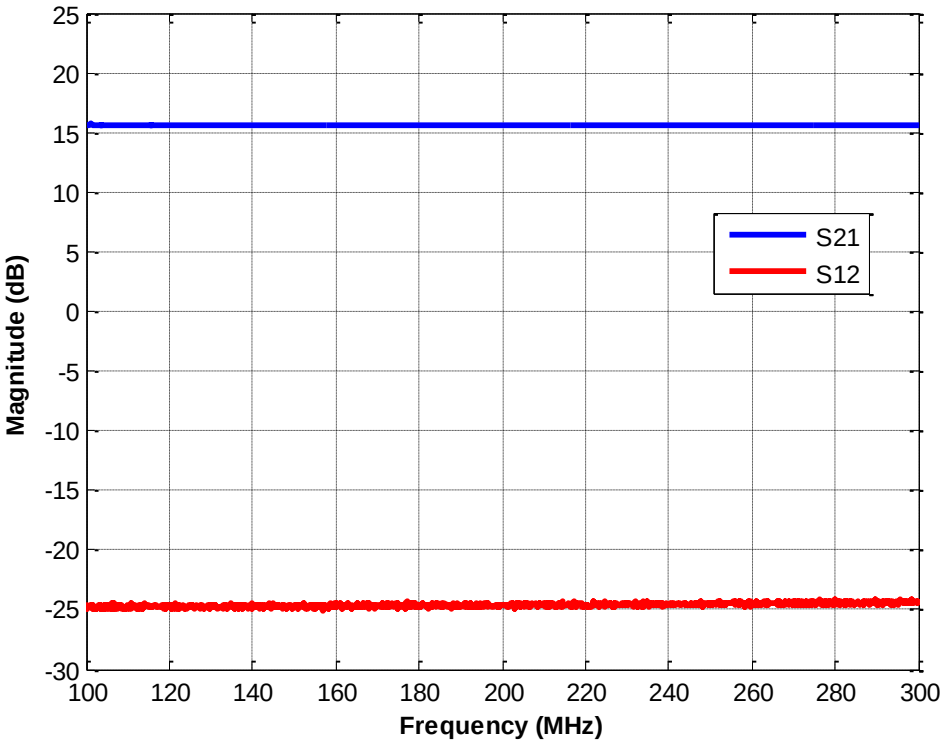


*Figure 3.9 - Measured S21 and S12 of RFHIC WL2208-L Low Noise Amplifier*

Figures 3.10 and 3.11 compare the S parameters of the LNA with the external output matching network connected and the LNA without the matching network. From the plots we can see that in the MCoRDS/I system bandwidth of 180 MHz - 210 MHz the output return loss is increased from 7.5 dB to approximately 16 dB. The input return loss and reverse isolation also increases for the output matched LNA. The tradeoff comes in the gain of the LNA which decreases 0.9 dB from 15.6 dB to 14.7 dB. It is typically desirable for the LNA to have a large gain which improves the noise performance of the receiver chain. In this case, less than 1 dB reduction in gain does not significantly impact the noise figure of the receiver chain.

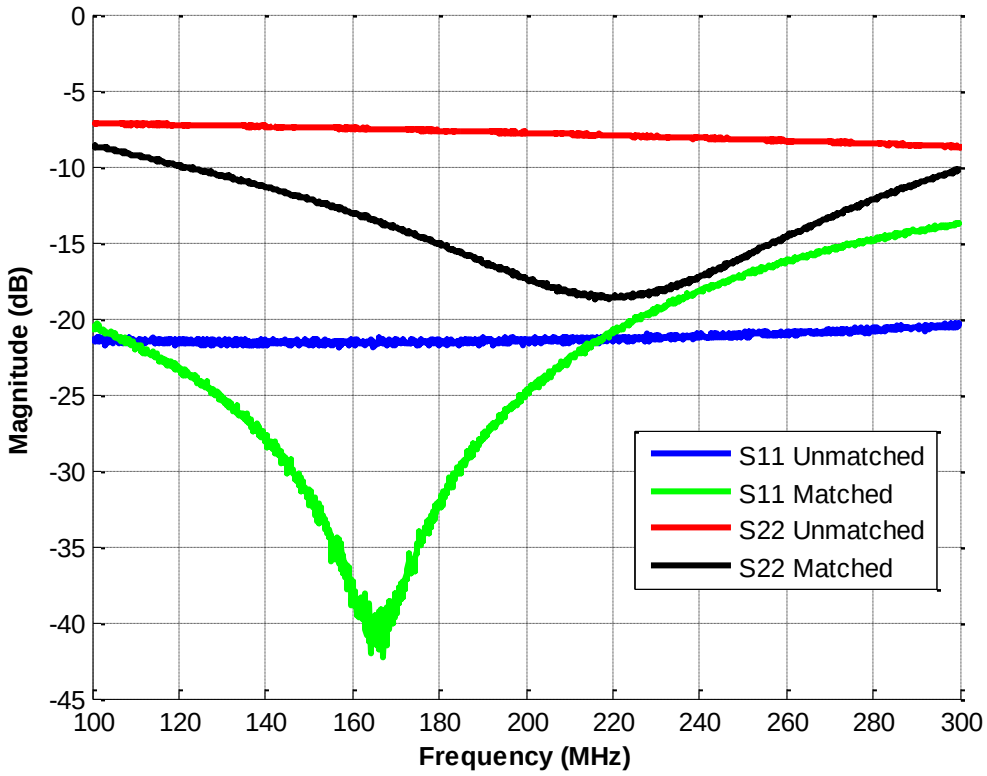


*Figure 3.10 - Comparison of S11 and S22 of the RFHIC WL2208-L Low Noise Amplifier With and Without the External Matching Network*

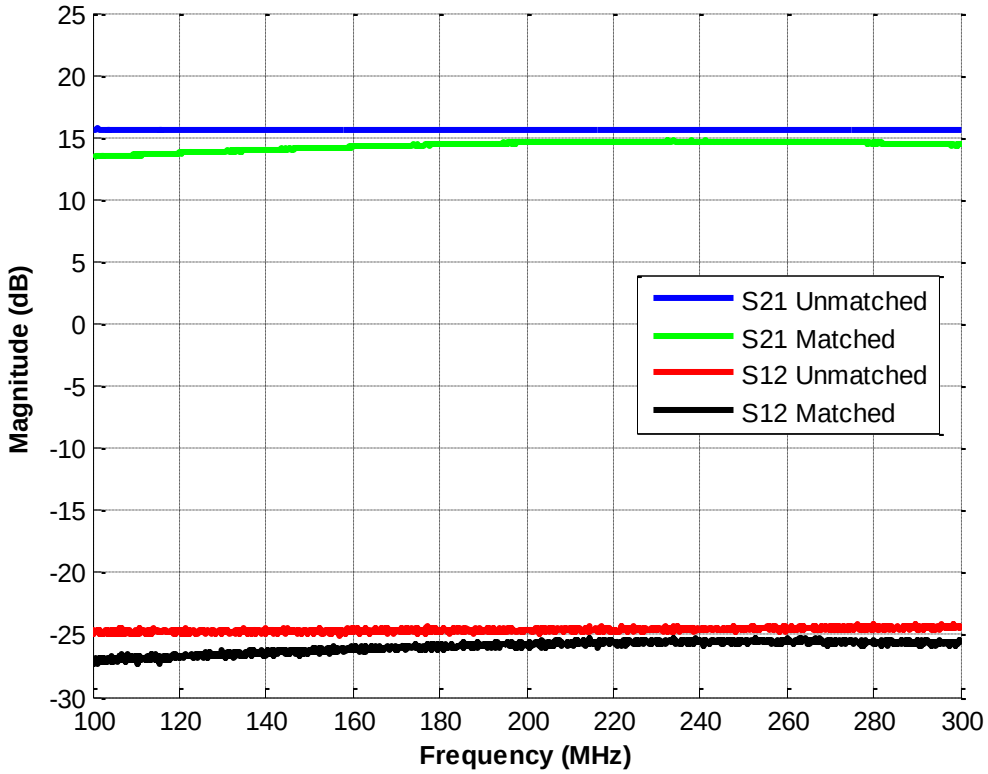


*Figure 3.11 - Comparison of S21 and S12 of the RFHIC WL2208-L Low Noise Amplifier With and Without the External Matching Network*

The 1 dB compression point of the LNA will be designed to set the compression point of the receiver channel in the low gain setting thus it is important to measure the compression point and the effect of the output matching on the compression point. As was discussed in Section 2.3.3, the receiver channel must not reach its 1 dB compression point at input powers below 3.1 dBm. To measure the compression point, an Agilent 8648D signal generator and an Agilent E4446A spectrum analyzer were used. The setup was calibrated by performing a through measurement for each of the input power settings then the LNA was inserted into the setup. Figure 3.12 is a plot of the variation in the gain

of the LNA with respect to input power for the RFHIC WL2208-L both with and without the output matching network. This plot shows that the input power at the 1 dB compression point is approximately 5 dBm which meets the design requirement and the matching network has only a very small affect on the input power at the 1 dB compression point. It is also shown that the LNA is still linear at the maximum expected input power of 0.1 dBm given by Table 2.1.

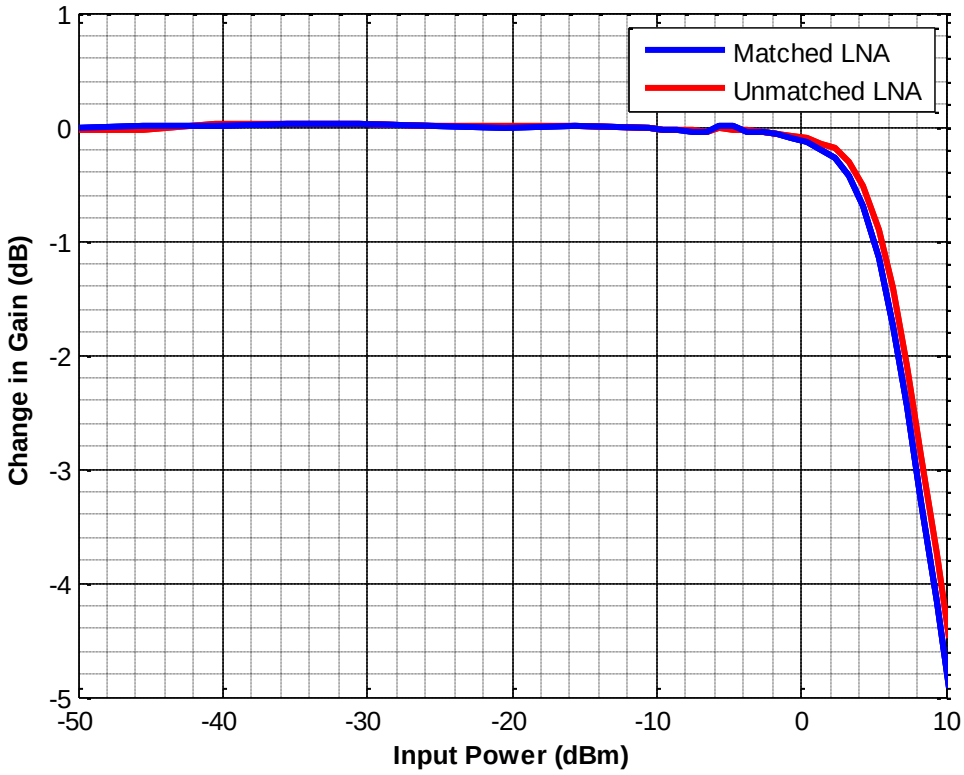


*Figure 3.12 - Measured Power Compression of the RFHIC WL2208-L Low Noise Amplifier With and Without the External Matching Network*

The LNA is the main component that contributes to the receiver's noise performance in the high gain setting thus it is important to measure the noise figure and make certain that the noise performance was not changed by the output matching network. To measure the noise figure of the LNA both with and without the output matching network, the noise figure was measured by the HP 8970B noise figure meter. Figure 3.13 plots the noise figure versus frequency of the LNA both with and without the output matching network. This figure confirms that the noise figure of the LNA is very close to the manufacturer's specification of 1.5 dB and that the output matching network slightly decreased the noise figure of the LNA by about 0.05 dB.

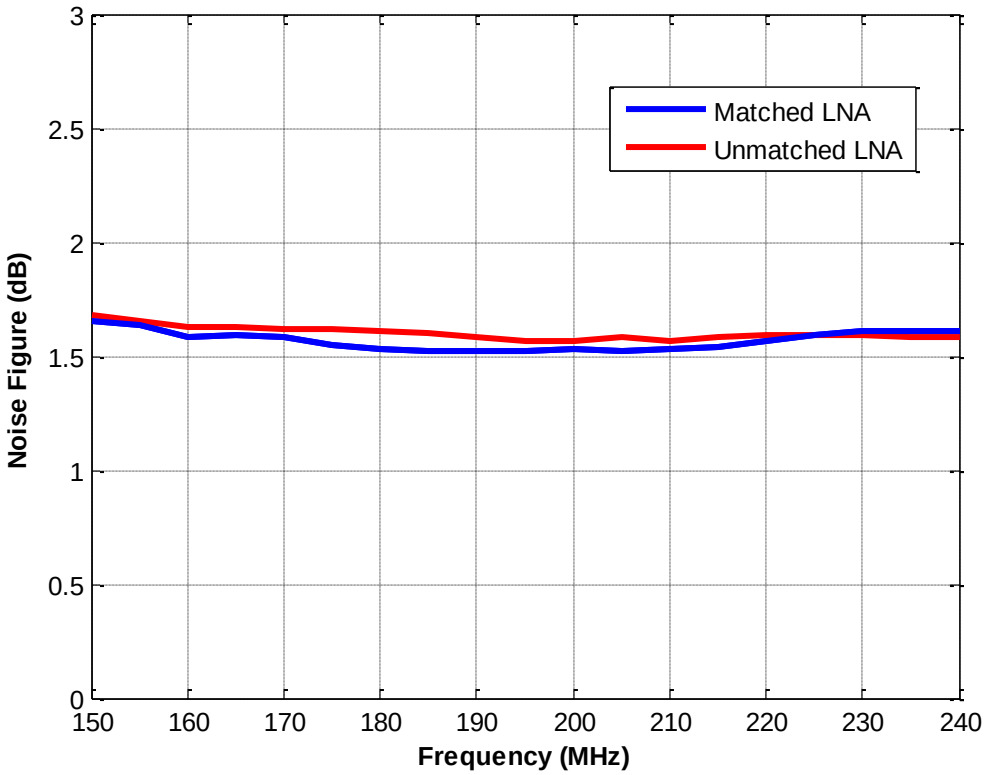


*Figure 3.13 - Measured Noise Figure Characteristics of the RFHIC WL2208-L Low Noise Amplifier With and Without the External Matching Network*

### *3.2.2 Hittite HMC624LP4E Digital Attenuator*

To accomplish the adjustable gain requirement of the receiver design, two Hittite HMC624LP4E digital attenuators were utilized. The HMC624LP4E is a broadband Gallium Arsenide (GaAs) device with attenuation settings in 0.5 dB steps from 0 dB to 31.5 dB. It can be can be controlled by either 3.3 V CMOS or 5 V TTL logic with either a parallel 6 bit word or a three wire serial input. It was chosen for several reasons. First the 0.5 dB attenuation steps allow for very fine gain control and allows the variations in the gain from channel to channel to be compensated for so all the channels can be set to within 0.5 dB of the same gain setting. The HMC624LP4E also has a 0.1 dB compression point of 27 dBm, 31.5 dB in dynamic range of attenuation settings, flexible programming controls, and can operate from a 3.3 V or 5 V DC power supply. Using the serial programming mode, the attenuation setting can be changed every 630 ns and the attenuator has a switching speed of 100 ns. To program the digital attenuators, the load enable line must be driven low and the 6 bit attenuation setting on the data line is clocked in most significant bit to least significant on the rising edge of the clock line. Once the 6 bits of data have been input the buffer holding the data is transferred to the attenuator switches on the rising edge of the load enable line and the attenuator is programmed. Figure 3.14 plots the measured S parameters for the HMC624LP4E with the attenuation set at 0 dB. It shows a return loss of -20 dB and an insertion loss of 1.2 dB.

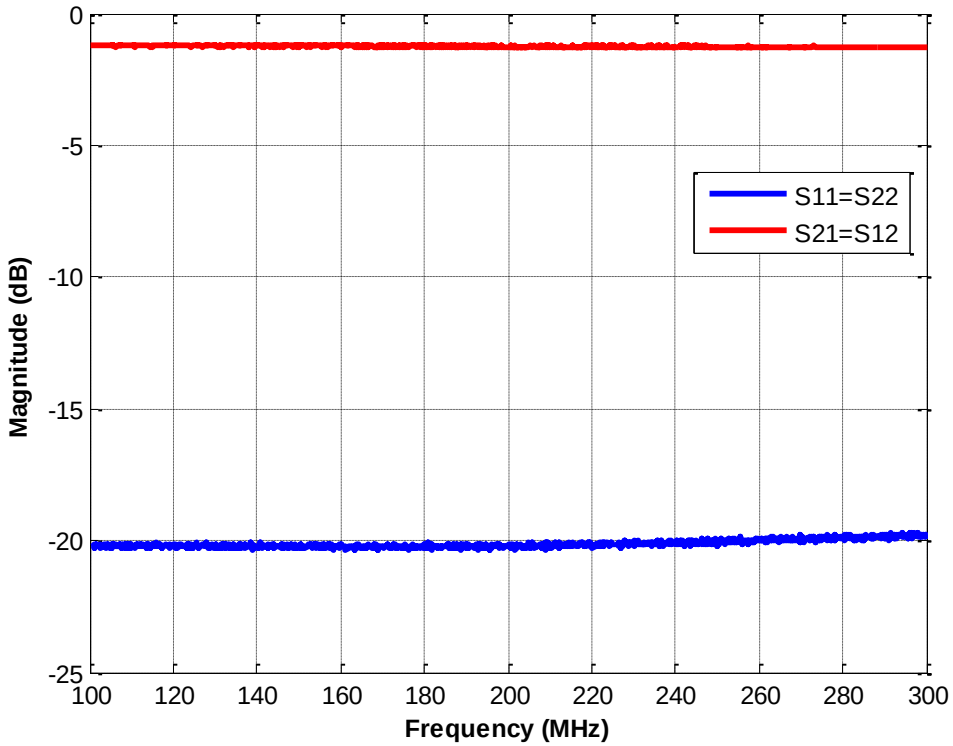


*Figure 3.14 - Measured S Parameter Data of the Hittite HMC624LP4E at 0 dB Attenuation*

### *3.2.3 Hittite HMC580STE Gain Block*

The Hittite HMC580STE amplifier was utilized in the gain stages of the receiver. It is a cascadable gain block that has a high compression point of 22 dBm, a stable gain over temperature variations, has a low number of required external bias components, and can operate from a 5 V DC power supply. Figures 3.15 and 3.16 plot the measured S parameter data for the HMC580STE. The plots show the amplifier has an input return loss of 21 dB, an output return loss of 12.5 dB, a gain of 22.7 dB and a reverse isolation of 26.58 dB.

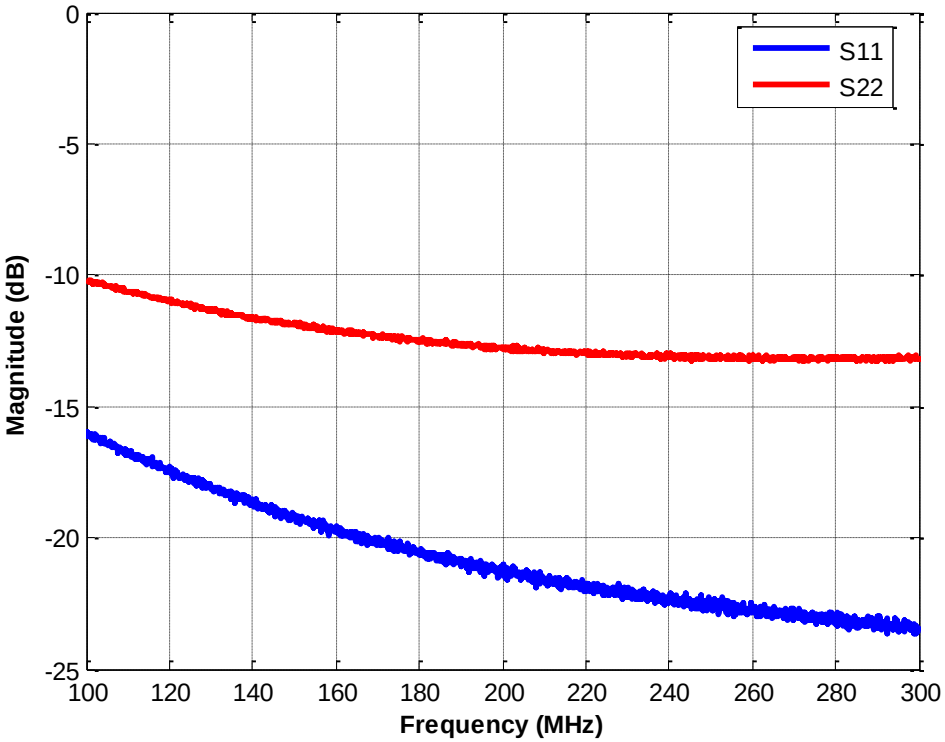


*Figure 3.15 - S11 and S22 for the Hittite HMC580STE Amplifier*

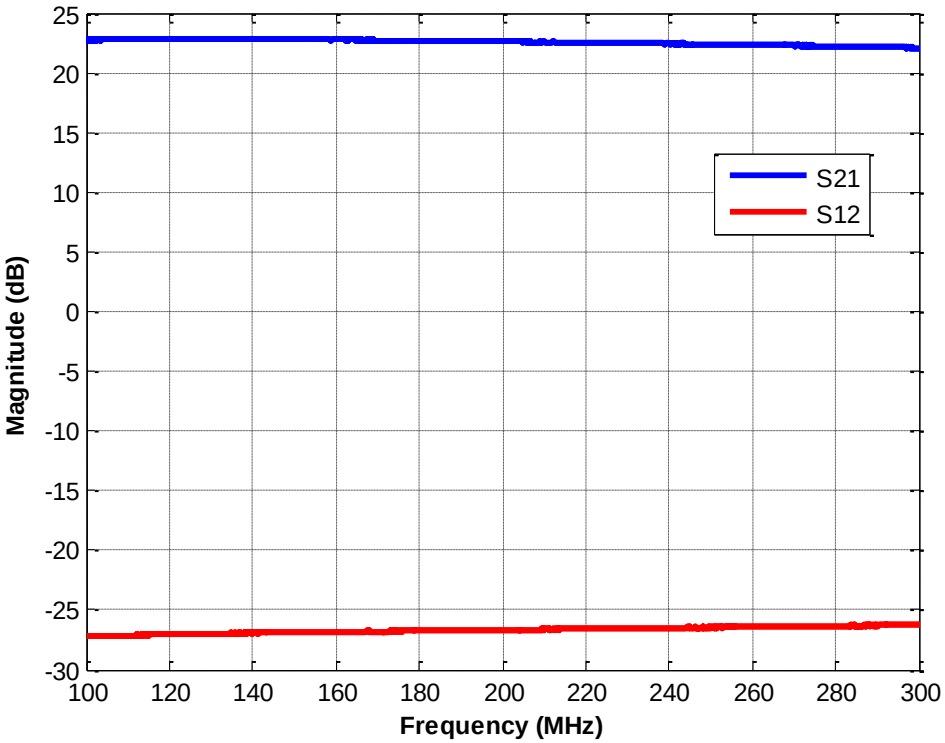


*Figure 3.16 - S21 and S12 for the Hittite HMC580STE Amplifier*

### *3.2.4 Minicircuits RLM-33+ RF Power Limiter*

To comply with the robustness requirement of the receiver the Minicircuits RLM-33+ RF power limiter was utilized. The power limiter protects each component by ensuring that the power level at every point in the receiver chain is below the damage level for each component while not interfering with the normal operation of the receiver. Figure 3.17 shows the S parameter data for the Minicircuits RLM-33+. This plot shows the limiter has a very low insertion loss of 0.05 dB and a return loss of 33.5 dB.

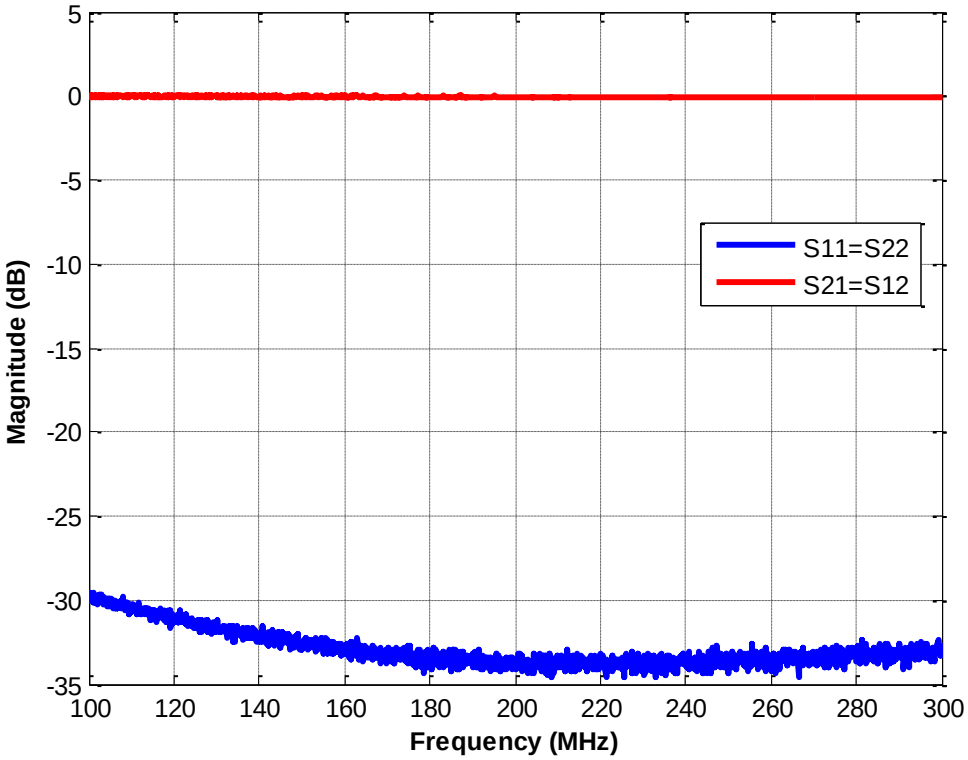


*Figure 3.17 - Measured S Parameter Data for the Minicircuits RLM-33+*

To ensure that the limiter properly protects each component and does not interfere with the normal operation of the receiver channel the power compression characteristics of the limiter should be measured. Figure 3.18 shows the inverse of the limiter's insertion loss (S21) over a range of input powers. As we can see from this plot the limiter has a very low insertion loss for input powers up to 6 dBm. The limiter reaches its 1 dB compression point at 9.5 dBm and effectively suppresses larger signals, limiting to a maximum output power of approximately 11 dBm. The RLM-33+ has a response time of 2 ns and recovery time of 10 ns.

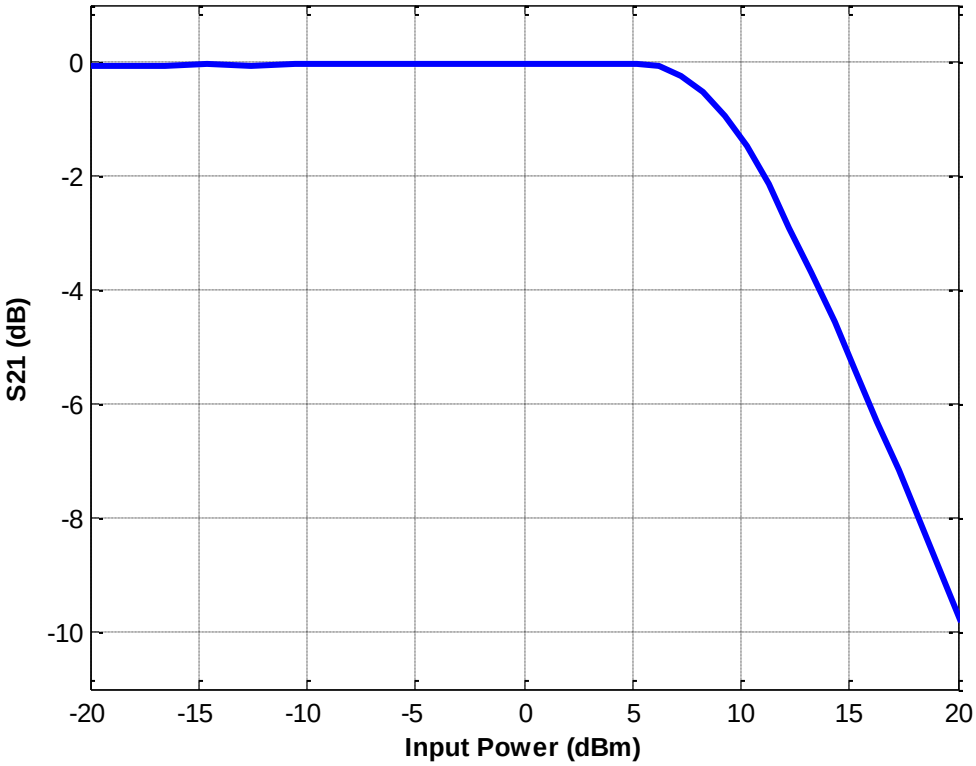


*Figure 3.18 - Measured Power Compression for the Minicircuits RLM-33+*

### *3.2.5 Minicircuits RLP-264 Low Pass Filter*

As described earlier in Section 2.2.3, a low pass filter is needed directly after the LNA to attenuate the switching transient signal created by the T/R switch changing states. To accomplish this, the Minicircuits RLP-264 was chosen for its low insertion loss and roll off characteristics. Figures 3.19 and 3.20 plot the S parameters of the RLP-264 across a narrow and wide bandwidth. These plots show that the filter has an insertion loss of 0.5 dB and a return loss greater than 17 dB across the MCoRDS/I frequency range.

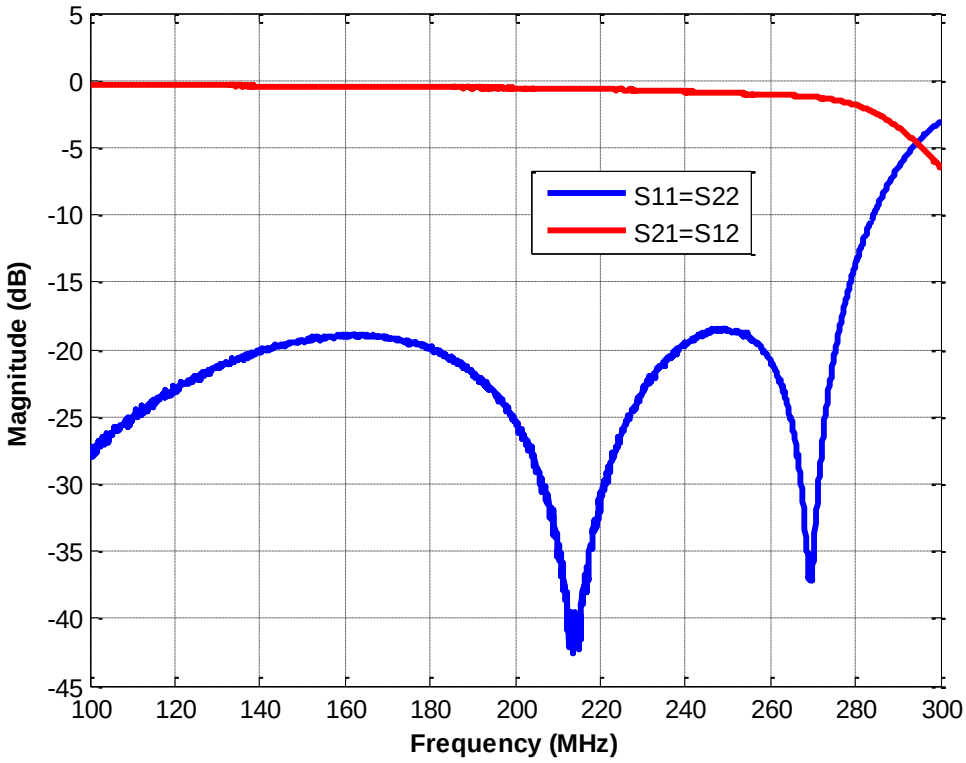


*Figure 3.19 - Measured S Parameter Data for the Minicircuits RLP-264*

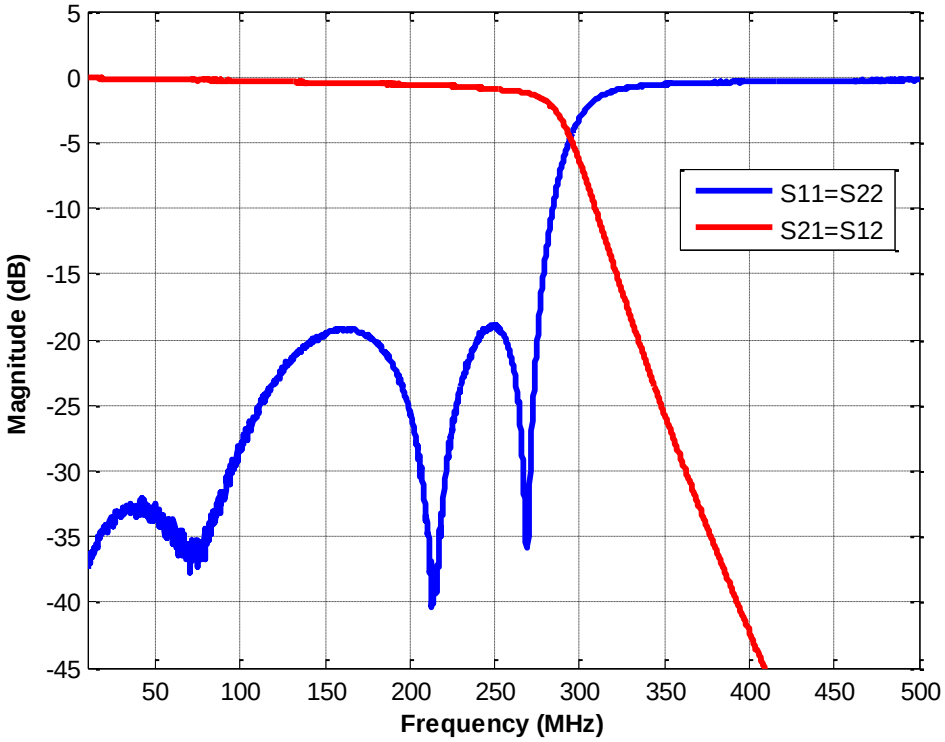


*Figure 3.20 - Measured S Parameter Wide Bandwidth Data for the Minicircuits RLP-264*

### *3.2.6 KR 2825-S2 Bandpass Filter*

The KR 2825-S2 bandpass filter was chosen for the anti-aliasing filter in the receiver chain. As described in Section 2.3.1, the MCoRDS/I system uses a bandpass sampling technique with a sample rate of 111.11 MHz placing the MCoRDS/I transmit signal in the fourth Nyquist zone. The anti-aliasing filter must attenuates signals in adjacent Nyquist zones to ensure they are not aliased into the MCoRDS/I frequency space. The key frequency ranges for the anti-aliasing filter are below 154 MHz and above 234 MHz. The filter must attenuate these signals by at least 50 dB to ensure they will not corrupt the recorded data. As can be seen from Figures 3.21 and 3.22 the 2825-S2 has an attenuation of at least 55 dB for signals lower than 154 MHz and at least 50 dB for signals above 234 MHz. The insertion loss of the filter is shown to be 1.1 dB with flatness of 0.3 dB within the bandwidth of the receiver.

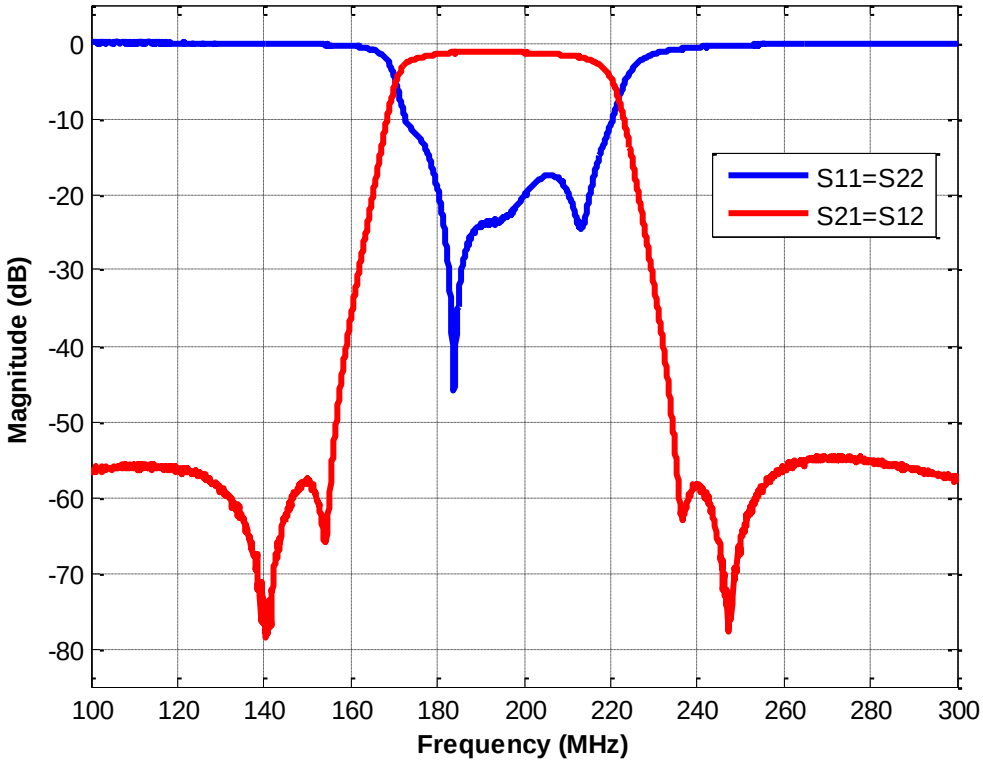


*Figure 3.21 - Measured S Parameter Data for the KR 2825 S-2*

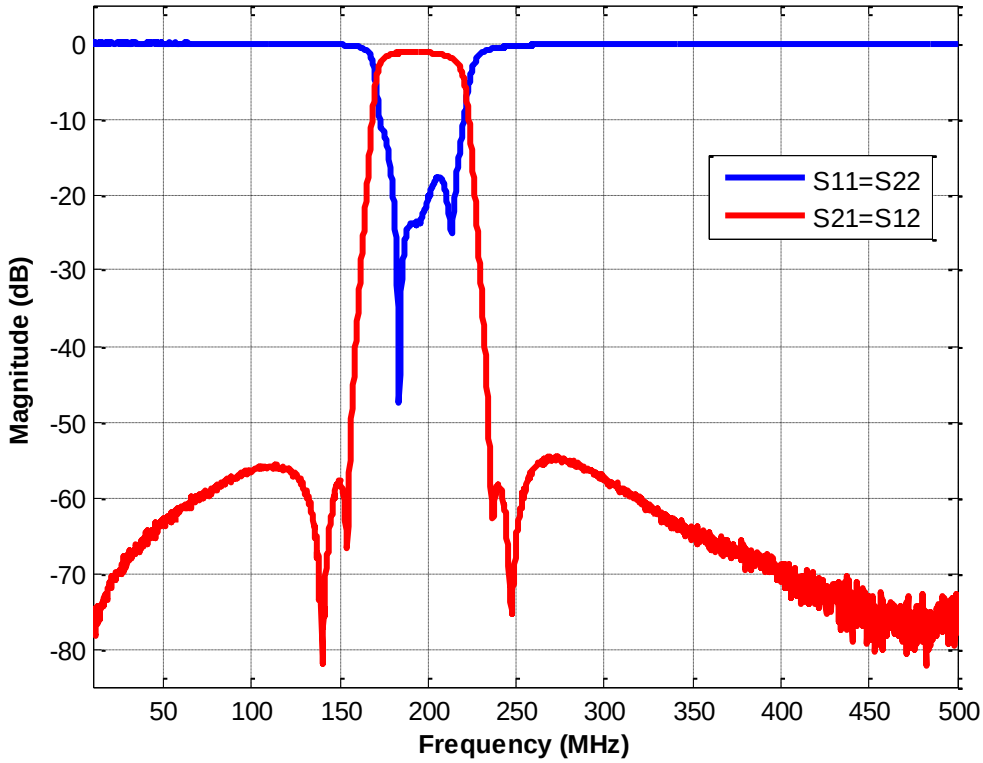


*Figure 3.22 - Measured S Parameter Wide Band Data for the KR 2825 S-2*

## *3.3 Receiver Chain Analysis*

To ensure that the receiver chain will operate as expected, an analysis of the gain, compression point and noise figure is necessary. Tables 3.2 and 3.3 use the measured gain, insertion loss, noise figure and 1 dB compression point data in the previous sections to illustrate several parameters about the receiver chain. Any noise figure, compression point, or maximum input power data that was not directly measured and presented in the previous section was taken from the component manufacturer datasheets. The tables show the input power to each component for a given set of attenuation settings and receiver input power. With the input power to each component given, it is possible to see which component in the chain will reach its 1 dB compression point first and thus set the compression point for the entire receiver chain with that particular attenuation setting. The tables also show the gain or insertion loss along with the noise figure for each component which allows the calculation of the receiver gain, thermal noise power, and noise figure at the output of each component in the chain. In the "high gain" setting, Table 3.2 shows when the attenuators are set to 0 dB and 5.5 dB respectively (in addition to the 1.2 dB of insertion loss), the receiver chain achieves the required gain of 46 dB and properly amplifies the thermal noise to -51 dBm or approximately 10 dB above the quantization noise floor of the ADC of -62 dBm. Table 3.2 also shows that in the high gain setting the receiver chain has a theoretical noise figure of

1.94 dB which is meets the design requirement of less than 2 dB. Maximum sensitivity is desired in the high gain setting thus any attenuation needed from the digital attenuators should be placed in the second attenuator component in the receiver chain. The compression point of the receiver in the high gain setting is not critical, however, Table 3.2 shows that the limiter at the end of the receiver chain just before the ADC sets the compression point of the receiver in the high gain setting at approximately -37 dBm.

In the "low gain" setting, the compression point of the receiver chain is the most critical parameter. Table 3.3 shows that with attenuation settings of 18 dB and 29 dB respectively (in addition to the 1.2 dB of insertion loss) the LNA sets the compression point in the low gain setting at 4.45 dBm which meets the design requirement of 3.1 dBm. It should be noted that the attenuator settings of the receiver can greatly affect the compression point as well as which component will compress first. The gain of the receiver chain is adjustable from approximately -11 dB to 52 dB thus the required minimum gain of 4 dB or less is achieved. Table 3.3 shows that the theoretical noise figure of the receiver chain in the low gain setting is approximately 20 dB but, as described in Section 3.1.1, the noise figure of the receiver chain in the low gain setting has very little impact on the receiver's performance.

The DC power requirement of a single receiver chain can be easily calculated. Each component is compatible with a 5 V DC power supply and thus the current required by each component can simply be added to obtain the amount current required by a single receiver. Table 3.1 gives the current required by each device as well as the current required by one receiver channel.

| Component | RFHIC LNA | Hittite Gain Block | Hittite Digital Atten |
|---|---|---|---|
| Current (mA) | 100 | 110 | 2 |
| Number in Chain | 1 | 2 | 2 |
| Total (mA) | 100 | 220 | 4 |
| | | | |
| Total Current per Channel | | 324 mA | |

*Table 3.1 - Receiver Chain DC Current Analysis*

| | | Limit | LNA | BPF | D Atten | Limit | Pad | Gain | D Atten | Limit | Pad | Gain | LPF | Limit | ADC |
|---|---|---|---|---|---|---|---|---|---|---|---|---|---|---|---|
| P in | dBm | -38 | -38.05 | -23.45 | -23.95 | -25.15 | -25.2 | -27.2 | -4.5 | -11.2 | -11.25 | -13.25 | 9.45 | 8.35 | 8.3 |
| Gain | dB | -0.05 | 14.6 | -0.5 | -1.2 | -0.05 | -2 | 22.7 | -6.7 | -0.05 | -2 | 22.7 | -1.1 | -0.05 | 0 |
| P out | dBm | -38.05 | -23.45 | -23.95 | -25.15 | -25.2 | -27.2 | -4.5 | -11.2 | -11.25 | -13.25 | 9.45 | 8.35 | 8.3 | 8.3 |
| | | | | | | | | | | | | | | | |
| P 1dB | dBm | 9.5 | 18.5 | | 27 | 9.5 | | 22 | 27 | 9.5 | | 22 | | 9.5 | 10 |
| Pin max | dBm | 33 | 25 | 27 | 30 | 33 | 30 | 10 | 30 | 33 | 30 | 10 | 30 | 33 | 13 |
| | | | | | | | | | | | | | | | |
| S Gain | dB | -0.05 | 14.55 | 14.05 | 12.85 | 12.8 | 10.8 | 33.5 | 26.8 | 26.75 | 24.75 | 47.45 | 46.35 | 46.3 | 46.3 |
| S Gain | lin | .99 | 28.51 | 25.41 | 19.28 | 19.05 | 12.02 | 2238.72 | 478.63 | 473.15 | 298.54 | 55590.43 | 43151.91 | 42657.95 | 42657.95 |
| F | dB | .05 | 1.52 | .5 | 1.2 | .05 | 2. | 2.8 | 6.7 | .05 | 2. | 2.8 | 1.1 | .05 | . |
| Therm N | dBm | -99.21 | -83.09 | -83.57 | -84.74 | -84.78 | -86.69 | -63.78 | -70.47 | -70.52 | -72.52 | -49.81 | -50.91 | -50.96 | -50.96 |
| Sys F | lin | 1.01 | 1.44 | 1.44 | 1.45 | 1.45 | 1.48 | 1.56 | 1.56 | 1.56 | 1.56 | 1.56 | 1.56 | 1.56 | 1.56 |
| Sys F | dB | .05 | 1.57 | 1.58 | 1.62 | 1.62 | 1.71 | 1.93 | 1.93 | 1.93 | 1.94 | 1.94 | 1.94 | 1.94 | 1.94 |

*Table 3.2 - Receiver Chain Analysis in the High Gain Setting*

| | | Limit | LNA | BPF | D Atten | Limit | Pad | Gain | D Atten | Limit | Pad | Gain | LPF | Limit | ADC |
|---|---|---|---|---|---|---|---|---|---|---|---|---|---|---|---|
| P in | dBm | 0.1 | 0.05 | 14.65 | 14.15 | -5.05 | -5.1 | -7.1 | 15.6 | -14.6 | -14.65 | -16.65 | 6.05 | 4.95 | 4.9 |
| Gain | dB | -0.05 | 14.6 | -0.5 | -19.2 | -0.05 | -2 | 22.7 | -30.2 | -0.05 | -2 | 22.7 | -1.1 | -0.05 | 0 |
| P out | dBm | 0.05 | 14.65 | 14.15 | -5.05 | -5.1 | -7.1 | 15.6 | -14.6 | -14.65 | -16.65 | 6.05 | 4.95 | 4.9 | 4.9 |
| | | | | | | | | | | | | | | | |
| P 1dB | dBm | 9.5 | 19 | | 27 | 9.5 | | 22 | 27 | 9.5 | | 22 | | 9.5 | 10 |
| Pin max | dBm | 33 | 25 | 27 | 30 | 33 | 30 | 10 | 30 | 33 | 30 | 10 | 30 | 33 | 13 |
| | | | | | | | | | | | | | | | |
| S Gain | dB | -0.05 | 14.55 | 14.05 | -5.15 | -5.2 | -7.2 | 15.5 | -14.7 | -14.75 | -16.75 | 5.95 | 4.85 | 4.8 | 4.8 |
| S Gain | lin | .99 | 28.51 | 25.41 | .31 | .3 | .19 | 35.48 | .03 | .03 | .02 | 3.94 | 3.05 | 3.02 | 3.02 |
| F | dB | .05 | 1.52 | .5 | 19.2 | .05 | 2. | 2.8 | 30.2 | .05 | 2. | 2.8 | 1.1 | .05 | . |
| Therm N | dBm | -99.21 | -83.09 | -83.57 | -97.66 | -97.67 | -98.18 | -73.14 | -97.79 | -97.80 | -98.27 | -73.19 | -74.29 | -74.34 | -74.34 |
| Sys F | lin | 1.01 | 1.44 | 1.44 | 4.67 | 4.71 | 6.65 | 11.4 | 40.88 | 41.23 | 58.69 | 101.53 | 101.6 | 101.61 | 101.61 |
| Sys F | dB | .05 | 1.57 | 1.58 | 6.7 | 6.73 | 8.23 | 10.57 | 16.12 | 16.15 | 17.69 | 20.07 | 20.07 | 20.07 | 20.07 |

*Table 3.3 - Receiver Chain Analysis in the Low Gain Setting*

## *3.4 Receiver Chain Simulation*

To simulate the S parameters of the receiver chain, Agilent's Advanced Design System (ADS) was utilized. An S parameter block was created in ADS for each component using the S parameter measurements from Section 3.2. These component blocks were cascaded together to form the receiver chain and an S parameter simulation was done. Figures 3.23 and 3.24 plot the simulated S parameter data for the receiver in the "high gain" setting using measured S parameter data with the digital attenuator in the 0 dB and 5.5 dB attenuation settings respectively. These plots show that the receiver chain behaves as expected in the simulation and meets the requirements for gain and bandwidth. Figures 3.25 and 3.26 show the simulated S parameter data for the receiver in the "low gain" setting using measured S parameter data with the digital attenuator in the 18 dB and 29 dB attenuation settings respectively. These plots also show that for the low gain setting the receiver chain behaves as expected in the simulation and meets the requirements for gain and bandwidth.

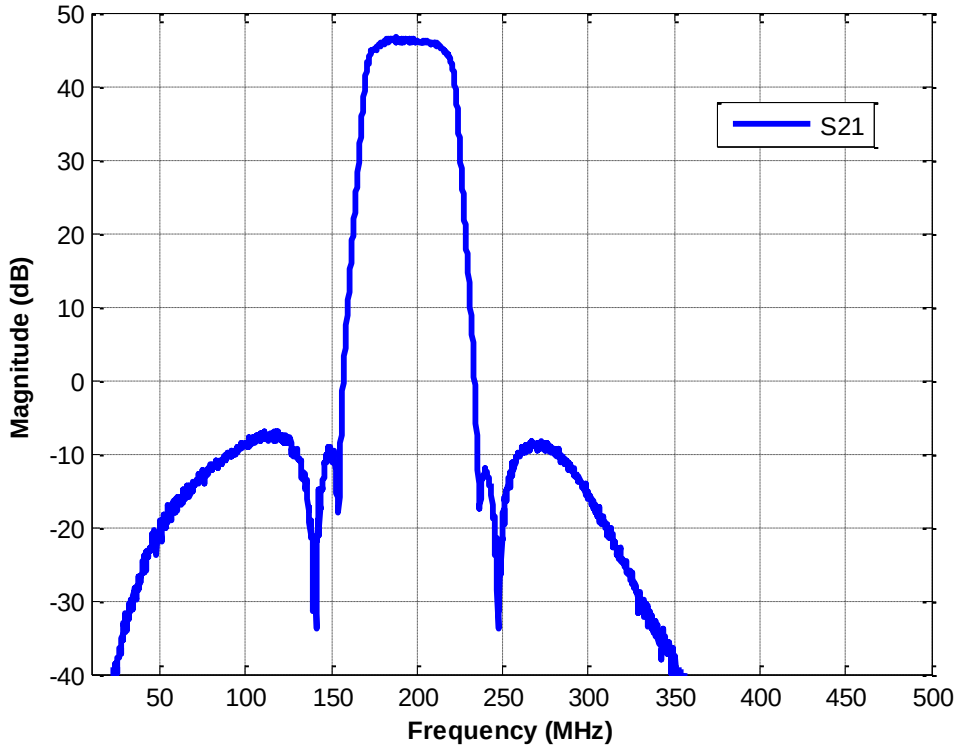


*Figure 3.23 - S21 Receiver Chain High Gain Simulation with Measured S Parameters of Components*

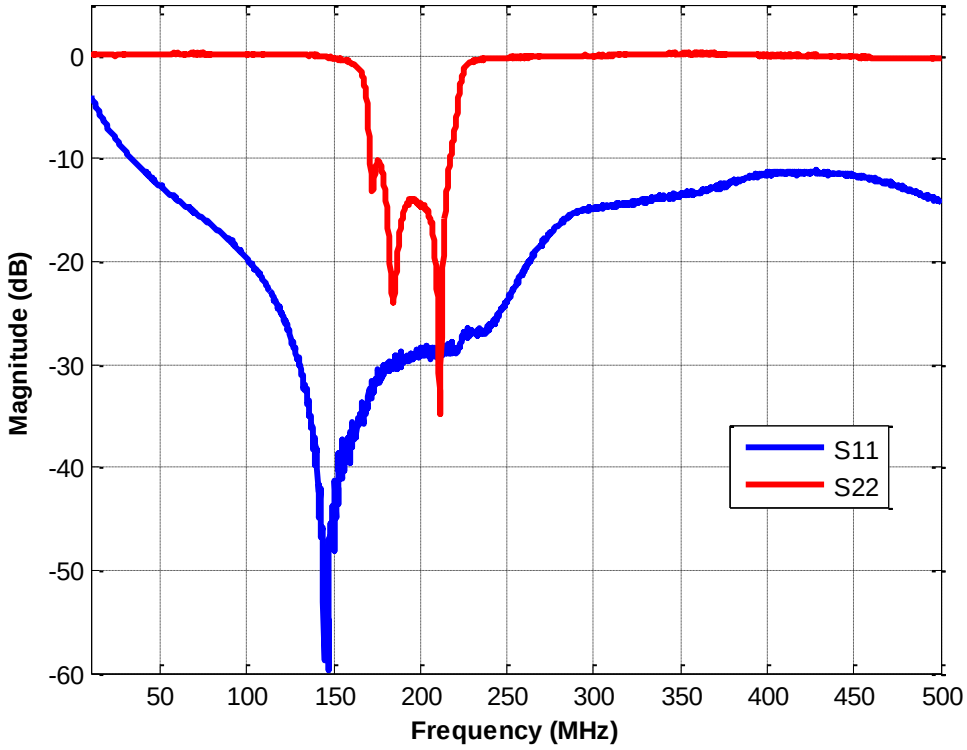


*Figure 3.24 - S11 and S22 Receiver Chain High Gain Simulation with Measured S Parameters of Components*

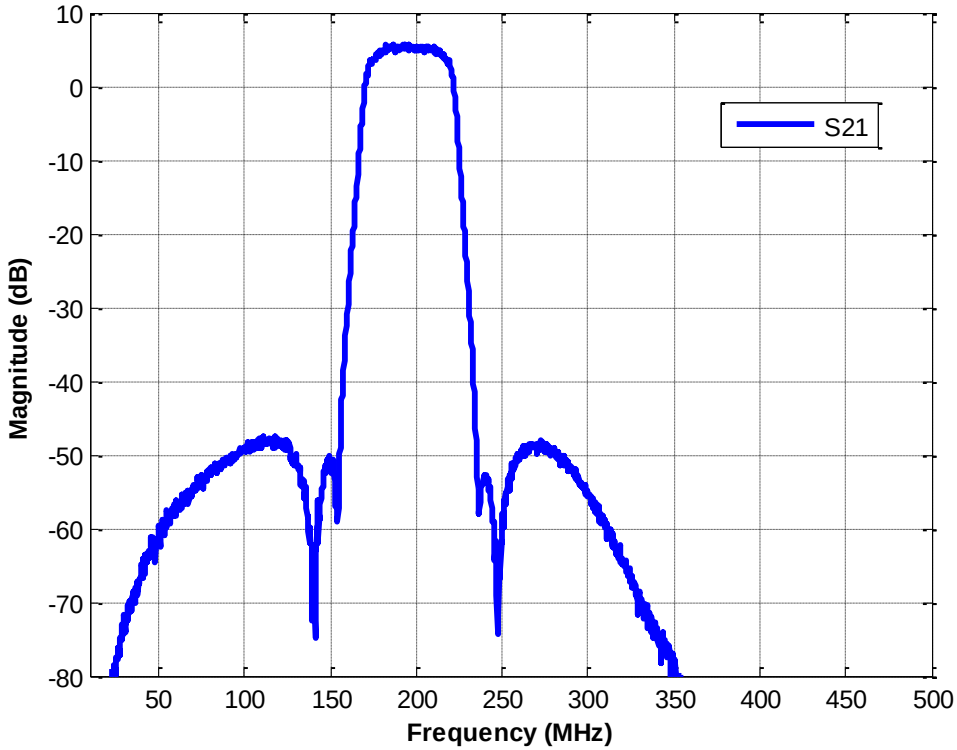


*Figure 3.25 - S21 Receiver Chain Low Gain Simulation with Measured S Parameters of Components*

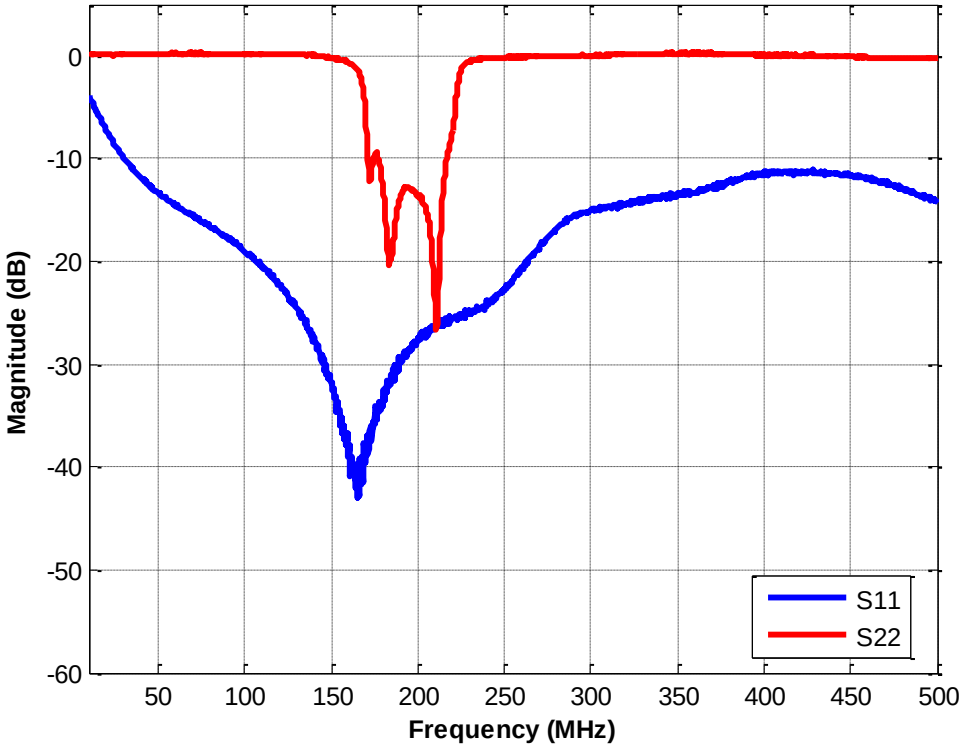


*Figure 3.26 - S11 and S22 Receiver Chain Low Gain Simulation with Measured S Parameters of Components*

# Chapter 4

## *Receiver Implementation*

### *4.1 RF Test board*

The next step in realizing the receiver design once the RF topology and components are determined is to design the PCB. To speed up the design cycle, the first PCB that was designed included only the receiver RF channels. Appendix A provides the schematic, board stack up, and board layout for the RF test board. The board was designed as a six layer PCB and was manufactured by Sierra Circuits. Each RF channel is arranged in a linear fashion with the input and output connectors adjacent at the edge of the board. Controlled impedance transmission lines were used for the RF traces on the PCB. Trace widths that provide a 50 ohm impedance are 15 mils for microstrip traces on the top and bottom layers and 7 mils for the asymmetric stripline transmission lines on the third layer [5]. A C-grid connector was used to power the board from a bench top power supply. To control the digital attenuators, a three wire serial connection was routed from the attenuators control inputs to C-grid connectors so an external device could program the attenuators to the desired setting.

### *4.1.1 RF Test board Verification*

To verify the performance of the RF test board meets the receiver requirements many tests were performed. Unfortunately, due to the very quick design cycle and long lead time for some parts, some of the components from the RF test boards were reused on the final design and the electronic data from these tests were not permanently saved. It would be difficult and time consuming to recreate them therefore the outcomes from these tests will be discussed without the raw data. The first tests that were performed measured the gain and bandwidth characteristics of the receiver channel. The adjustable gain of the receiver worked properly and the minimum and maximum gain settings were close to the theoretical analysis. The bandwidth of the receiver was tested to match the simulation results. The input and output return loss of the receiver channel was dominated by the LNA and anti-aliasing filter respectively and were greater than 10 dB for the system bandwidth thus deemed acceptable. The 1 dB compression point of the receiver channel was tested and was approximately the same as the theoretical analysis of 4.45 dBm in the low gain setting and -37 dBm in the high gain setting. The receiver channel's noise figure was tested with an HP 8970B noise figure meter at 195 MHz to be 1.96 dB in the high gain setting which is very close to the theoretical noise figure calculation of 1.94 dB. To test the receiver channel's robustness, the receiver was set to the maximum gain and a signal of 30 dBm was injected into the input of the receiver.

After being subjected to the 30 dBm signal overnight the receiver channel was tested and proved to be fully functional.

The last test that was performed was to measure the channel to channel isolation of the RF test board. Due to the large gain of the receiver channels, any small coupling between channels could result in very poor channel to channel isolation. In an attempt to increase the channel to channel isolation, each receiver channel was split up into a small signal section and a large signal section with the solder mask relieved all the way around each small and large signal section. Once the boards were populated, a separate copper shielding lid was placed around the small and large signal sections of each receiver channel to better isolate the receiver chains. To test the channel to channel isolation port 1 of a network analyzer was connected to the input port of one of the receiver channels and the output to that channel was terminated in a matched load. The input to the receiver channel you are measuring the isolation of is connected to a matched load and the output of that channel is connected to port 2 of the network analyzer. Both receiver channels are set to full gain and the S21 parameter was measured. By subtracting the receiver channel's gain from the S21 measurement we arrive at the effective channel to channel isolation. The channel to channel isolation for the RF test board was measured to be approximately 40 dB. This measurement was done both before and after the copper shielding lids were installed and it was discovered that the

copper shielding lids had no effect on the channel to channel isolation. Upon further investigation it was determined that the coupling from one channel to another was occurring by the signal coupling onto the shared power plane. A test was done by disconnecting the LNA and gain blocks from the shared power plane and powering them from a separate bench top power supply than the rest of the RF test board. This test showed that when the two receiver channels did not share the same power supply the channel to channel isolation increased by approximately 10 dB. To solve this issue in the next revision, each receiver channel was given a separate power plane that was connected to the main power plane through an inductor which acted as a low pass filter allowing the DC power to pass but attenuating the signals in the MCoRDS/I band thus decreasing the coupling between channels and increasing the channel to channel isolation.

## *4.2 Final Receiver Design*

Once the RF test board testing and verification was completed the full receiver module was designed. This design included a CPLD to interface with the PXI chassis and control the digital attenuators, high density backplane connectors that are the physical interface between the receiver module and the PXI chassis, and isolated power planes that, as described in the previous section, increase the channel to channel isolation and allows for the receiver module to be powered either from

the PXI backplane or an external power supply. Appendix B provides the schematic, board layout, board stack up, and photos of the final design of the receiver module.

The digital section of the receiver module consists of a Xilinx XC95144-15I CPLD. A CPLD was used due to their non-volatile memory and low number of required external components. The CPLD is used to decode the attenuation settings information sent over the PXI backplane by the MCoRDS/I system controller and program each digital attenuator on the receiver module with proper attenuation setting. A simple three wire serial communication scheme is used for the communication from the MCoRDS/I system controller to the CPLD. When the load enable (LE) line is driven low, the data (DATA) is input to the CPLD on the rising edge of the clock (CLK) line. The first bit of data is a reset bit which, if high, immediately sets every attenuator on the receiver module to the maximum attenuation setting. If the reset bit is low, first the 6 bits for the second attenuator in the receiver chain are input least significant bit to most significant bit then the 6 bits for the first attenuator in the receiver chain are input in the same manner. After the last bit of data is input the load enable line is driven high and the CPLD programs all the attenuators on the receiver module with the attenuation settings. Figure 4.1 illustrates the serial communication scheme between the MCoRDS/I system controller and the receiver module CPLD with a timing diagram.

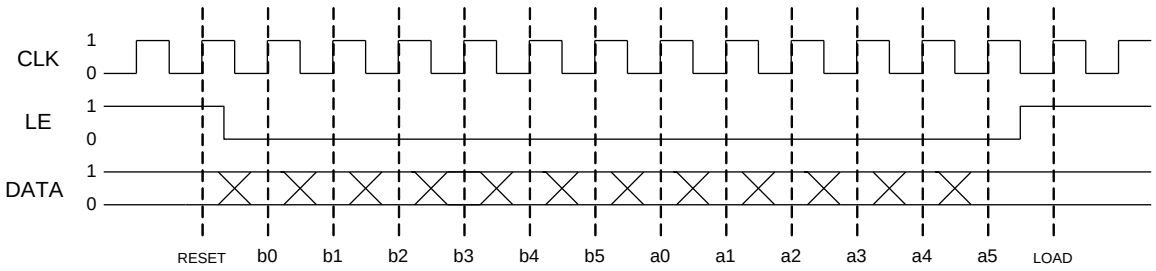


*Figure 4.1 - CPLD Programming Timing Diagram*

It was determined during the testing of the RF test board that separate shielding of each channel did not have an effect on the channel to channel isolation of the receiver, however, because of the large gain of the receiver channels it is desired that they are shielded from outside electromagnetic interference (EMI) sources. To shield the receiver modules a copper shielding lid was constructed to fit over the entire RF section. The EMI shielding lid is soldered to the board on seven pads around its perimeter and clips are used on the edge with the RF connectors to both solidly affix the shield to the PCB and to create a good ground connection between the shield and the PCB. Because the RF traces for the input signal lie on the top layer, notches were cut out of the EMI shield where the traces run under the shield to make sure they do not short the trace to ground and do not disturb the controlled impedance of the trace. Appendix B provides photos of the receiver module with and without the EMI shield connected.

The receiver modules were designed to be powered either from the PXI chassis backplane or with an external power supply by simply

populating or depopulating a DC power filter. The power that is provided by the PXI chassis backplane comes from a switching power supply inside the chassis. These switching power supplies are not of the low noise variety and thus may introduce noise onto the DC power plane of the receiver modules. This noise can get coupled into the RF output of the receiver channels and thus the modules were designed such that they can easily be configured to be powered by an external power supply or the PXI chassis backplane power.

## *4.3 Receiver Testing and Verification*

To ensure that the receiver modules operate properly a large amount of testing must be done. To measure the S parameters the Agilent N5230C network analyzer was used with an output power of -45 dBm for the high gain setting and -10 dBm for the low gain setting. In the high gain setting, attenuation values of 0 dB in the first attenuator and 5.5 dB in the second attenuator were used while the low gain setting used attenuation values of 18 dB in the first attenuator and 29 dB in the second. Figures 4.2 through 4.7 compare the measured S parameters of the receiver channel in both the high and low gain settings to the ADS simulation of the receiver chain S parameters in the using the measured S parameter data of every component. These plots show that the receiver module S parameters closely follow the simulation results and are acceptable for the receiver operation.

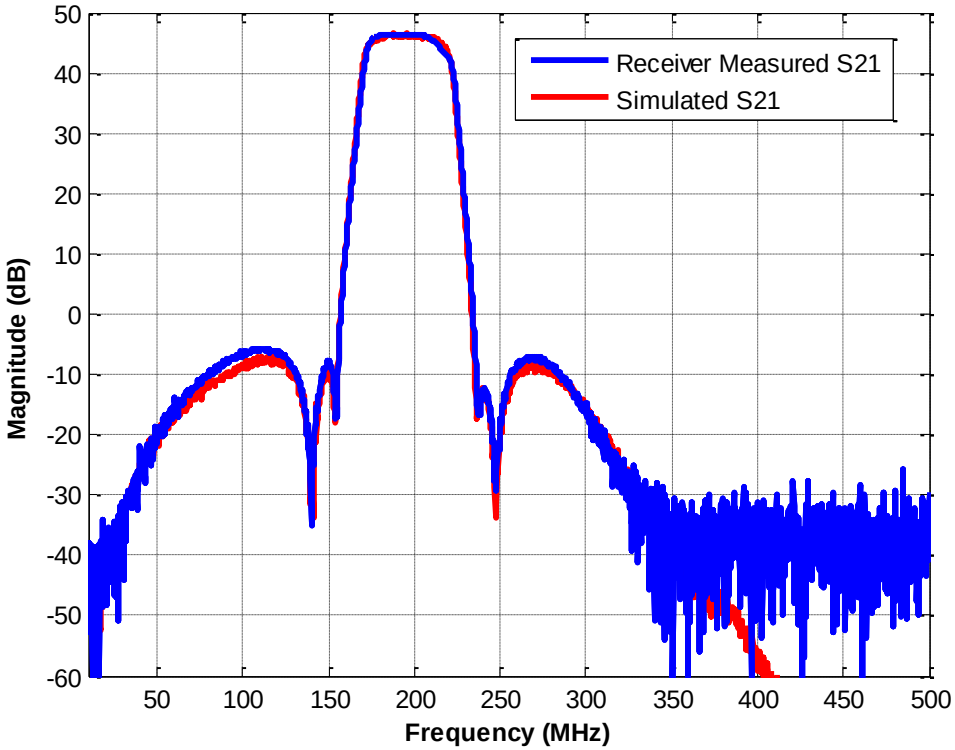


*Figure 4.2 - Comparison of Receiver Channel Measured and Simulated S21 in the High Gain Setting*

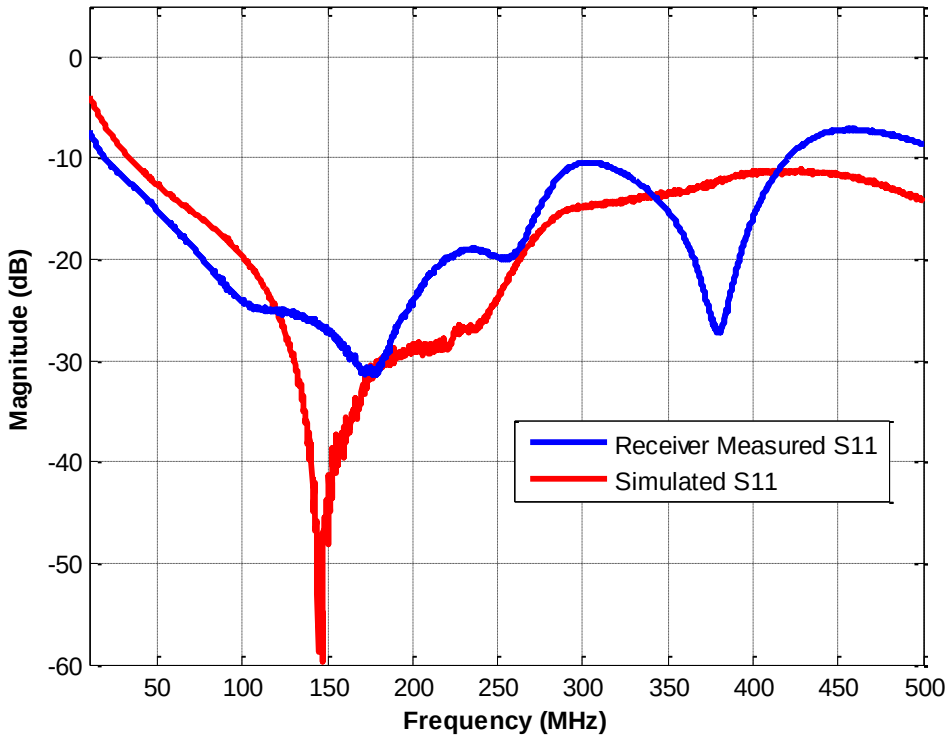


*Figure 4.3 - Comparison of Receiver Channel Measured and Simulated S11 in the High Gain Setting*

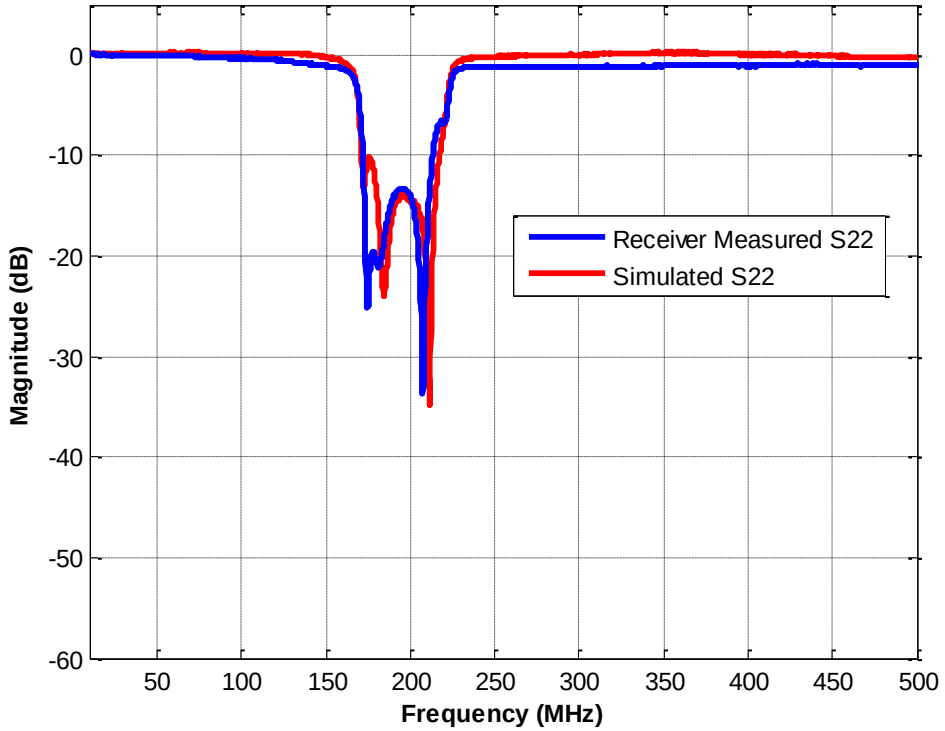


*Figure 4.4 - Comparison of Receiver Channel Measured and Simulated S22 in the High Gain Setting*

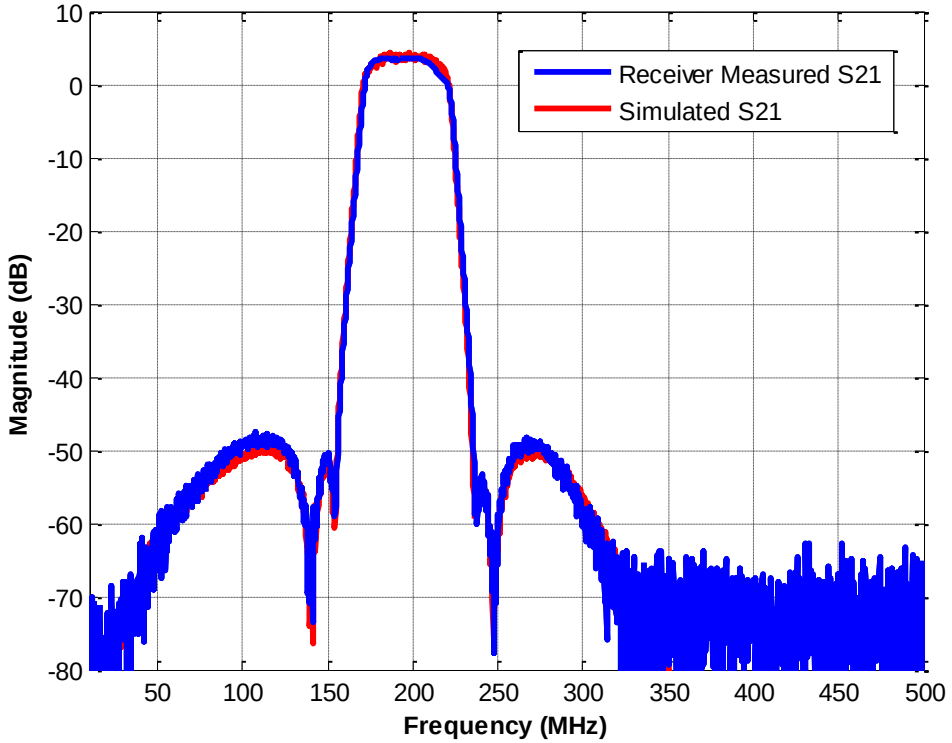


*Figure 4.5 - Comparison of Receiver Channel Measured and Simulated S21 in the Low Gain Setting*

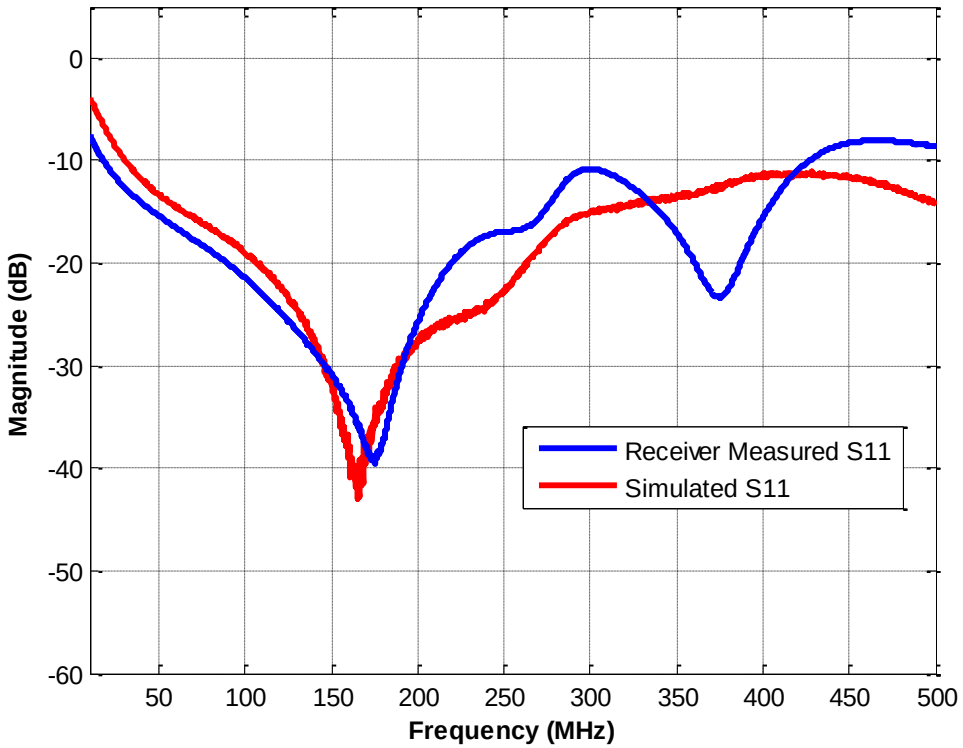


*Figure 4.6 - Comparison of Receiver Channel Measured and Simulated S11 in the Low Gain Setting*

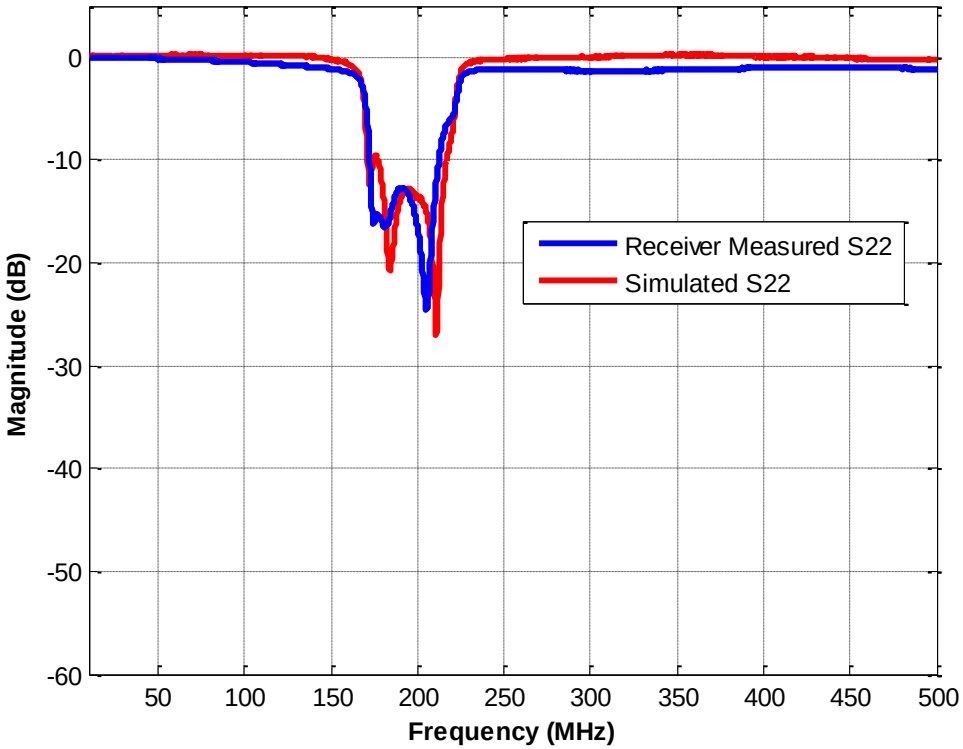


*Figure 4.7 - Comparison of Receiver Channel Measured and Simulated S22 in the Low Gain Setting*

To measure the compression point of the receiver channel, again an Agilent 8648D signal generator and an Agilent E4446A spectrum analyzer were calibrated and used for the measurement. Figure 4.8 plots the change in the gain of the receiver in the low gain setting with respect to the input power to the receiver. The plot shows that the 1 dB compression point of the receiver channel in the low gain setting is approximately 4.5 dBm and the plot closely resembles Figure 3.12 indicating that, as expected, the LNA is setting the compression point of the receiver channel in the low gain setting. Figure 4.9 illustrates the compression point of the receiver in the high gain setting is approximately -38 dBm which closely coincides with the theoretical calculation in Section 3.3.

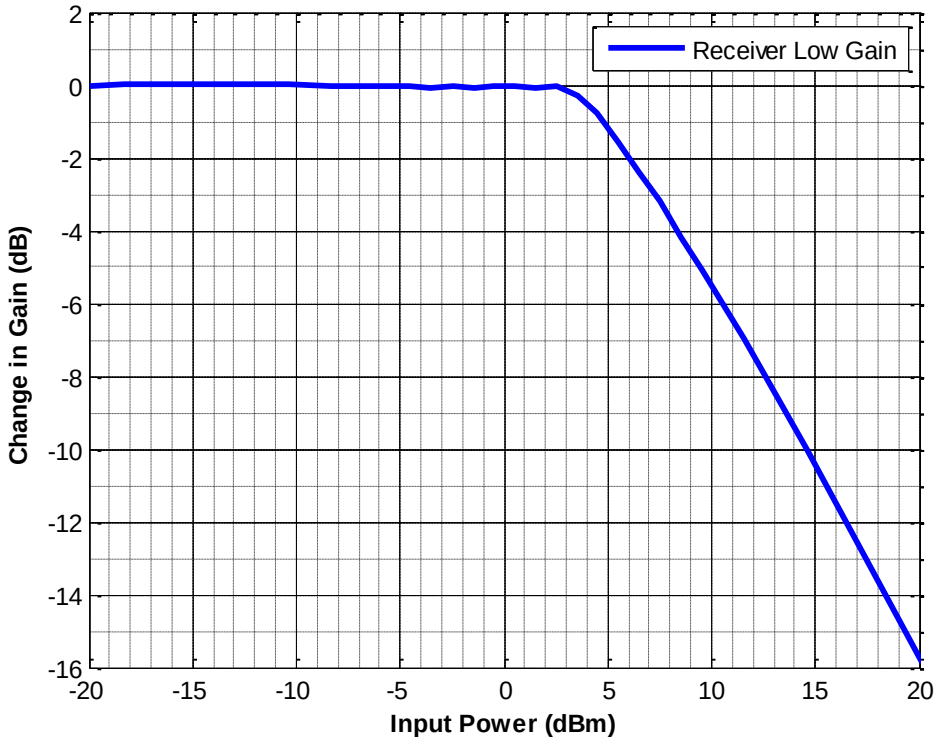


*Figure 4.8 - Measured Power Compression Characteristics for the Receiver Channel in the Low Gain Setting*

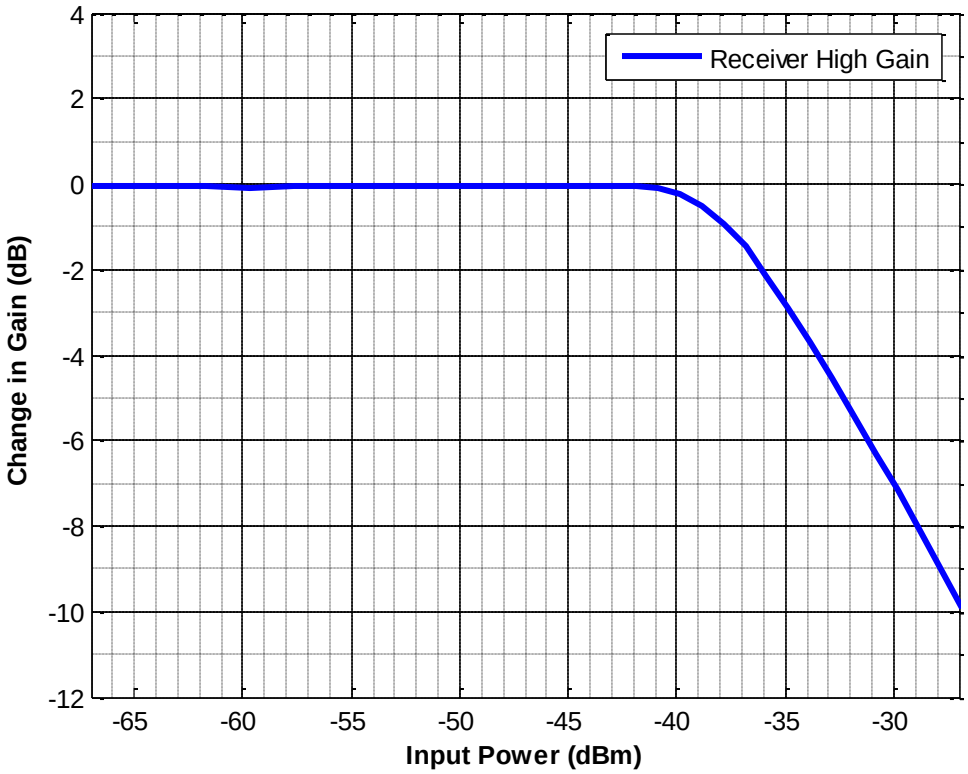


*Figure 4.9 - Measured Power Compression Characteristics for the Receiver Channel in the High Gain Setting*

The noise figure of the receiver channel in the high gain setting is an important parameter in its performance. Figure 4.10 below plots the receiver's noise figure in the high gain setting as measured by an HP 8970B noise figure meter. This plot illustrates that the receiver has a noise figure of approximately 1.96 dB across the bandwidth of the system which is very close to the theoretical noise figure calculation of 1.94 dB. Figure 4.11 shows the noise figure of the receiver in the low gain setting also agrees with the theoretical calculation of approximately 20 dB.

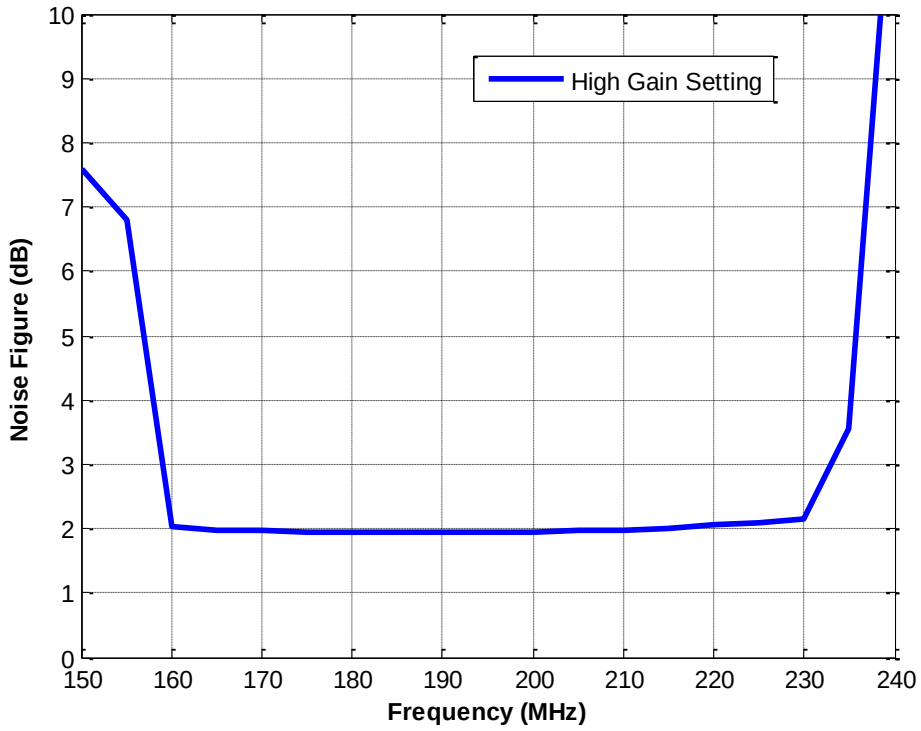


*Figure 4.10 - Measured Noise Figure for the Receiver Channel in the High Gain Setting*

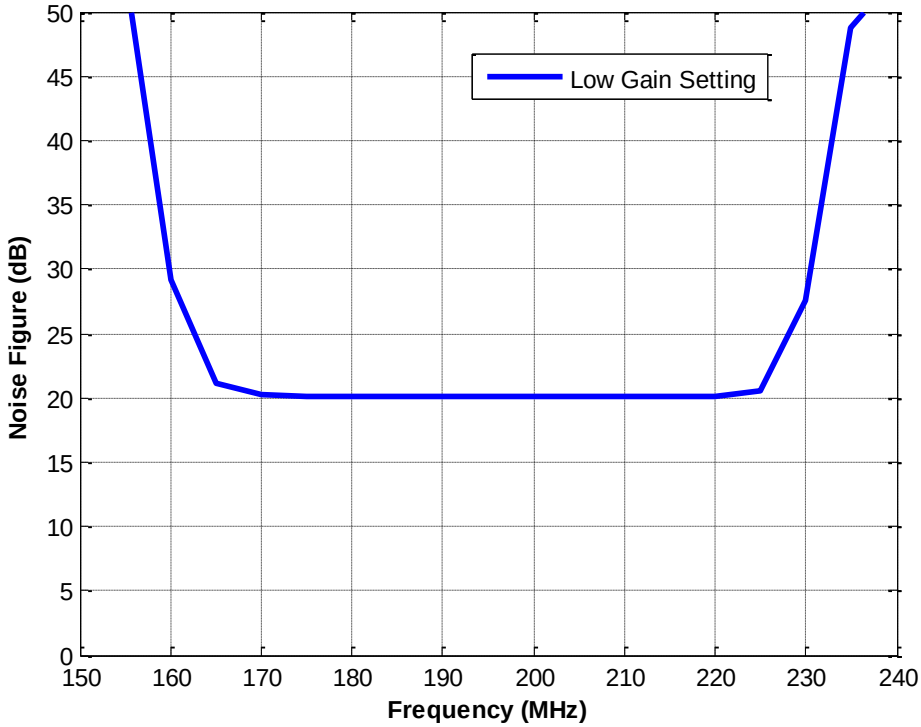


*Figure 4.11 - Measured Noise Figure for the Receiver Channel in the Low Gain Setting*

The channel to channel isolation of the receiver was measured with an Agilent N5230C network analyzer. All channels of the receiver module were programmed to the high gain setting and port 1 of the network analyzer was connected to the input of a channel while a matched load was connected to its output. Port 2 of the network analyzer was connected to the output of another channel with a matched load connected to its input. The S21 measurement minus the gain of the receiver channel gives the ratio of the coupled signal power to the output signal power. All 12 possible configurations of channel to channel isolation measurements were done and Figure 4.12 shows the worst case channel to channel isolation for the receiver module between channel 2 as the input channel and 3 as the output channel. The plot shows that the channel to channel isolation is greater than 50 dB in the worst case. The channel to channel isolation for adjacent channels with the lower channel as the input were all consistent with Figure 4.12 to within 3 dB. The other configurations of channel to channel isolation were greater than 10 dB more than what the figure illustrates.

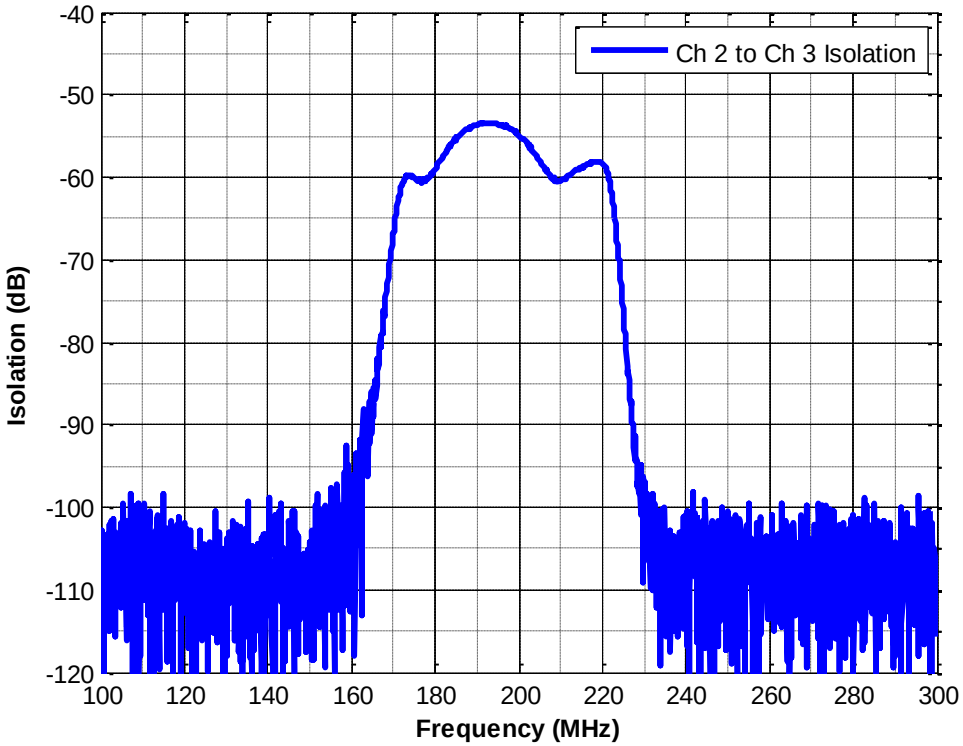


*Figure 4.12 - Measured Worst Case Channel to Channel Isolation of Receiver Module*

Ideally, the gain of the receiver channel would be perfectly constant with linear phase over the bandwidth of the system. Due to the non-ideal characteristics of the receiver components the receiver channel has some variation in gain and non-linear phase response. Figure 4.13 shows a detailed plot of the receiver channel's gain across the 180 MHz to 210 MHz bandwidth. The variation in gain of the receiver channel is approximately 0.8 dB. Figure 4.14 plots the group delay of the receiver channel. If the phase response of the receiver channel was perfectly linear, the group delay would be constant but, as you can see from the plot, the phase response is not perfectly linear and the group delay varies by approximately 10 ns across the 180 MHz to 210 MHz bandwidth.

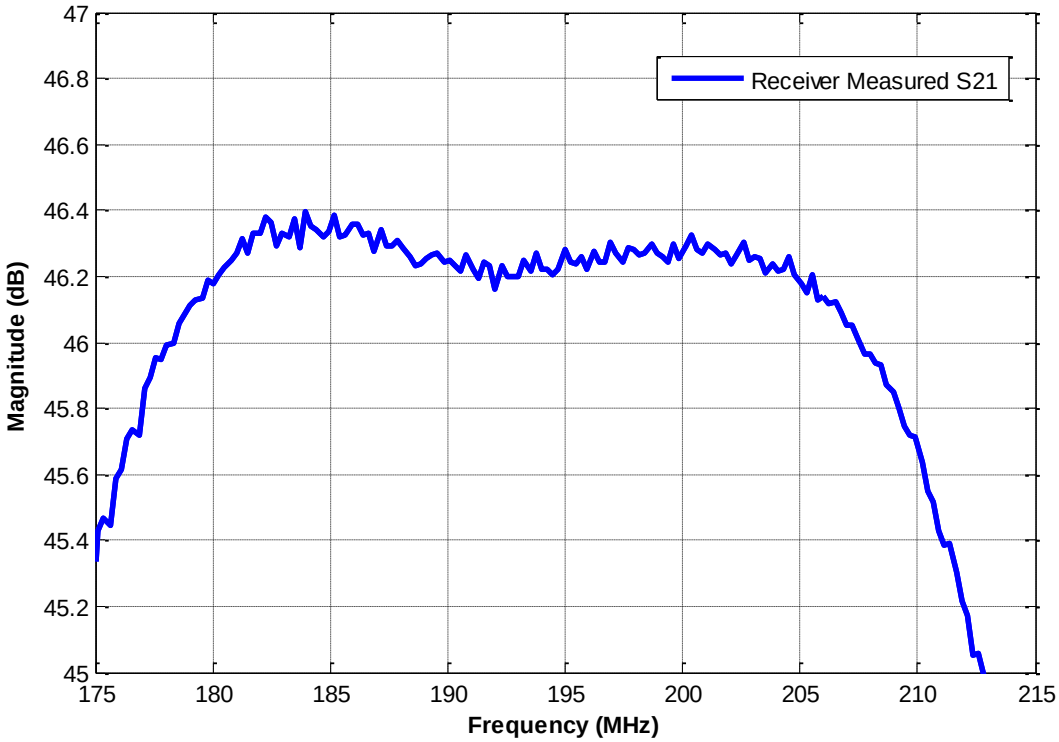


*Figure 4.13 - Measured Gain of Receiver Module in the High Gain Setting*

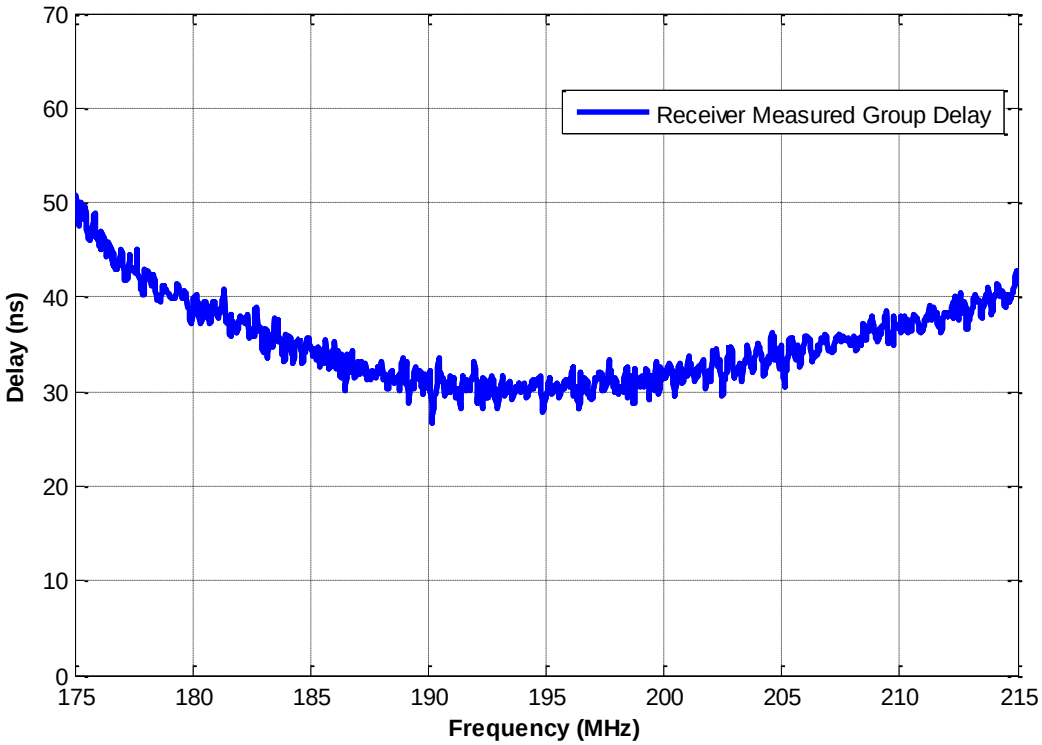


*Figure 4.14 - Measured Group Delay of Receiver Module in the High Gain Setting*

To characterize how the non-ideal channel response will affect the system performance, a MATLAB simulation was done. The simulation uses a 1 μs linear FM chirp pulse from 180 MHz to 210 MHz with a weighted cosine (Tukey) window of α=0.2. This pulse is then multiplied in the frequency domain by the channel response and converted back into the time domain where pulse compression is done on the resulting signal with the original pulse. This simulation was done for an ideal channel response with constant gain and linear phase, the receiver's gain response with a linear phase response, and the receiver's gain and phase response. Figure 4.15 compares the ideal channel response with the receiver's gain response and linear phase. This plot shows that the variation in gain of the receiver has a very small affect on the peak sidelobe level increasing it by 0.2 dB and almost no affect on the main lobe. Figure 4.16 compares the ideal channel response with the receiver's gain and phase response. This plot shows that the non-linear phase response of the receiver causes the sidelobes to become asymmetrical with the left sidelobes being larger than the ideal case and the right sidelobes being smaller. This causes an increase in the peak sidelobe level of 0.8 dB and slight distortion of the main lobe. This small decrease in the peak sidelobe performance has very little effect on the overall system performance and can be almost completely mitigated by characterizing the channel with a loopback calibration and using the non-ideal channel response during pulse compression.

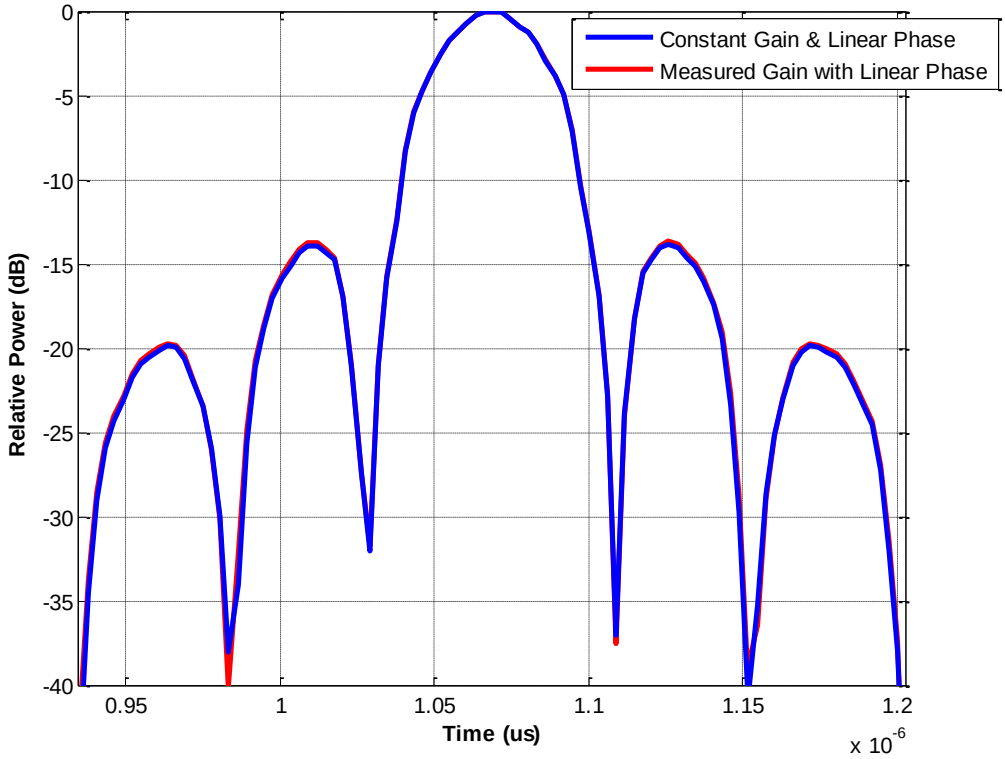


*Figure 4.15 - Simulation of Sidelobe Performance for Ideal Channel Response and Receiver Gain Response with an Ideal Linear Phase*

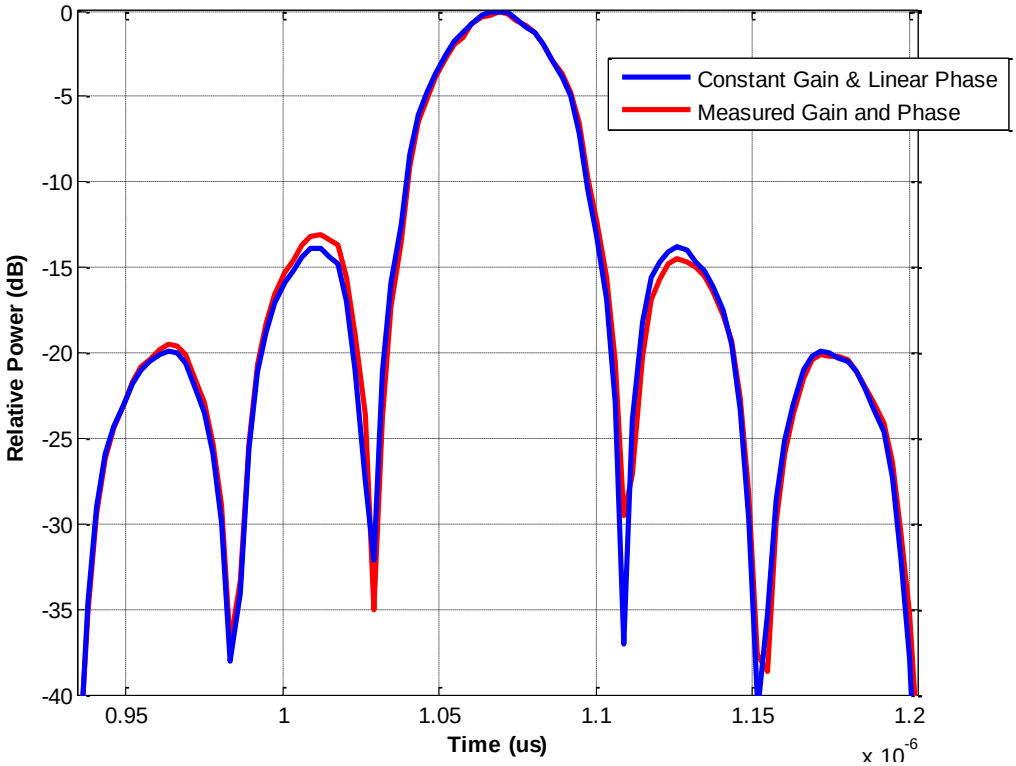


*Figure 4.16 - Simulation of Sidelobe Performance for Ideal Channel Response and Receiver Channel Response*

The receiver modules were integrated into the MCoRDS/I system on the P3 platform and data was collected for a noise analysis and over the ocean from high altitude. Figure 4.17 shows the power in the frequency spectrum across the system bandwidth at the output of the receiver module with the input terminated in a matched load and the receiver channel set to 45.75 dB of gain. The inset of the plot shows the raw voltage data used in the plot. This figure shows the noise floor to be relatively constant across the bandwidth and does not contain any noise sources at discrete frequencies coupling into the receiver and being amplified. The plot also illustrates that as presumming is preformed, the noise floor drops as described in Section 2.2.4; 2 presums will result in a 3 dB reduction of the noise floor, 10 presums in a 10 dB reduction, and 32 presums in a 15 dB reduction.

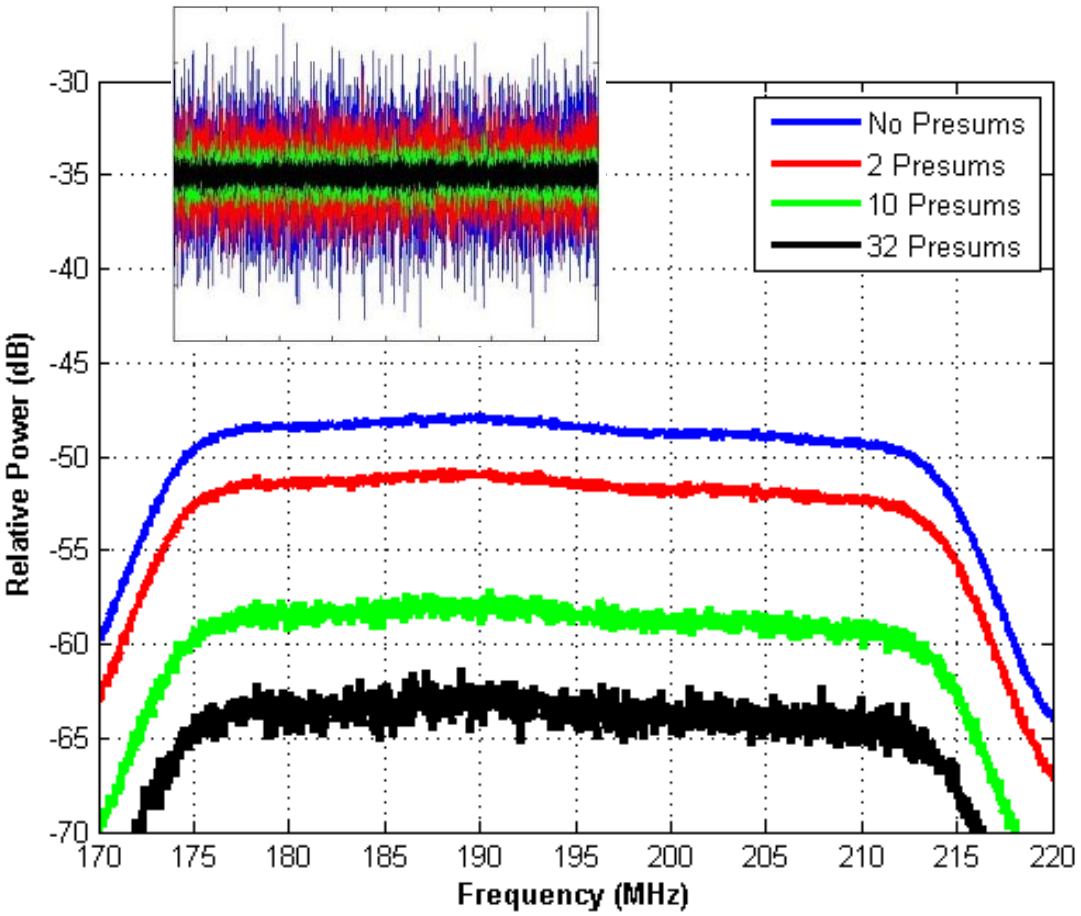


*Figure 4.17 - Receiver Noise Floor Performance in the High Gain Setting on the P3 Platform*

Figure 4.18 is a plot of the pulse compressed signal return over the ocean from an altitude of 24,000 feet in the high gain setting using a weighted cosine window (α=0.2) on the transmit pulse and a Blackman window during pulse compression. This plot shows the receiver module operating properly when integrated with the MCoRDS/I system and capturing the signal return from the ocean surface successfully. The first 20 μs of the plot shows a strong direct path feed through from the transmitter followed by the signal return from the ocean surface at 58.5 μs. Figure 4.19 is a zoomed in plot of the ocean surface return.

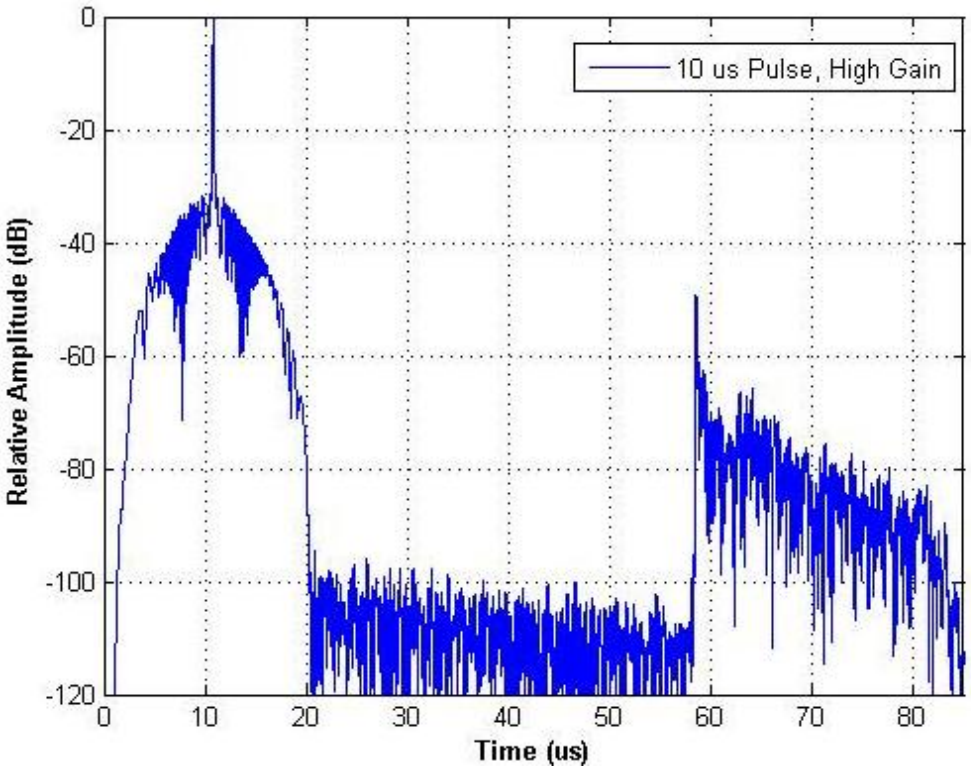


*Figure 4.18 - High Altitude Receiver Testing Over the Ocean in the High Gain Setting*

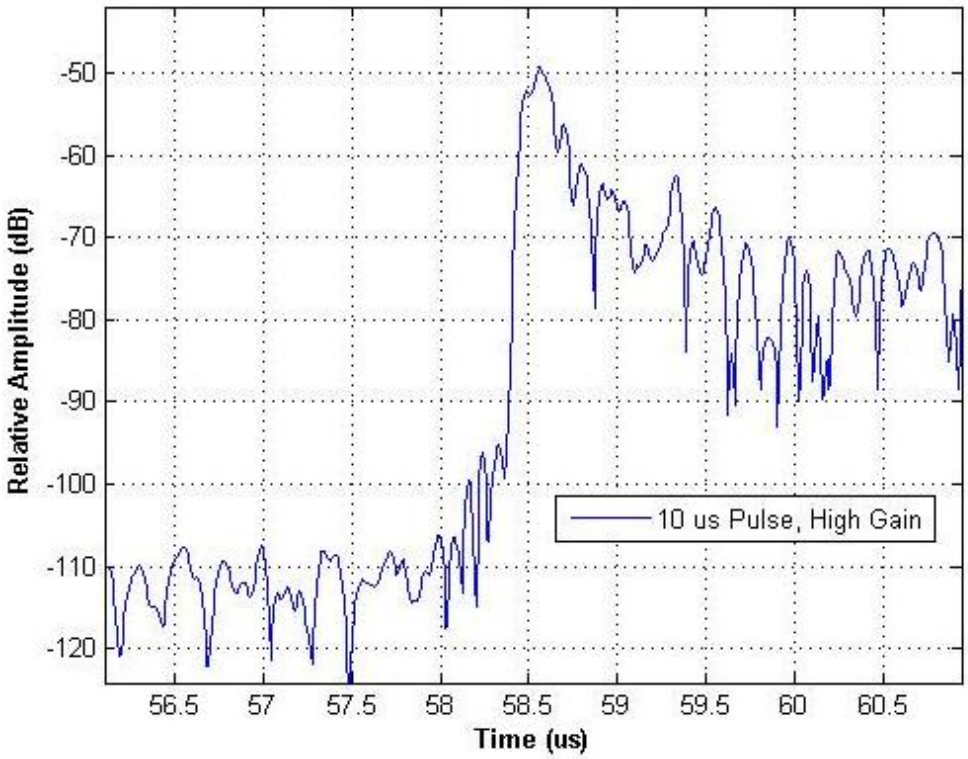


*Figure 4.19 - Ocean Surface Return of High Altitude Receiver Testing in the High Gain Setting*

# Chapter 5

## *Conclusion*

### *5.1 Conclusion*

A compact receiver module for the MCoRDS/I ice penetrating radar system was designed, simulated, implemented, and field tested. Design parameters for the receiver module was determined from the MCoRDS/I system by considering all possible operating conditions as well as taking into account future improvements of the system. The receiver chain was simulated using ADS and the measurements of the implemented design agree well with the simulation results. The receiver modules were integrated into the MCoRDS/I system on the P3 platform and tested in the field under typical operating conditions. These tests showed that the receiver modules operate properly and accomplished the design parameters.

### *5.2 Future Work*

Due to the short design cycle and unavailability of the MCoRDS/I system for testing in the lab, extensive testing of the receiver modules when integrated inside the NI PXI chassis was unable to be done. The MCoRDS/I system is very sensitive to noise due to the very small signals that are being captured and any noise from the receiver modules will

degrade the performance of the system. There are two main sources that could contribute to increased noise output of the receiver modules should it arise: the DC power supply input and EMI radiation coupling onto the receiver channels. To mitigate the EMI radiation, a copper shield was soldered to the receiver modules but definitive testing was not able to be done to quantify their effectiveness. Noise from the power supply input to the receiver modules is also a concern and testing should be done to ensure that if the backplane power from the NI system is used that it does not affect the noise performance of the receiver modules. If the NI power supply increases the noise of the receiver modules, an external power supply can be implemented. This external supply should have very low conducted noise power. The cabling of the external power supply should also be tested as proper shielding of the power supply cables may lower the noise output of the receiver module.

## References


[1] Julian A. Dowdeswell. “The Greenland Ice Sheet and Global Sea-Level Rise.” *Science*, Vol. 311, (2006:963-964)

[2] B. Douglas and W.R. Peltier.”The Puzzle of Global Sea-Level Rise.” *Physics Today*. pp. 35-40, March 2002.

[3] B. Douglas, M. Kearney and S. Leatherman. “Sea Level Rise: History and Consequences.” *International Geophysics Series*, Vol. 75, Academic Press: Sandiego, CA. 2001.

[4] T. Yoshino. "The Reflection Properties of Radio Waves on the Ice Cap." Antennas and Propagation, IEEE Transactions on, vol.15, no.4, pp. 542- 551, Jul 1967

[5] H. Johnson and M Graham. High-Speed Digital Design: A Handbook of Black Magic. Upper Saddle River, NJ: Prentice Hall. 1993

# *APPENIDX A*

## *RF Test Board Schematic and Layout*

# RF TEST BOARD

| REV | WHO | WHEN | WHAT |
|---|---|---|---|
| 1 | ARA | 11/10/2011 | INITIAL RF TEST BOARD DESIGN |
| | | | |
| | | | |
| | | | |
| | | | |
| | | | |

## Board Stackup - 6 Layer - 6/6

FR-4: er = 4.5

| | | |
|---|---|---|
| Layer 1 = Route = 0.7 mil - 0.5 oz Copper | RF routing | 50 ohm = 15 mil |
| 8.4 Mil Prepreg | | |
| Layer 2 = Plane = 1.4 mil - 1 oz Copper | Ground Plane | |
| 16.8 Mil Core | | |
| Layer 3 = Route = 1.4 mil - 1 oz Copper | RF routing | 50 ohm = 7 mil |
| 7.4 Mil Prepreg | | |
| Layer 4 = Plane = 1.4 mil - 1 oz Copper | Ground Plane | |
| 16.8 Mil Core | | |
| Layer 5 = Plane = 1.4 mil - 1 oz Copper | Power Plane | |
| 8.4 Mil Prepreg | | |
| Layer 6 = Route = 0.7 mil - 0.5 oz Copper | Digital Routing | |

CReSIS - University of Kansas
2335 Irving Hill Rd.
Lawrence, KS 66045
(785) 864-4390
http://www.cresis.ku.edu/

CReSIS

| | |
|---|---|
| Project: | MCoRDS NI COMPACT RECEIVER |
| Engineer: | Austin Arnett |
| Date: 6/7/2012 12:53:49 AM | Sheet: 1/5 |

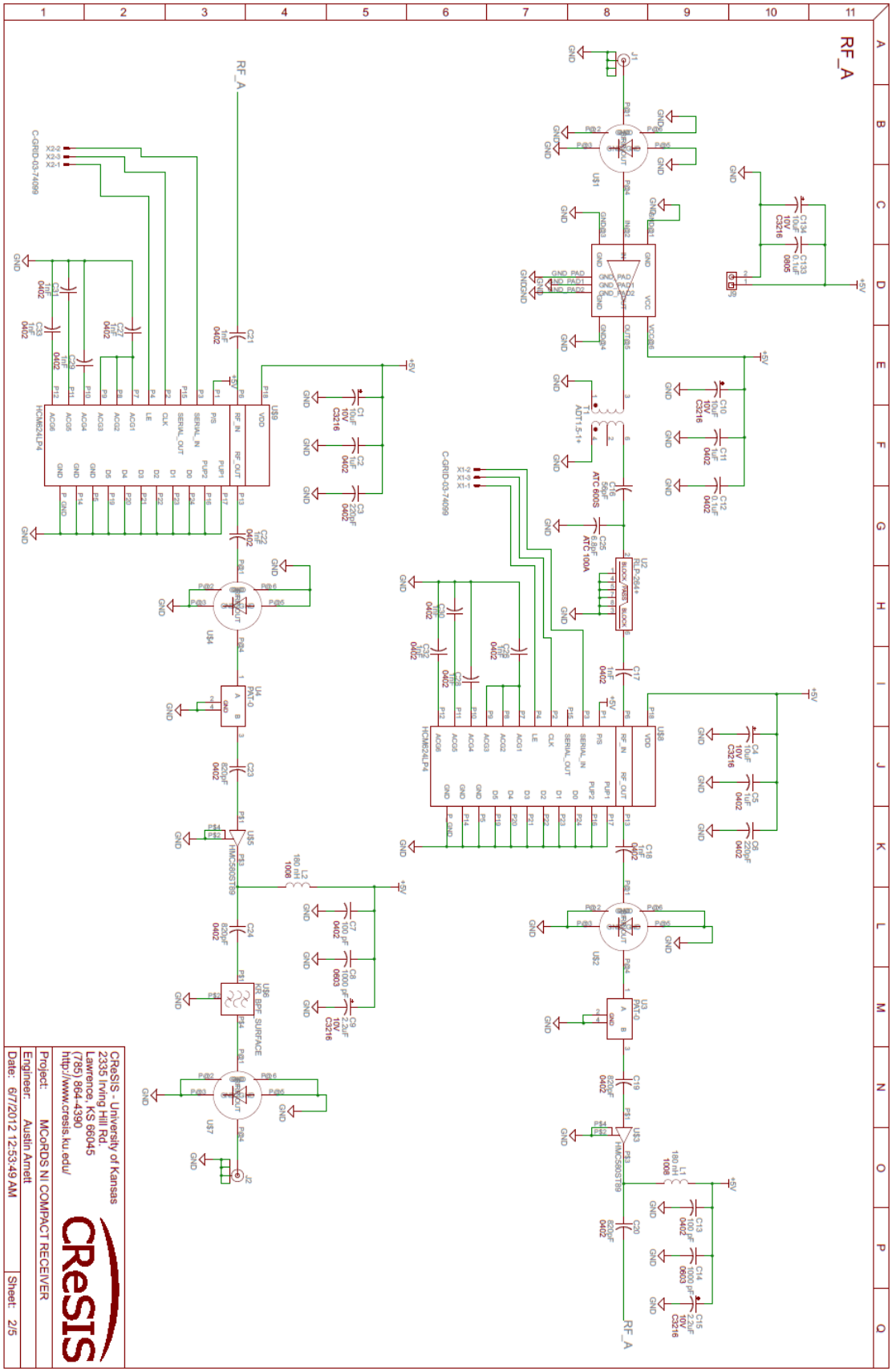
RF_A
CReSIS - University of Kansas
2335 Irving Hill Rd.
Lawrence, KS 66045
(785) 864-4390
http://www.cresis.ku.edu/
Project: MCoRDS NI COMPACT RECEIVER
Engineer: Austin Arnett
Date: 6/7/2012 12:53:49 AM
Sheet: 2/5

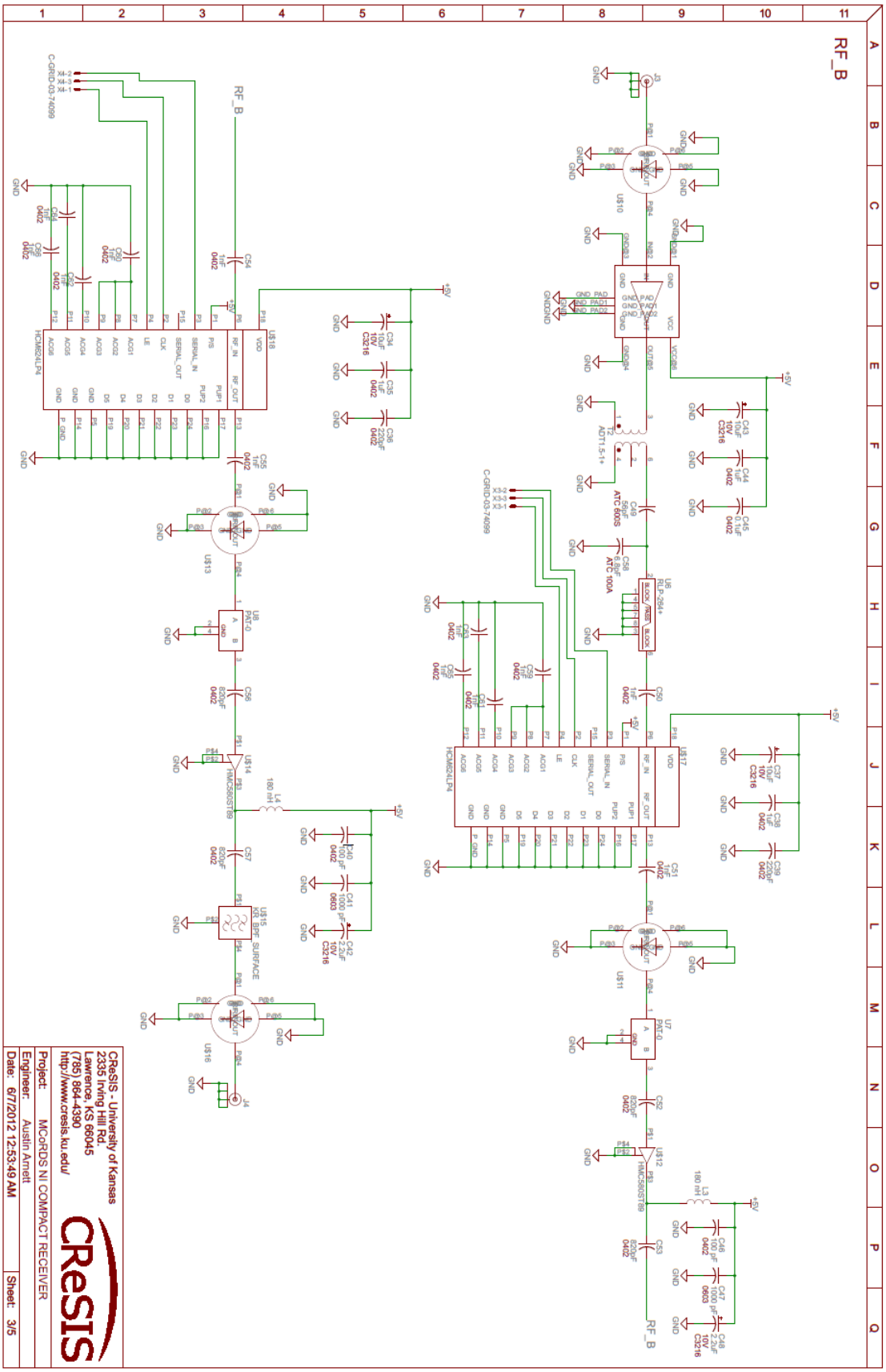
CReSIS - University of Kansas
2335 Irving Hill Rd.
Lawrence, KS 66045
(785) 864-4390
http://www.cresis.ku.edu/
CReSIS
Project: MCoRDS NI COMPACT RECEIVER
Engineer: Austin Arnett
Date: 6/7/2012 12:53:49 AM
Sheet: 3/5

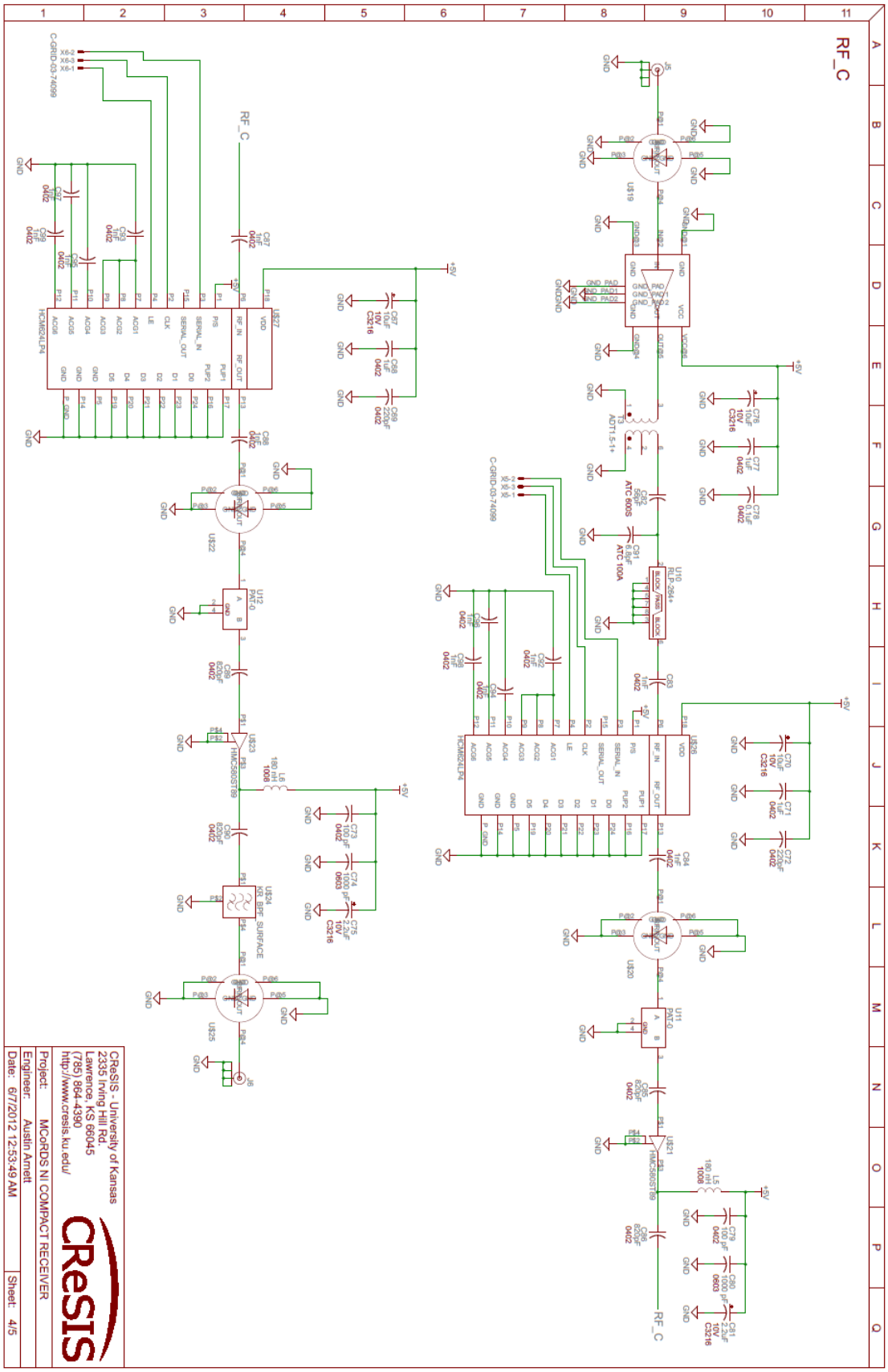
RF_C
CReSIS - University of Kansas
2335 Irving Hill Rd.
Lawrence, KS 66045
(785) 864-4390
http://www.cresis.ku.edu/
CReSIS
Project: MCoRDS NI COMPACT RECEIVER
Engineer: Austin Arnett
Date: 6/7/2012 12:53:49 AM
Sheet: 4/5

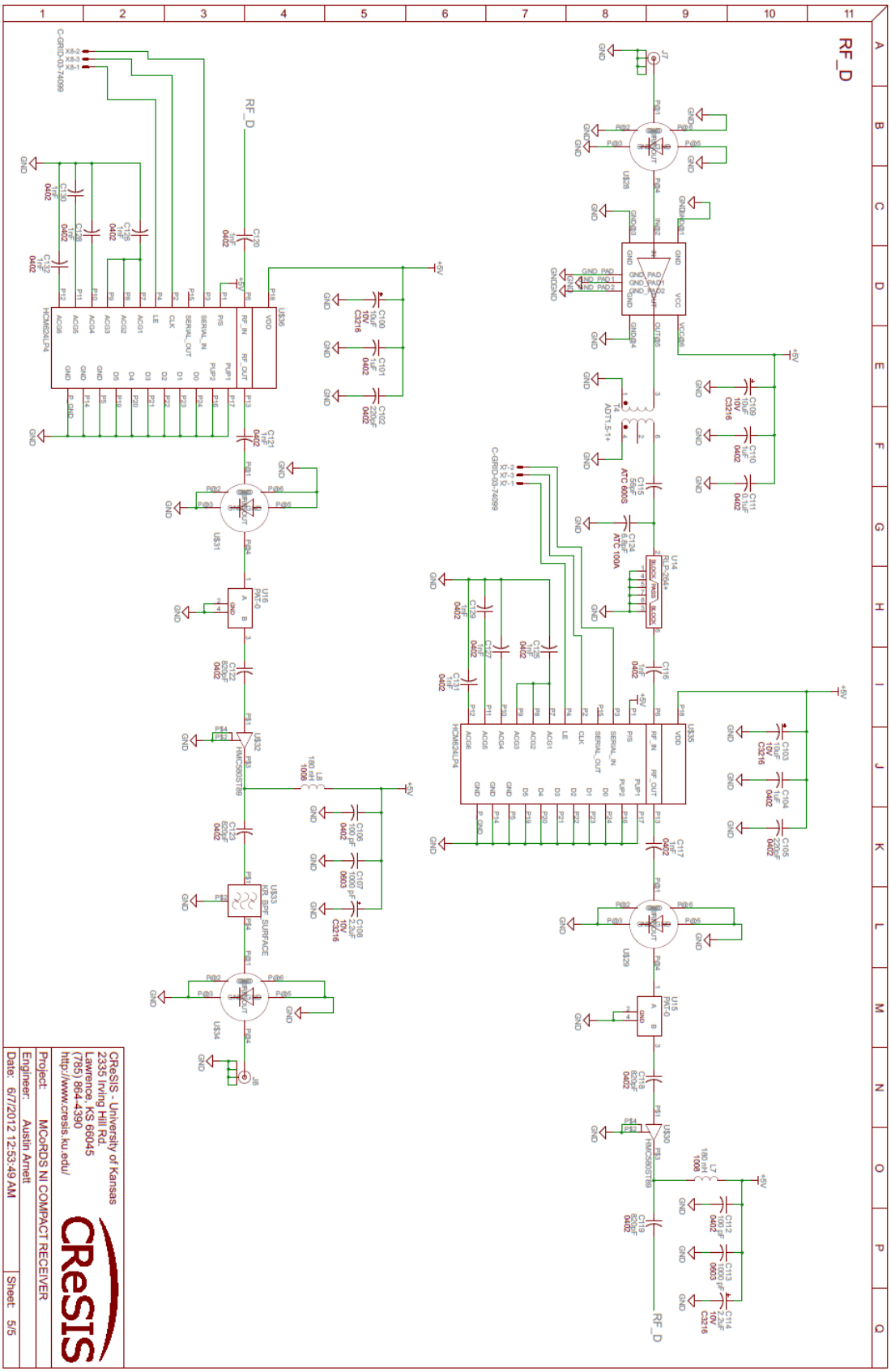
RF_D
CReSIS - University of Kansas
2335 Irving Hill Rd.
Lawrence, KS 66045
(785) 864-4390
http://www.cresis.ku.edu/
CReSIS
Project: MCoRDS NI COMPACT RECEIVER
Engineer: Austin Arnett
Date: 6/7/2012 12:53:49 AM
Sheet: 5/5

## *Layer 1 – RF Routing*

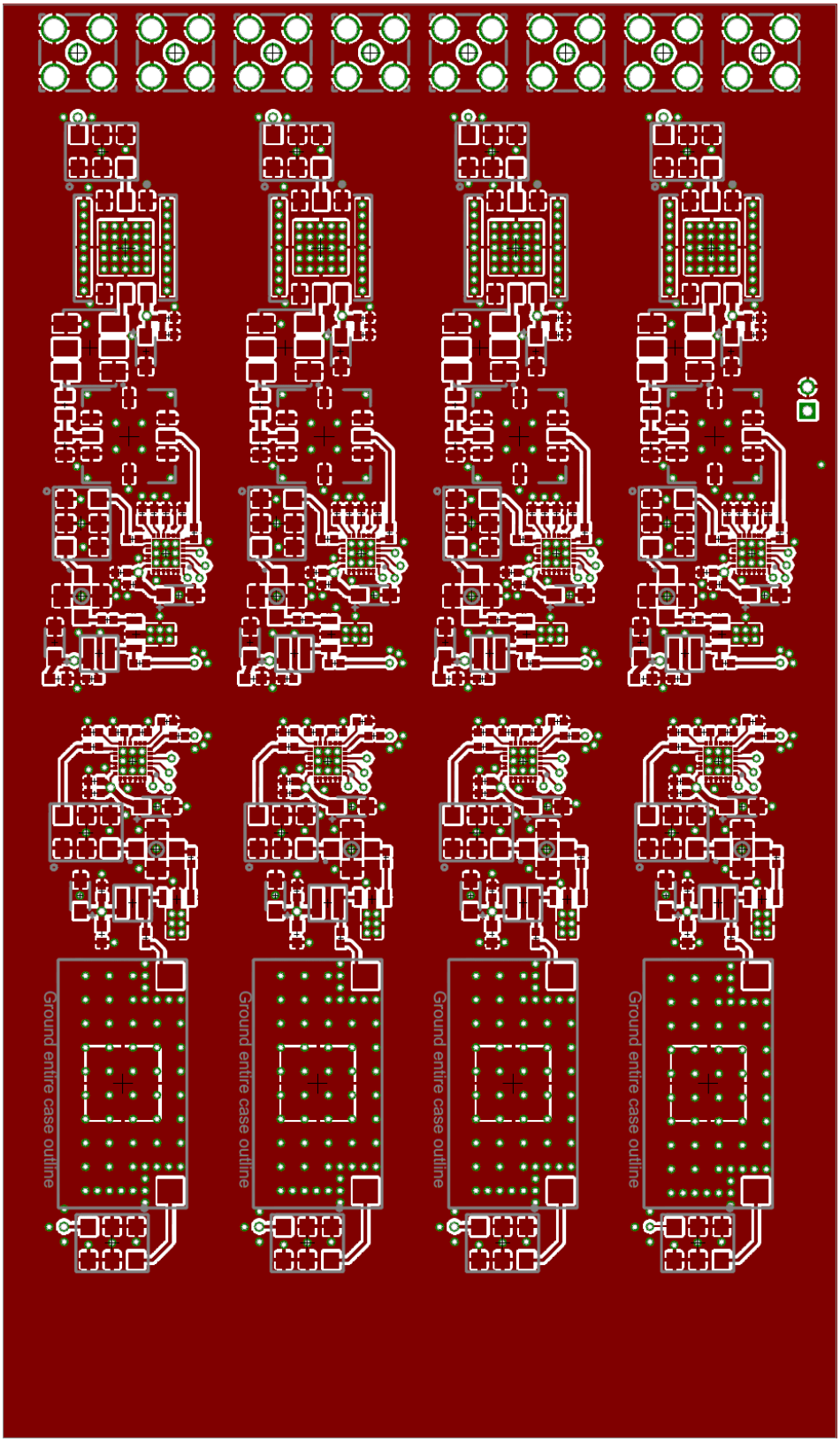

## *Layer 2 – Ground Plane*

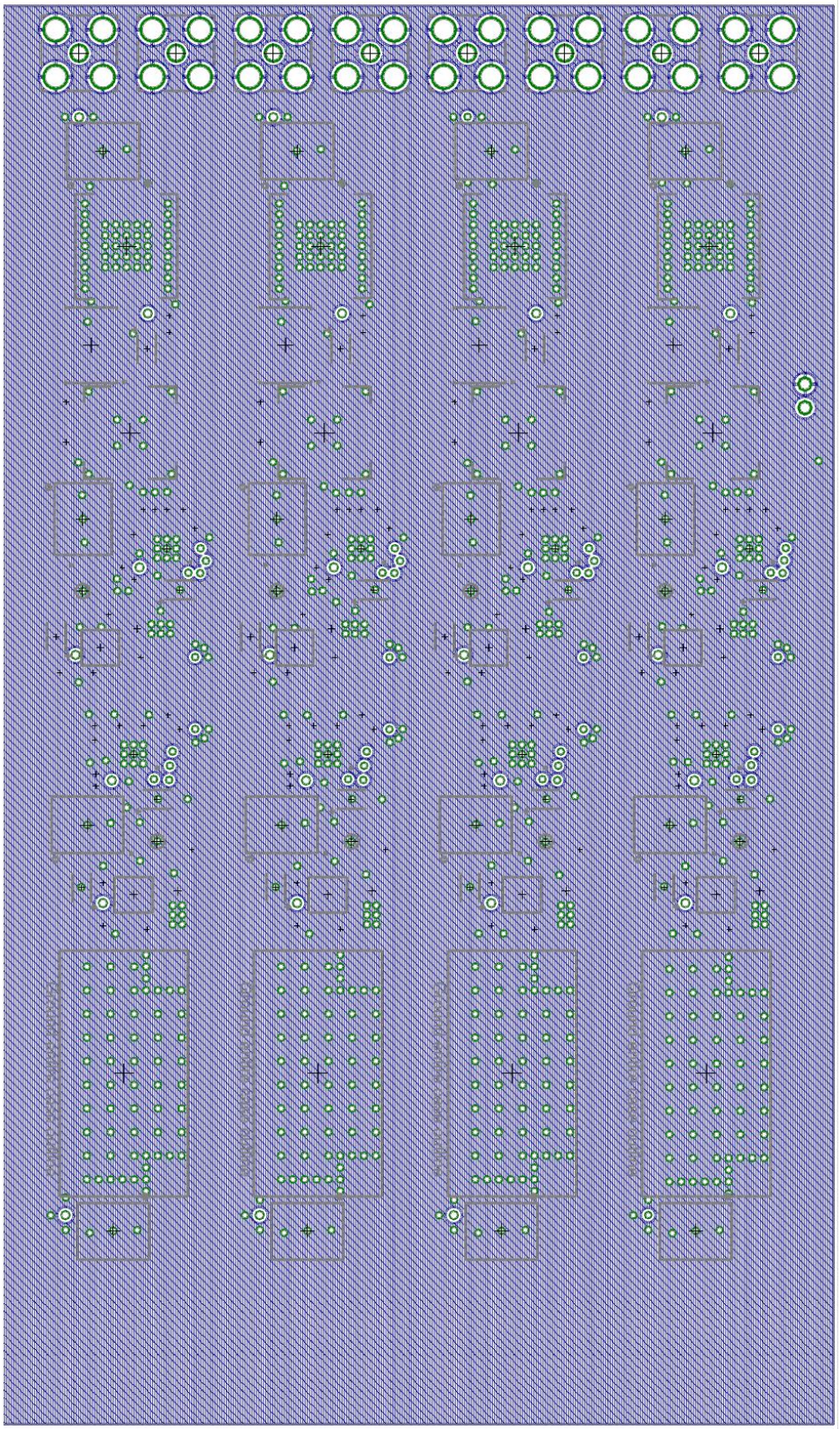

## *Layer 3 – RF Routing*

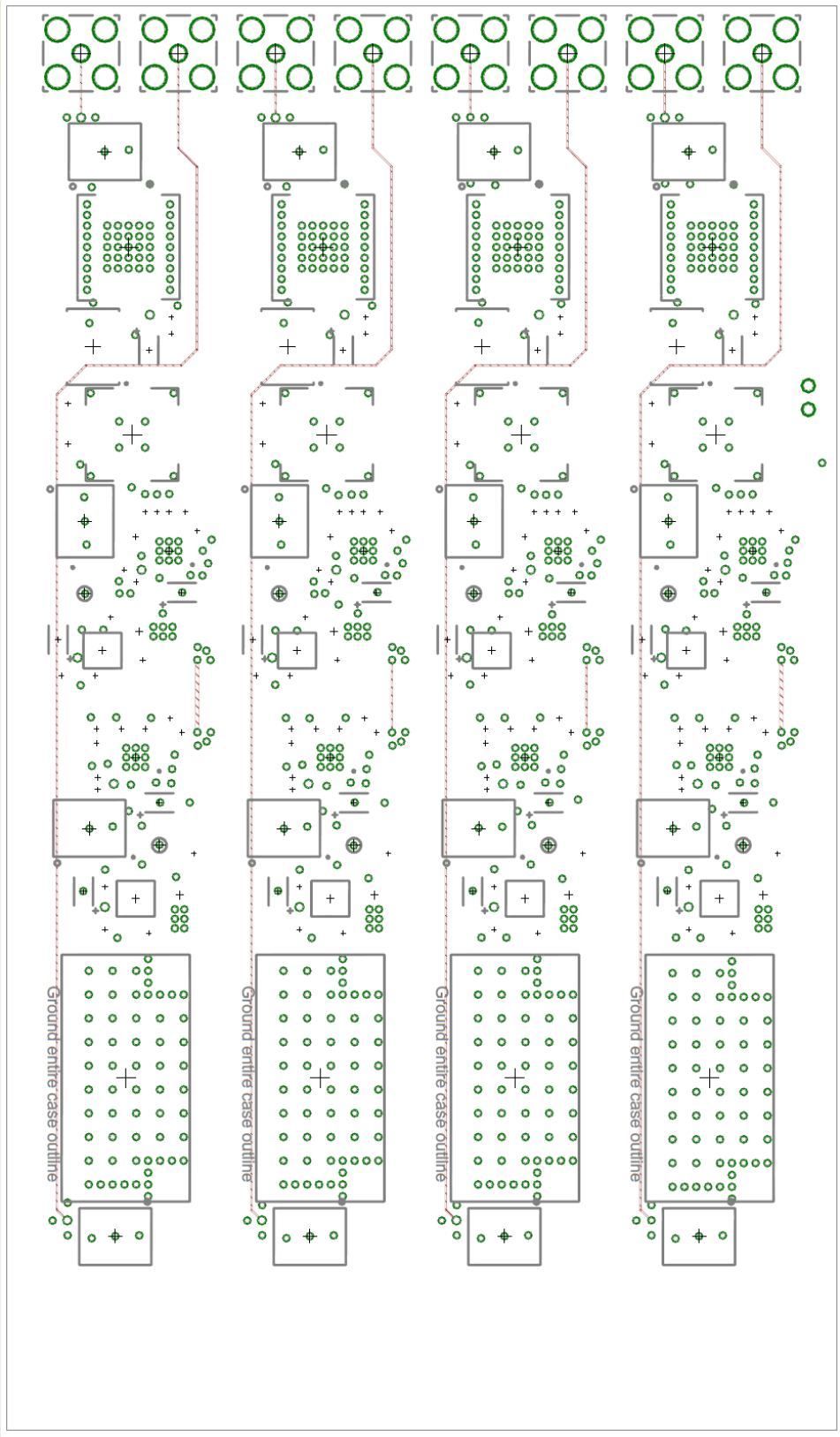

## *Layer 4 – Ground Plane*

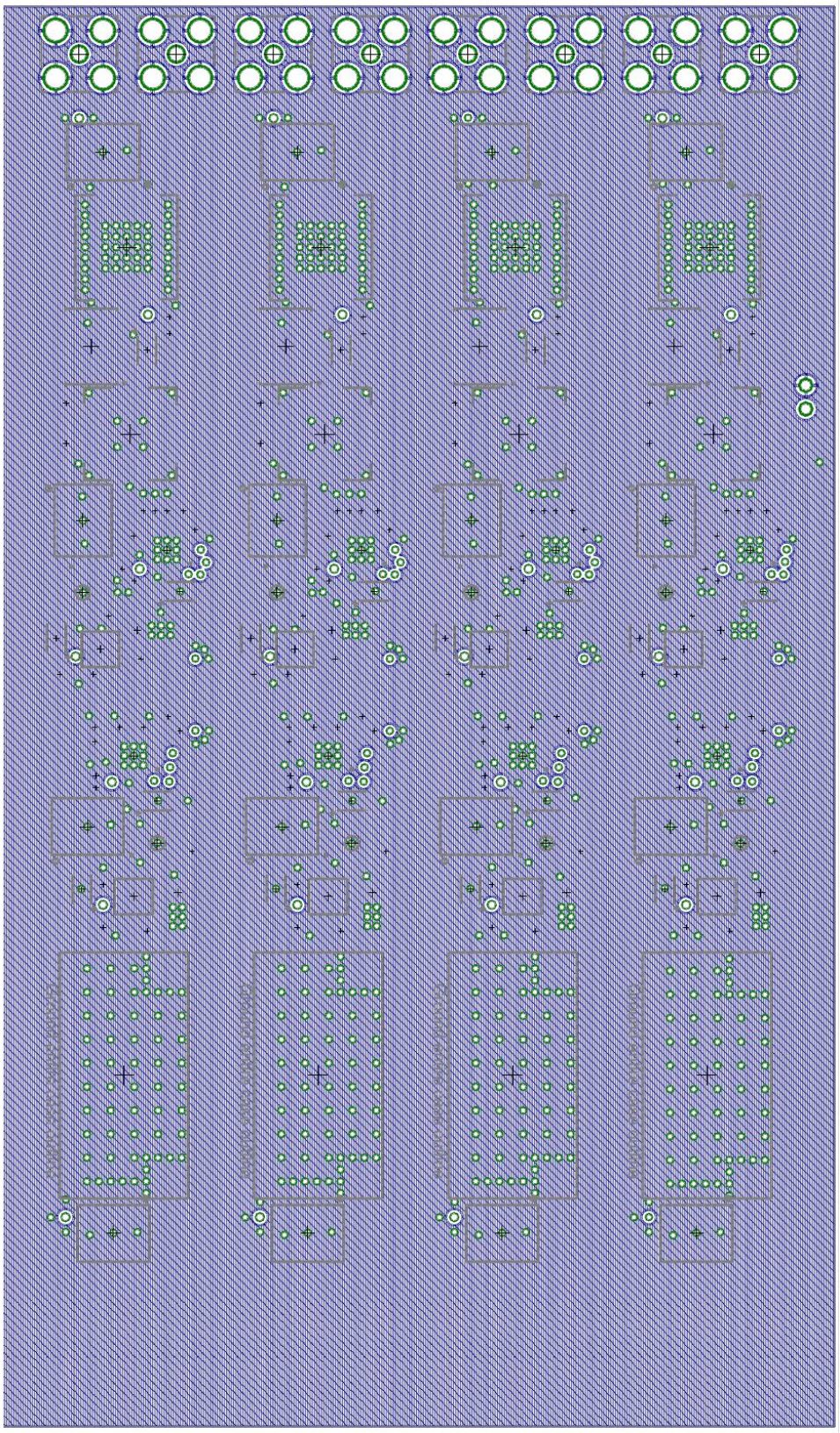

## *Layer 5 – 5V Power Plane*

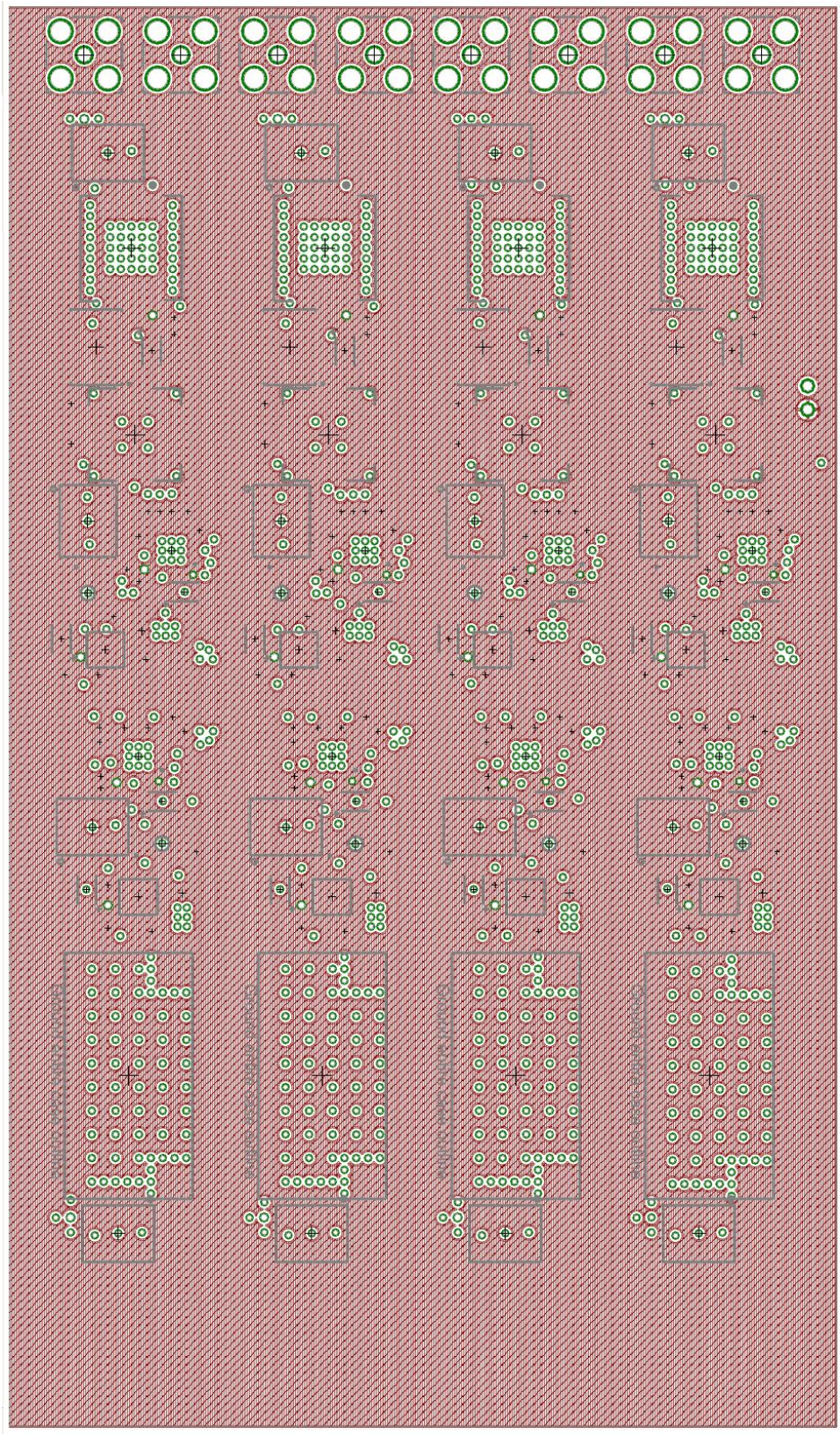

## *Layer 6 – Digital Routing*

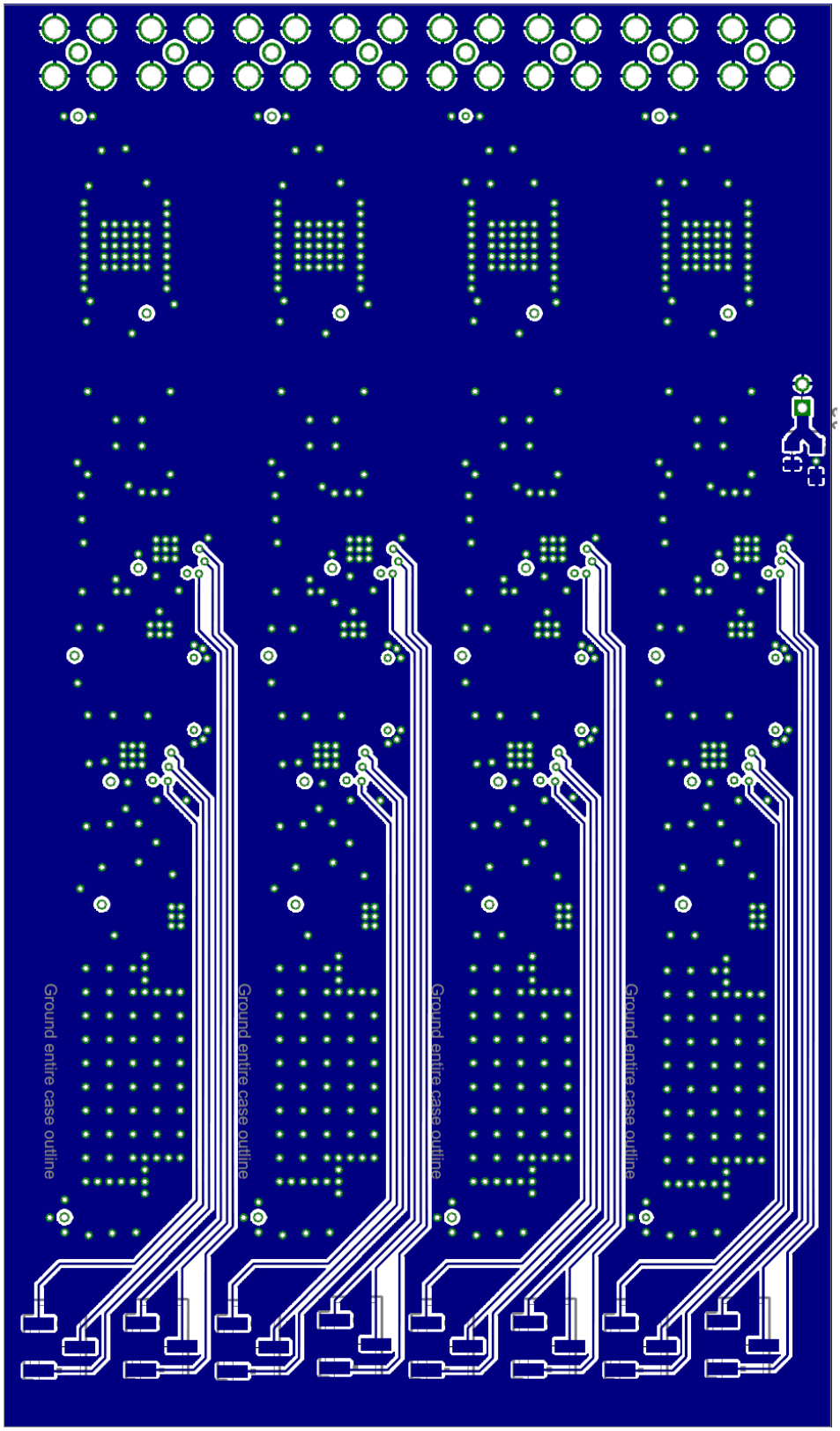

# *Appendix B*

## *Final Receiver Module Design Schematic, Layout, and Photos*

# NI MCORDS COMPACT RECEIVER MODULE

| REV | WHO | WHEN | WHAT |
|---|---|---|---|
| 1 | ARA | 11/10/2011 | INITIAL RF TEST BOARD DESIGN |
| 2 | ARA | 11/30/2011 | ADD DIGITAL SECTION, MITER RF ROUTING |
| 3 | ARA | 12/12/2011 | REMOVE FENCE BETWEEN RX CHAINS, MOVE ALL RF ROUTING TO TOP LAYER |
| 4 | ARA | 1/8/2012 | MAKE SEPERATE POWER PLANES FOR RF POWER |
| 5 | ARA | 1/18/2012 | ADD BOARD SELECTOR SWITCH, MOVE MOUNTING HOLE UP, ADD +5v TO JTAG CONNECTOR |

## Board Stackup - 6 Layer - 6/6 FR-4: er = 4.5

| | | |
|---|---|---|
| Layer 1 = Route = 0.7 mil - 0.5 oz Copper | RF routing | 50 ohm = 15 mil |
| 8.4 Mil Prepreg | | |
| Layer 2 = Plane = 1.4 mil - 1 oz Copper | Ground Plane | |
| 16.8 Mil Core | | |
| Layer 3 = Route = 1.4 mil - 1 oz Copper | RF routing | 50 ohm = 7 mil |
| 7.4 Mil Prepreg | | |
| Layer 4 = Plane = 1.4 mil - 1 oz Copper | Ground Plane | |
| 16.8 Mil Core | | |
| Layer 5 = Plane = 1.4 mil - 1 oz Copper | Power Plane | |
| 8.4 Mil Prepreg | | |
| Layer 6 = Route = 0.7 mil - 0.5 oz Copper | Digital Routing | |

CReSIS - University of Kansas
2335 Irving Hill Rd.
Lawrence, KS 66045
(785) 864-4390
http://www.cresis.ku.edu/

CReSIS

Project: MCoRDS NI Compact Receiver
Engineer: Austin Arnett
Date: 6/7/2012 12:16:33 AM
Sheet: 1/7

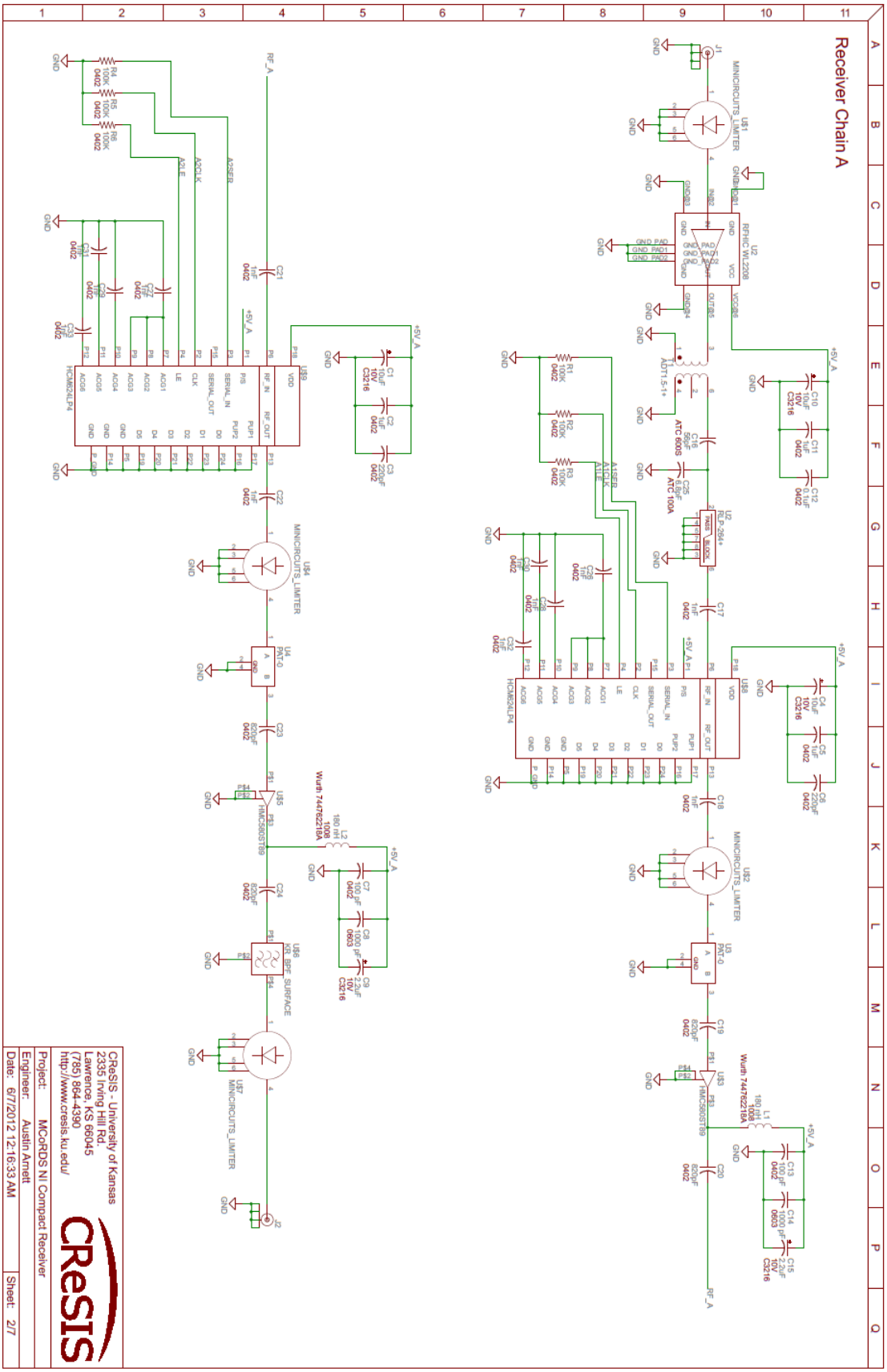
Receiver Chain A
CReSIS - University of Kansas
2335 Irving Hill Rd.
Lawrence, KS 66045
(785) 864-4390
http://www.cresis.ku.edu/
Project: MCoRDS NI Compact Receiver
Engineer: Austin Arnett
Date: 6/7/2012 12:16:33 AM
Sheet: 2/7

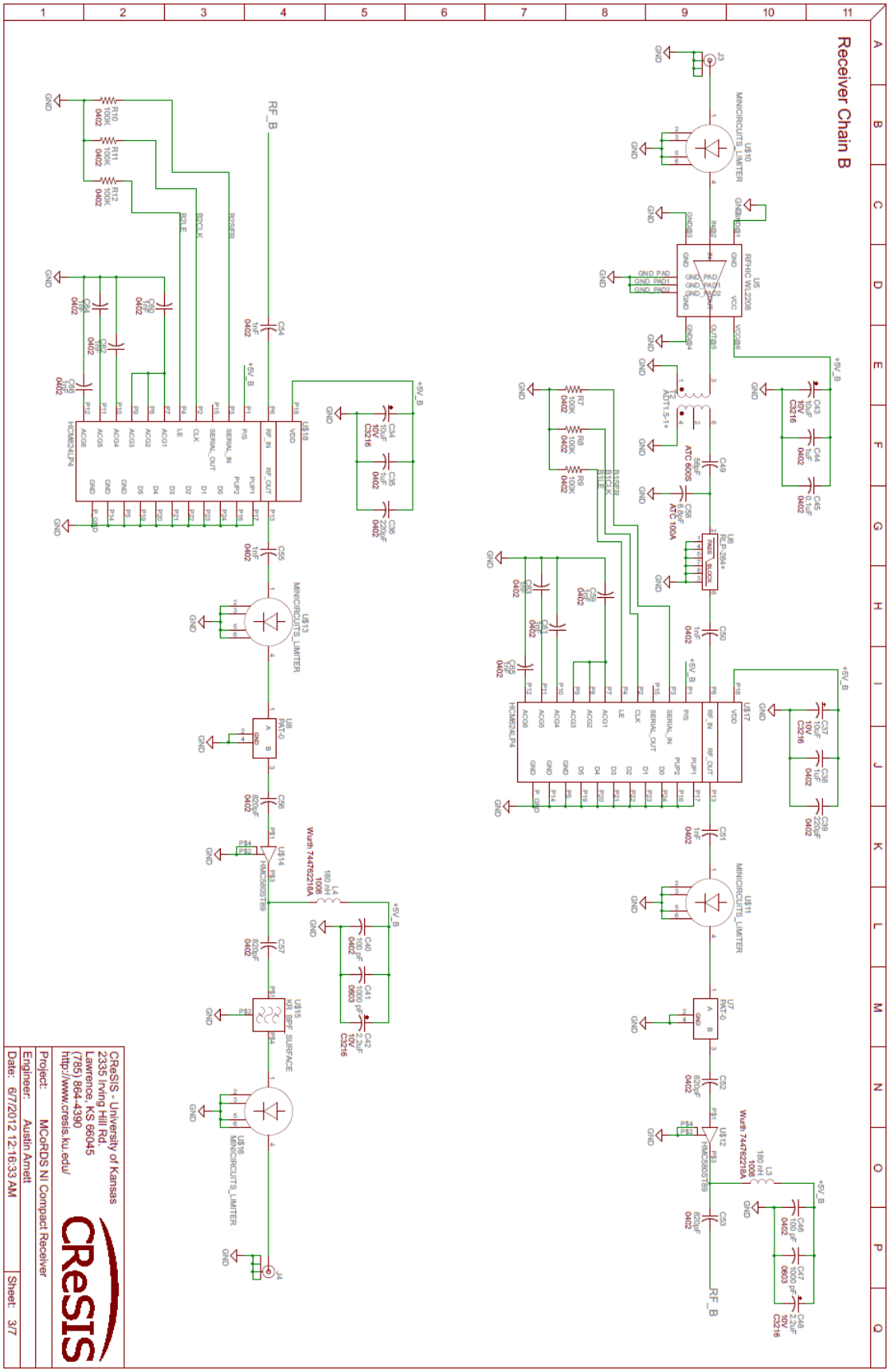
Receiver Chain B
CReSIS - University of Kansas
2335 Irving Hill Rd
Lawrence, KS 66045
(785) 864-4390
http://www.cresis.ku.edu/
CReSIS
Project: MCoRDS NI Compact Receiver
Engineer: Austin Arnett
Date: 6/7/2012 12:16:33 AM
Sheet: 3/7

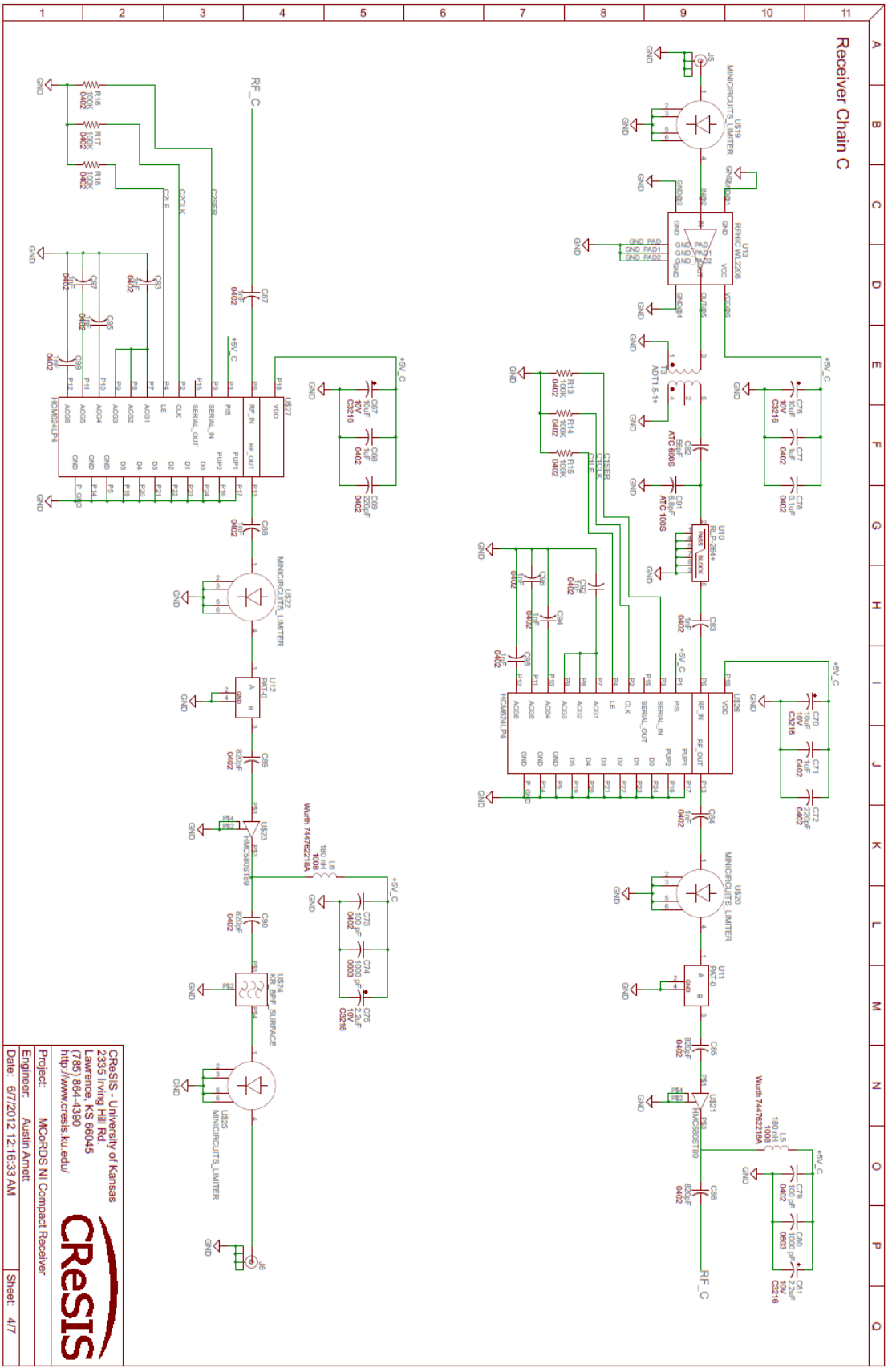
Receiver Chain C
CReSIS - University of Kansas
2335 Irving Hill Rd.
Lawrence, KS 66045
(785) 864-4390
http://www.cresis.ku.edu/
Project: MCoRDS NI Compact Receiver
Engineer: Austin Arnett
Date: 6/7/2012 12:16:33 AM
Sheet: 4/7
RF_C
+5V_C
GND

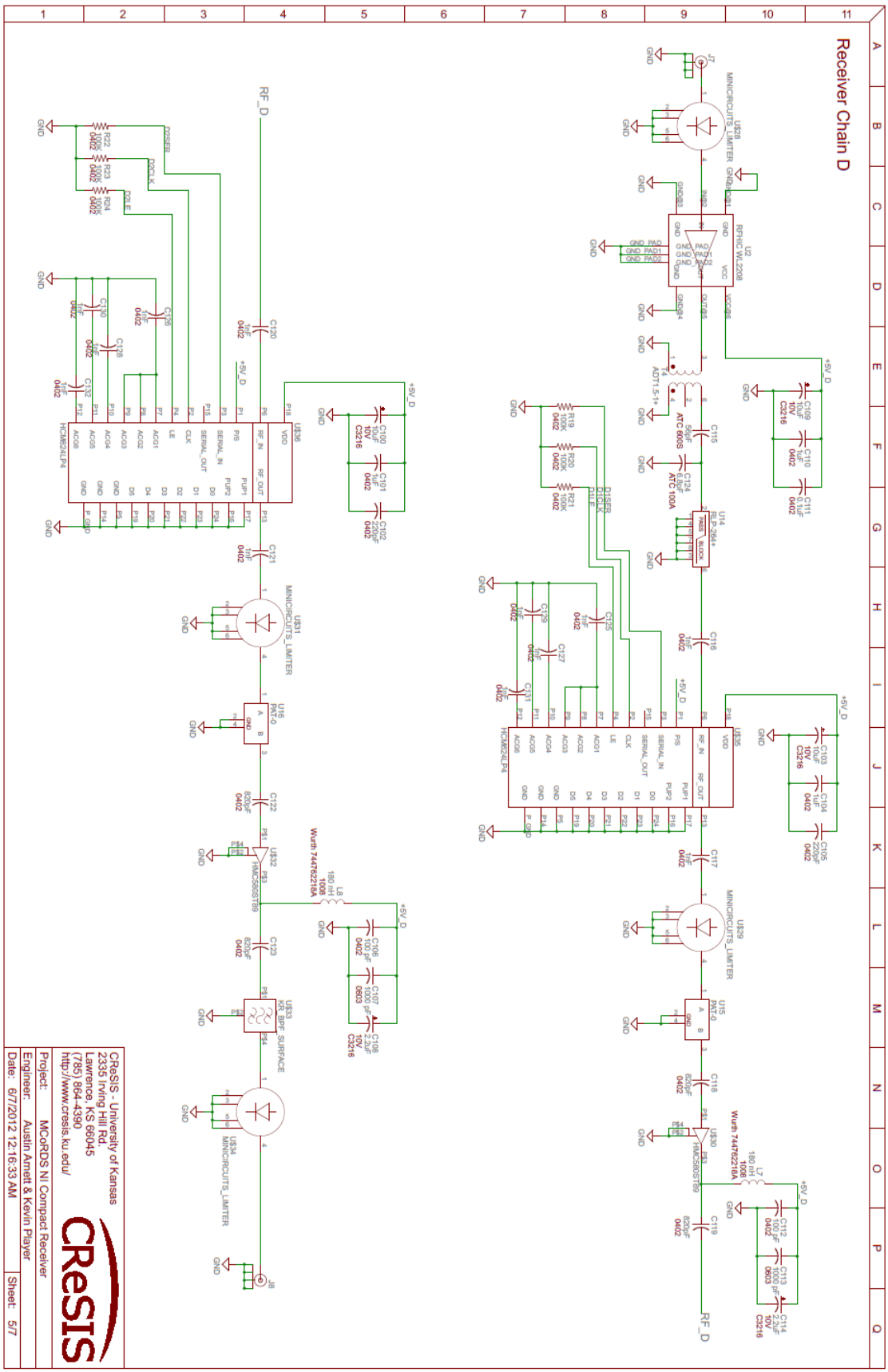
Receiver Chain D
CReSIS - University of Kansas
2335 Irving Hill Rd.
Lawrence, KS 66045
(785) 864-4390
http://www.cresis.ku.edu/
Project: MCoRDS NI Compact Receiver
Engineer: Austin Arnett & Kevin Player
Date: 6/7/2012 12:16:33 AM
Sheet: 5/7
RF_D
+5V_D
GND

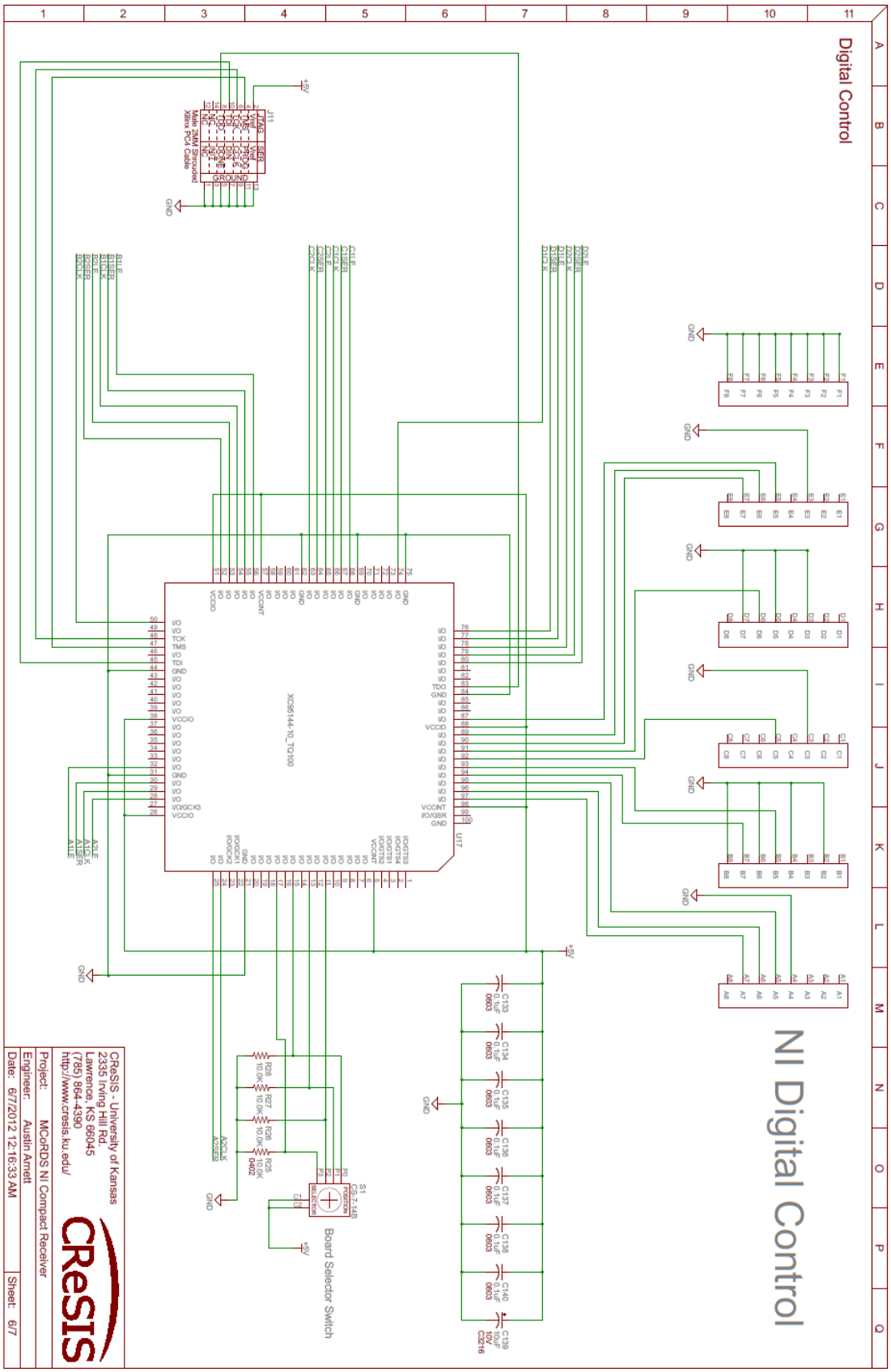
Digital Control
NI Digital Control
Board Selector Switch
CReSIS - University of Kansas
2335 Irving Hill Rd.
Lawrence, KS 66045
(785) 864-4390
http://www.cresis.ku.edu/
Project: MCoRDS NI Compact Receiver
Engineer: Austin Arnett
Date: 6/7/2012 12:16:33 AM
Sheet: 6/7

DC Power and Shielding

## Aux Power Input

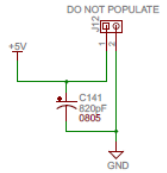


## NI Power Filter

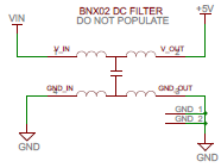


## RF Power Filters

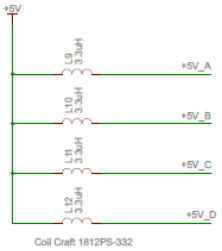


Coil Craft 1812PS-332

## EMI Shield Pads

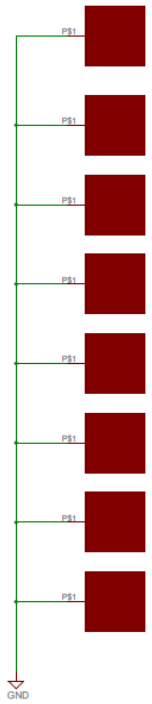


## NI Power Input

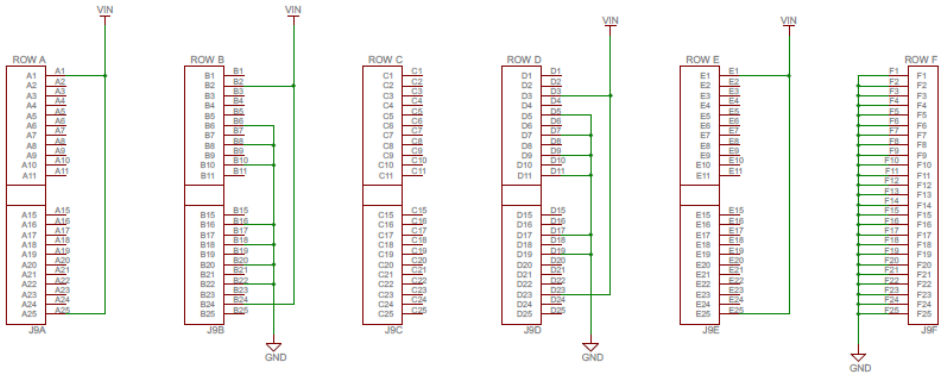



CReSIS - University of Kansas
2335 Irving Hill Rd.
Lawrence, KS 66045
(785) 864-4390
http://www.cresis.ku.edu/


| | |
|---|---|
| Project: | MCoRDS NI Compact Receiver |
| Engineer: | Austin Arnett |
| Date: 6/7/2012 12:16:33 AM | Sheet: 7/7 |

## *Layer 1 – RF Routing*

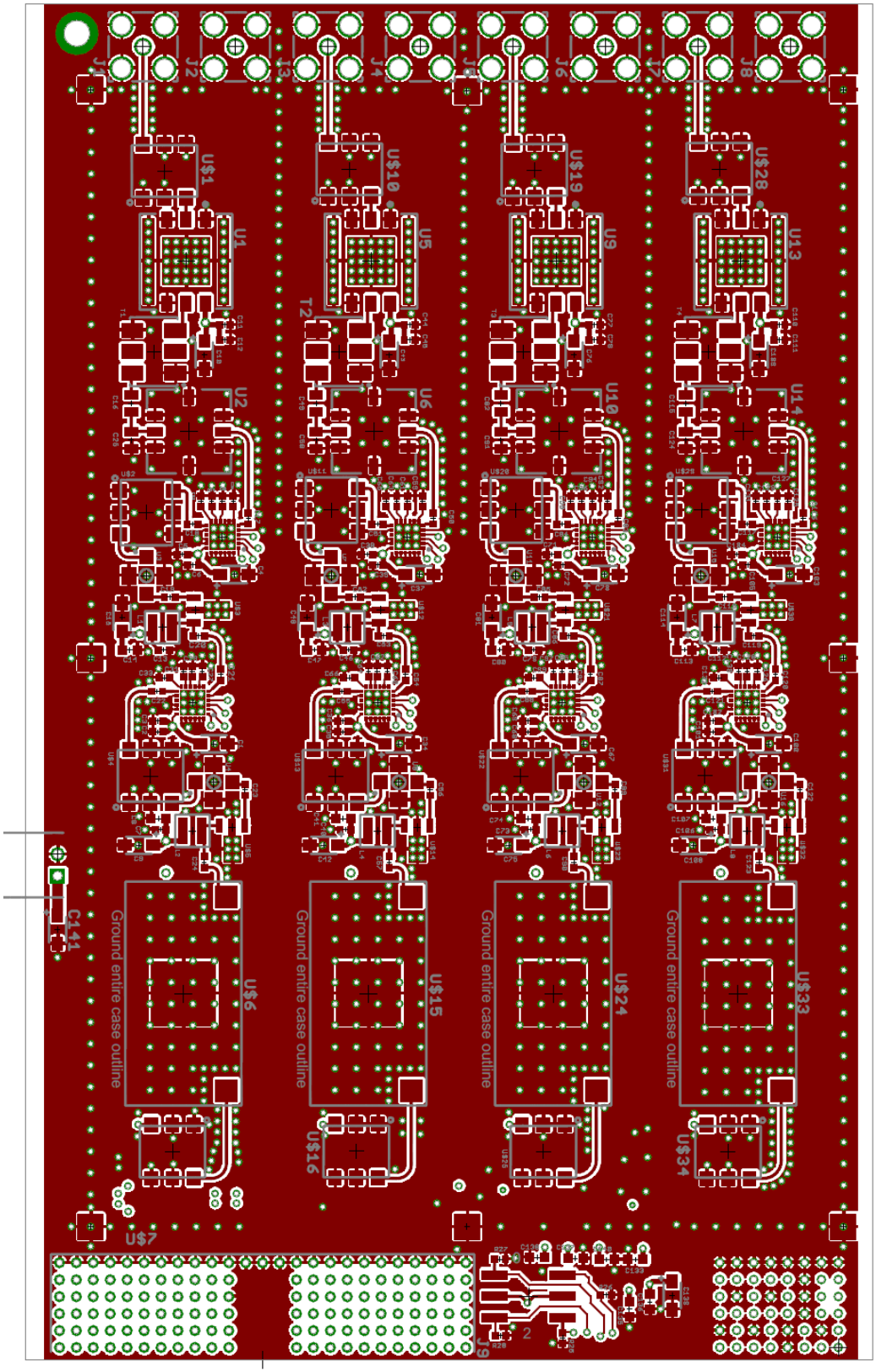

## *Layer 2 – Ground Plane*

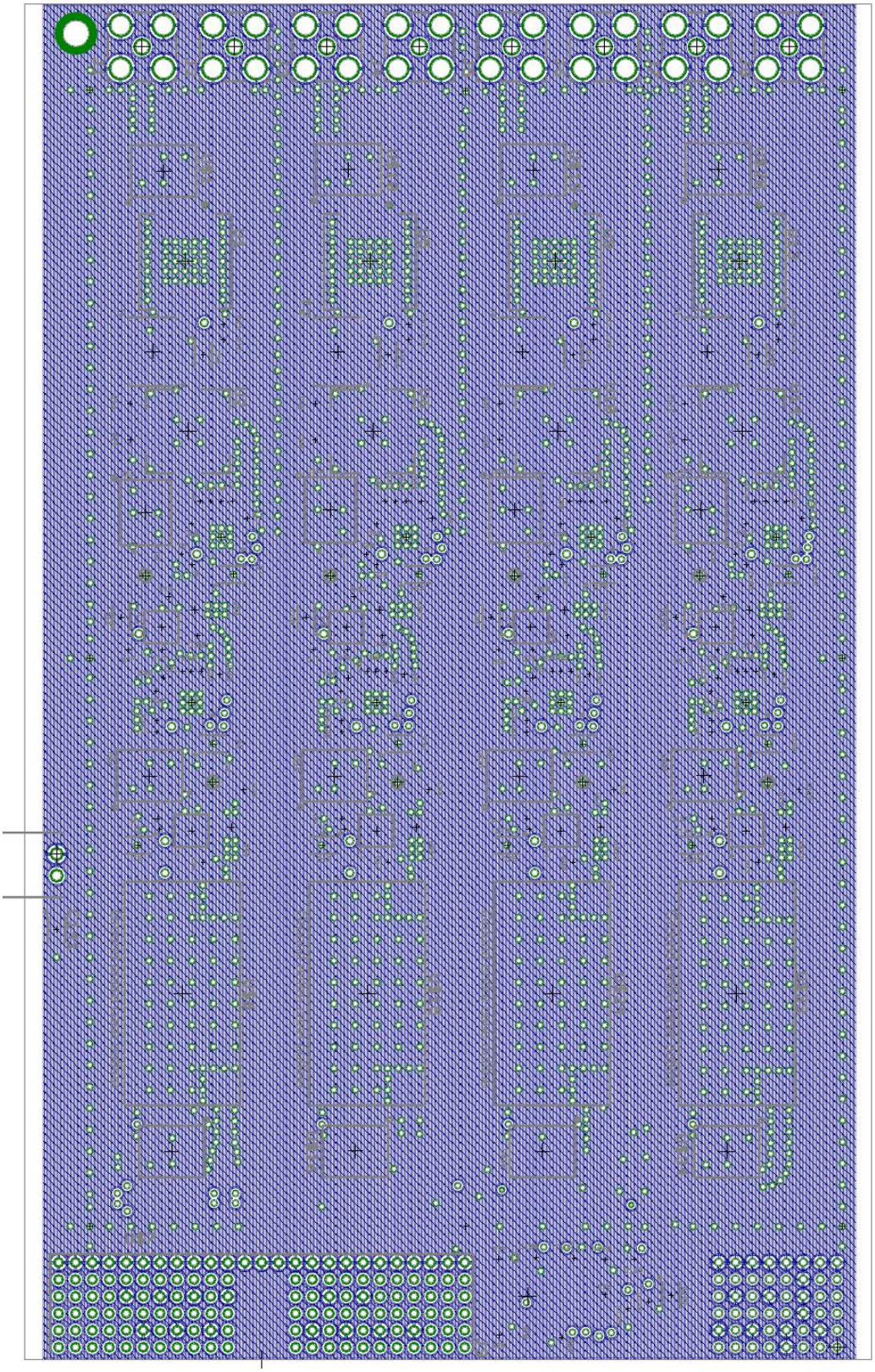

## *Layer 3 – RF Routing*

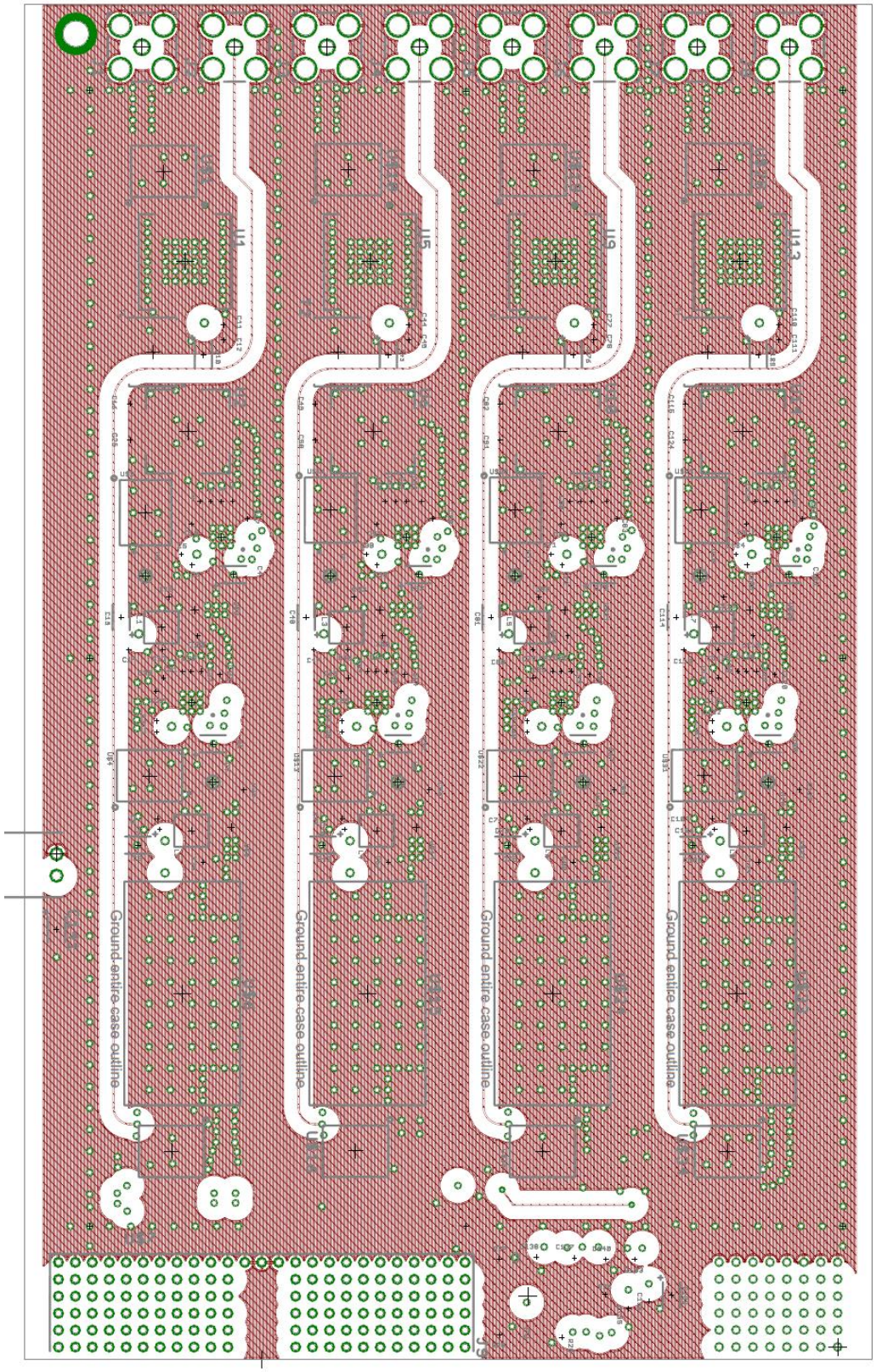

## *Layer 4 – Ground Plane*

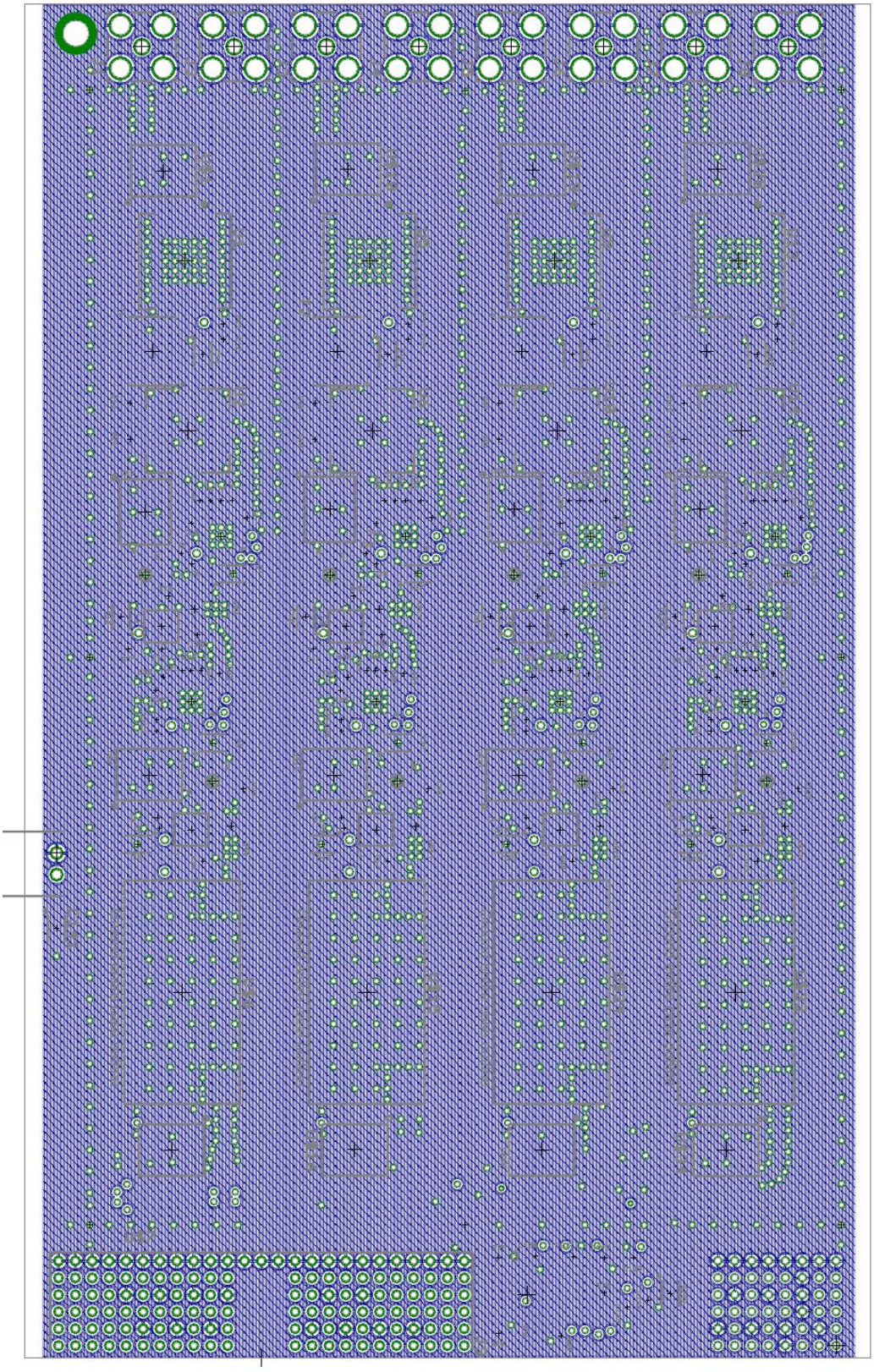

## *Layer 5 – 5 V Power Plane*

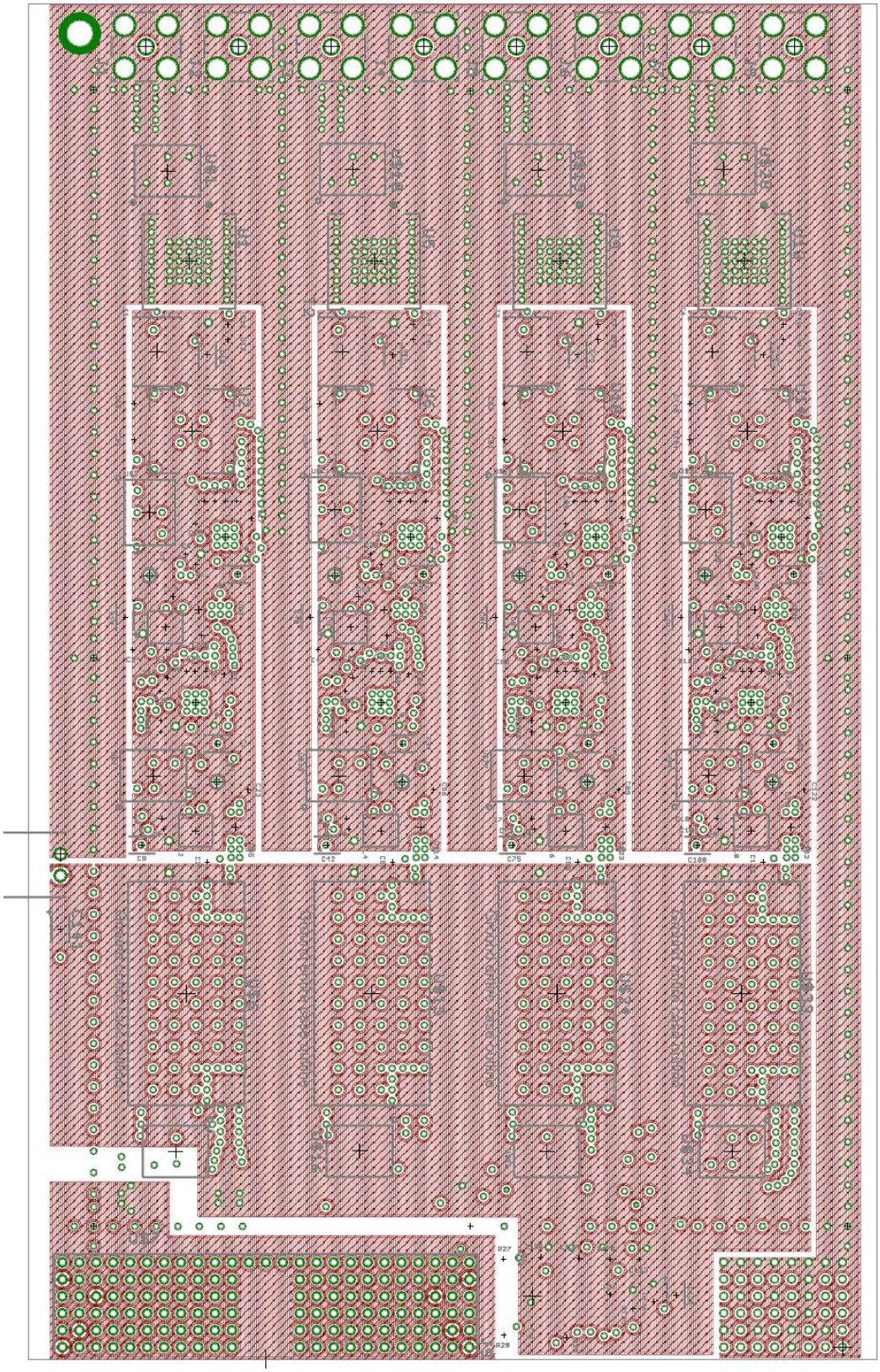

## *Layer 6 – Digital Routing*

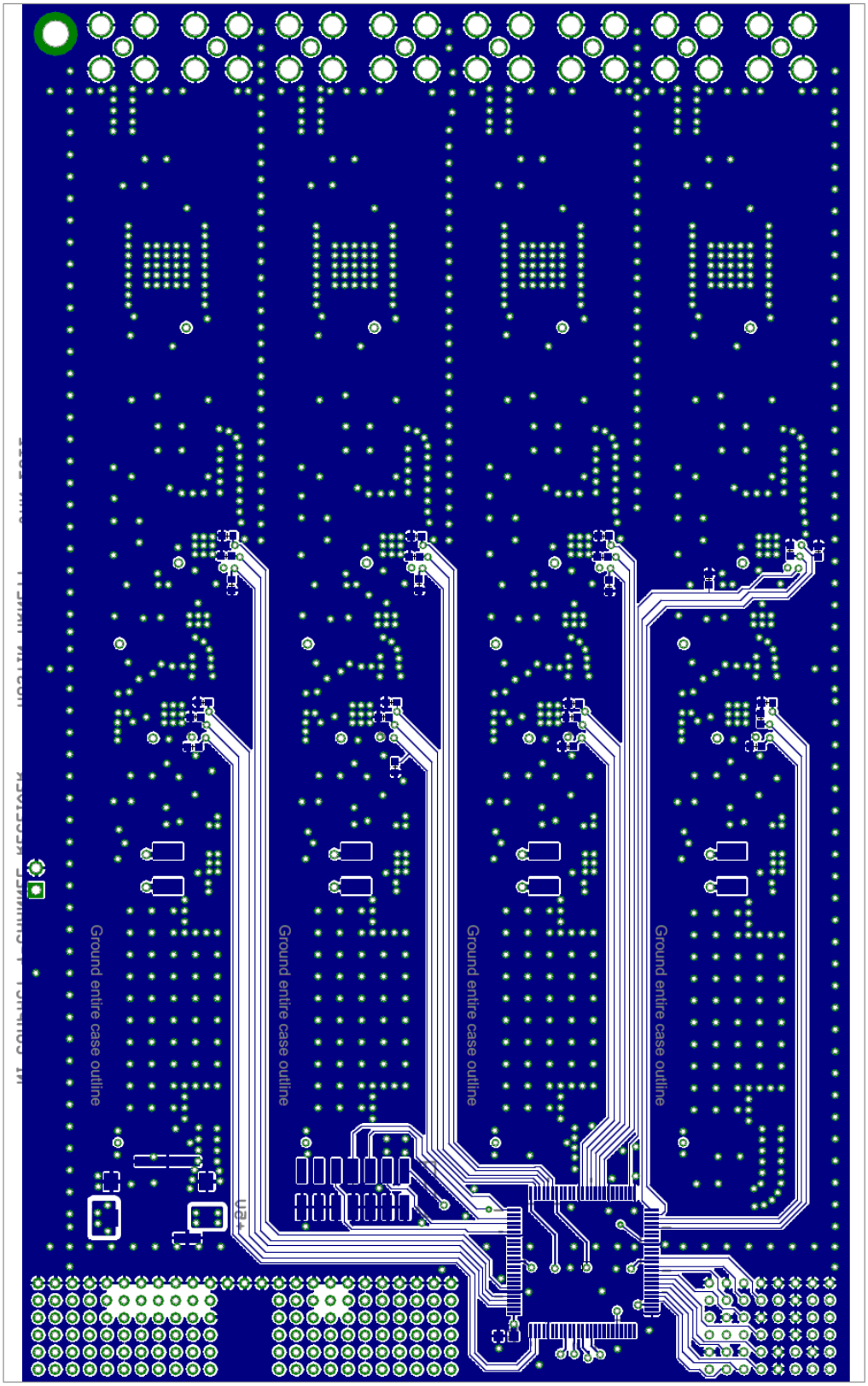

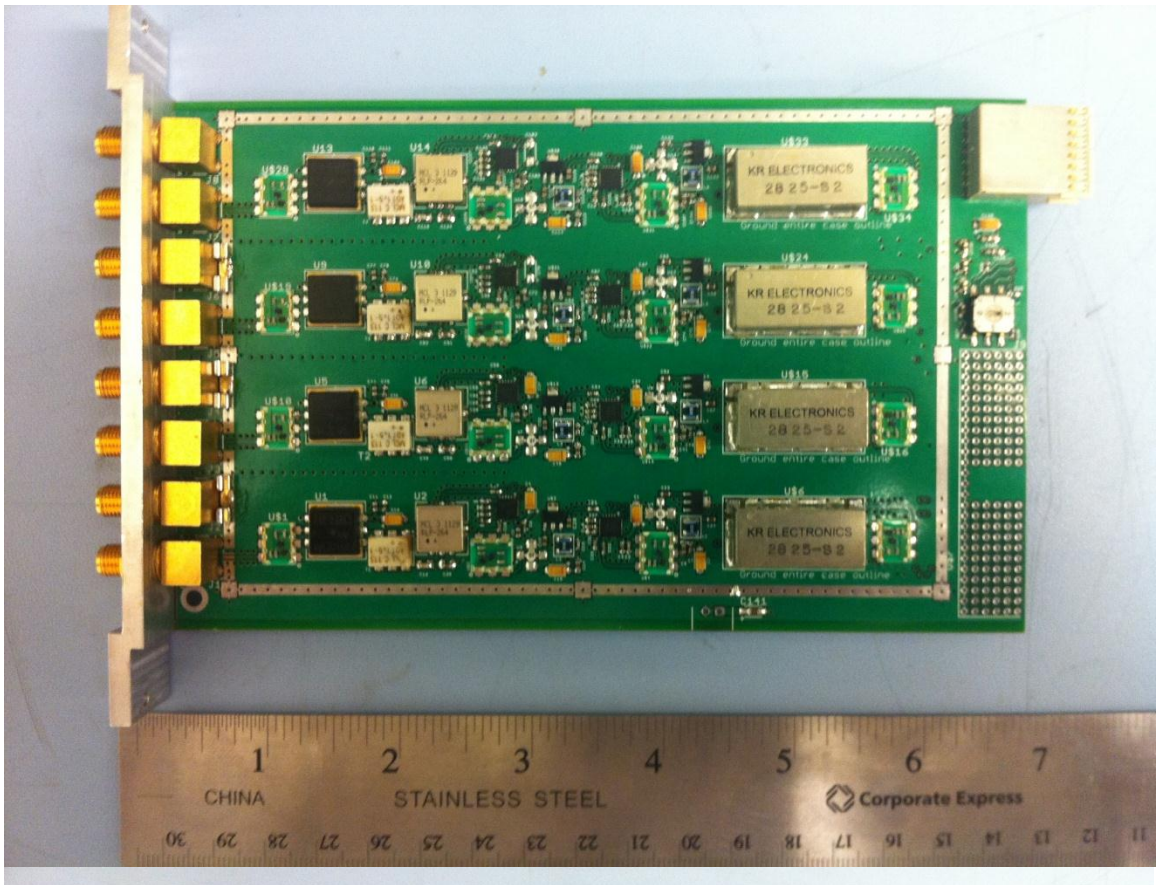
KR ELECTRONICS
2825-S2
CHINA
STAINLESS STEEL
Corporate Express

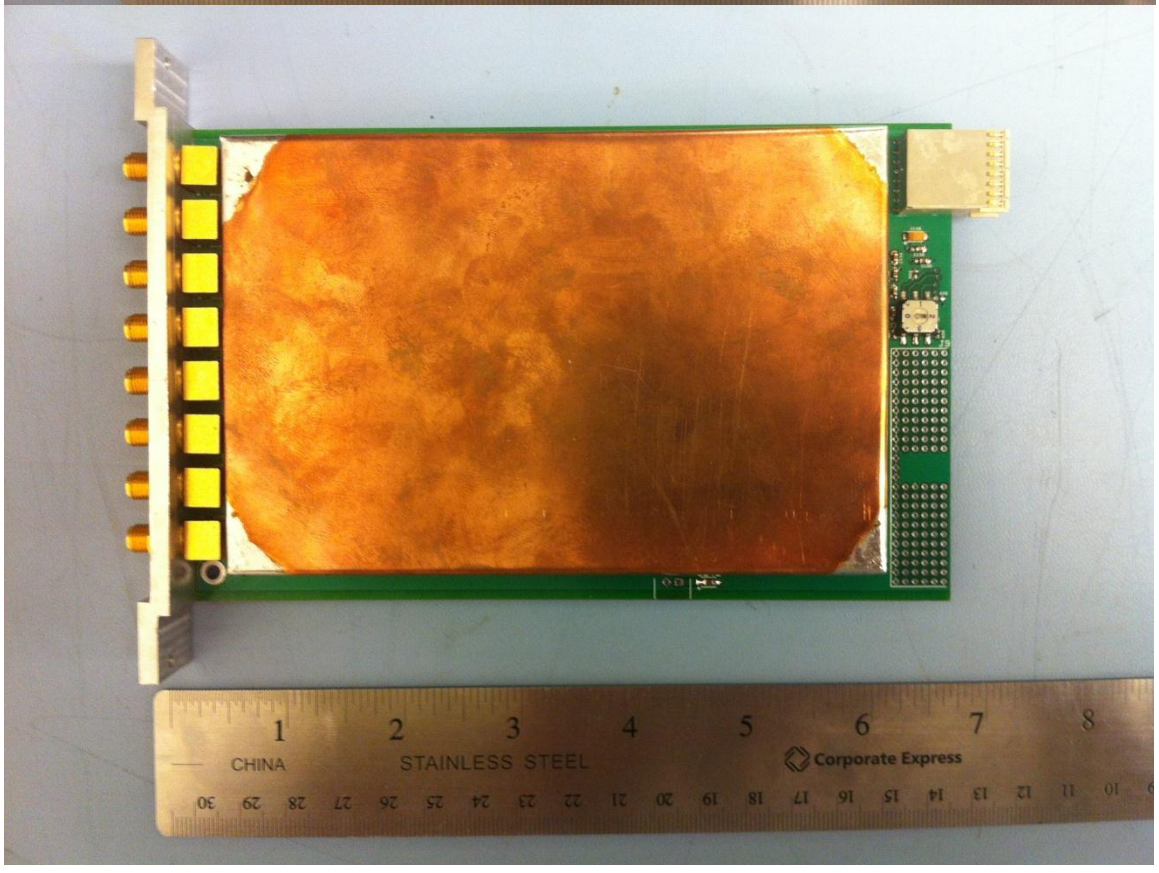
CHINA
STAINLESS STEEL
Corporate Express

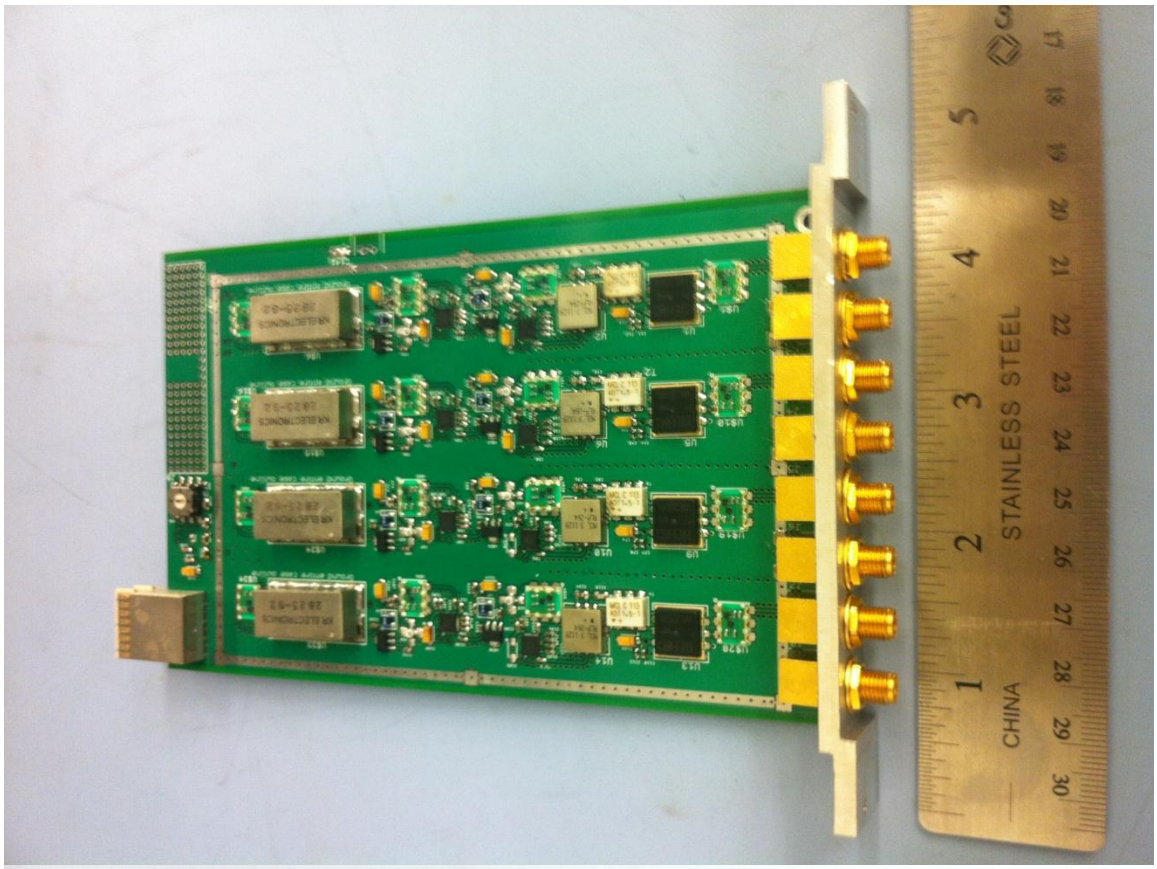
STAINLESS STEEL
CHINA

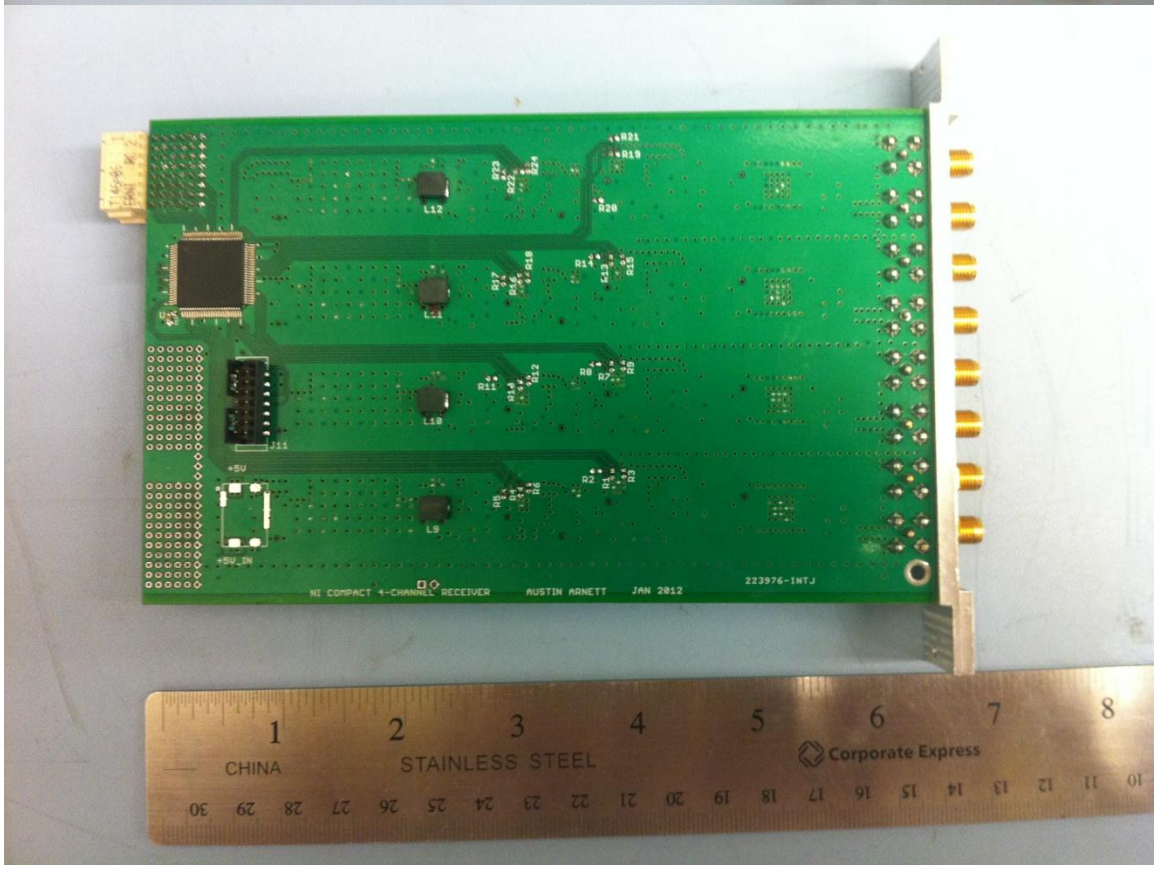
NI COMPACT 4-CHANNEL RECEIVER
AUSTIN ARNETT
JAN 2012
223976-INTJ
STAINLESS STEEL
CHINA
Corporate Express


CHINA